NATIONAL TECHNICAL UNIVERSITY OF ATHENS
SCHOOL OF NAVAL ARCHITECTURE & MARINE ENGINEERING
DIVISION OF MARINE STRUCTURES
SHIPBUILDING TECHNOLOGY LABORATORY

Diploma Thesis

Redesign options of large container vessels in order to comply better with the COFASTRANS system for loading/unloading from both sides

TSAGANOS Leonidas – Nektarios

Thesis Committee:

Supervisor:	**N. Tsouvalis, Professor NTUA**
Members:	**G. Zaraphonitis, Professor NTUA**
	D. Lyridis, Associate Professor NTUA

Athens, March 2020

ΕΘΝΙΚΟ ΜΕΤΣΟΒΙΟ ΠΟΛΥΤΕΧΝΕΙΟ
ΣΧΟΛΗ ΝΑΥΠΗΓΩΝ ΜΗΧΑΝΟΛΟΓΩΝ ΜΗΧΑΝΙΚΩΝ
ΤΟΜΕΑΣ ΘΑΛΑΣΣΙΩΝ ΚΑΤΑΣΚΕΥΩΝ
ΕΡΓΑΣΤΗΡΙΟ ΝΑΥΠΗΓΙΚΗΣ ΤΕΧΝΟΛΟΓΙΑΣ

Διπλωματική Εργασία

Ανασχεδίαση πλοίων μεταφοράς εμπορευματοκιβωτίων έτσι ώστε να είναι συμβατά με το σύστημα COFASTRANS για φορτοεκφόρτωση και από τις δύο πλευρές

ΤΣΑΓΑΝΟΣ Λεωνίδας - Νεκτάριος

Εξεταστική Επιτροπή:

Επιβλέπων:	**Ν. Τσούβαλης, Καθηγητής ΕΜΠ**
Μέλη:	**Γ. Ζαραφωνίτης, Καθηγητής ΕΜΠ**
	Δ. Λυρίδης, Αναπληρωτής Καθηγητής ΕΜΠ

Αθήνα, Μάρτιος 2020

Table of Contents

Table of Figures

List of Tables

Acknowledgements

This Diploma Thesis marks the end of my undergraduate studies in the School of Naval Architecture and Marine Engineering of NTUA. It was a difficult and bumpy road, but a pleasant trip, that enforced my fondness for Naval Architecture. I would like to express my gratitude to all those people who supported me during the past five years and made this work feasible.

First of all, my sincere thanks goes to my supervisor Dr. Nicholas Tsouvalis, for trusting me with this Thesis subject and for the perfect collaboration for the completion of the present study. I would also like to thank him for being my mentor, both for the present work and for my personal development.

Furthermore, it was an honor to have met and discussed with Mr. Vladimir Nevsimal-Weidenhoffer, the inventor of the Ship-to-Shore Multi Trolley Portal Gantry Container Crane. Mr. Nevsimal offered me constructive criticism and advice, that proved to be of great importance for my study. The same goes for Mr. Hannu Oja, with whom I have had a conference call that assisted with the further understanding of cranes' operation.

Special thanks goes to Dr. George Zaraphonitis and Dr. Dimitris Lyridis, Professor and Associate Professor of NTUA. They verified the design and economic procedures, that had to be applied during the study.

Moreover, I appreciate Mrs. Eleftheria Eliopoulou's intervention in the application of preliminary design methodologies. Many thanks goes to Chroni D., Kanellopoulou A., Alisafaki E., Foteinos M. and Bilalis E., too.

I would like to express my gratitude to my friend Manos Alexantonakis, that despite his busy schedule, devoted some personal time to help me with the development of the, much needed, algorithmic tool. What is more, my friend Pavlos Alexantonakis provided great advice about the procedure of searching information regarding basic particulars of the vessels. Special thanks go to Alexis Orfanidis and Tasos Meggos for assisting me with the graphics of the Thesis.

At this point, I would like to thank, from the bottom of my heart, my parents George and Vicky, for supporting me all my life and for making sacrifices to raise me to the man that I am today.

It goes without saying that I am deeply grateful to my girlfriend Marielpi for standing by my side, supporting and encouraging me and understanding everything that I am going through. I also wish her to accomplish her goals and graduate soon.

Last but not least I would like to thank my friends for their patience, encouragement and all the experiences and memories that will stay with us forever.

"The best is yet to come."

Leonidas Tsaganos
March 2020

Abstract

The increase in the population of the Earth has led to an increase in demand for transportation of goods worldwide. The most efficient way to transport them is by sea. This was the main reason that led to the construction of larger ships and the development of new types. Container ships are considered to be a modern type of ship, considering that shipbuilding has emerged since antiquity.

From the 1950s, when standardized dimensions' cargo (containers) first appeared, since today, these ships have evolved considerably. Investment in such vessels depends on demand, and this was the main reason for the impressive development of this type of ship. The increase in population, in economic terms, is translated into an increase in demand, which ideally leads to an increase in the size of ships in order to carry larger capacities (TEUs).

In reality, though, this cannot be achieved for reasons of navigation and construction obstacles during the route of the vessel (e.g. bridges), but also because of the inability of the cargo to be loaded/unloaded by the present technology (vessel's beam restriction). In addition, the increase of the ship size results in slower loading and unloading rates, which reduces the operations efficiency of both port and ship owner processes, resulting in the increase of the vessel's remaining time at port.

According to literature, many attempts have been made to optimally solve the above problems. The most promising system is believed to be the COFASTRANS one, in which loading/unloading is carried out in an indented berth using new design cranes (Ship-to-Shore Portal Cranes, SSPCs). For this reason, possible changes to the main dimensions of the large container vessels were investigated to make them compatible to the new COFASTRANS system for loading/unloading from both sides. The analysis was done for 2 case study vessels, and 6 new designs were proposed for each case.

Initially, it was considered necessary to investigate the feasibility of these cases, which was achieved by using statistical preliminary design methods. The investigation of suitability of these methods for their application to this type and size ships, was considered essential, due to their past date.

The calculation of loading/unloading times for all proposed cases was also necessary. A software tool has been developed to reduce computational time and to repeat all the calculations for each case, because of their large number.

An important point of the study was the economic evaluation of each case using the introduced index FCT (Fuel Cost per TEU) in order for the above procedure to "come to life".

Last but not least, a detailed evaluation of the results as well as suggestions were made, for further improvement of the above study and for future applications.

Key words: ISO containers; Twenty-foot Equivalent Unit (TEU); containerships; main dimensions; preliminary design; logistics; loading/unloading; present container technology; Ship-to-Shore Gantry (SSG) cranes; COFASTRANS; Ship-to-Shore Portal Cranes (SSPC); Fuel Cost per TEU (FCT)

Abstract in Greek

Η αύξηση του πληθυσμού της Γης έχει οδηγήσει στην αύξηση της ζήτησης για την μεταφορά αγαθών ανά την υφήλιο. Ο πιο αποδοτικός τρόπος για την μεταφορά αυτών είναι δια θαλάσσης. Αυτός ήταν και ο κύριος λόγος που οδήγησε στην κατασκευή μεγαλύτερων πλοίων καθώς και στην ανάπτυξη νέων τύπων. Τα πλοία μεταφοράς εμπορευματοκιβωτίων θεωρούνται σύγχρονος τύπος πλοίου, αν αναλογιστεί κανείς ότι η ναυπήγηση εμφανίστηκε από την αρχαιότητα.

Από το 1950, που πρωτοεμφανίστηκαν τα τυποποιημένα φορτία (εμπορευματοκιβώτια), μέχρι σήμερα, τα πλοία αυτά έχουν εξελιχθεί αρκετά. Η επένδυση σε τέτοιου είδους πλοία εξαρτάται από τη ζήτηση, και αυτός ήταν και ο κύριος λόγος της εντυπωσιακής ανάπτυξης αυτού του τύπου πλοίων. Η αύξηση του πληθυσμού, σε οικονομικούς όρους μεταφράζεται ως αύξηση της ζήτησης και αυτό οδηγεί ιδανικά στην αύξηση του μεγέθους των πλοίων με σκοπό να μεταφέρουν μεγαλύτερες ποσότητες.

Στη πραγματικότητα, όμως, αυτό δεν μπορεί να επιτευχθεί για λόγους ναυσιπλοΐας και κατασκευαστικών εμποδίων κατά το ταξίδι (π.χ. γέφυρες) αλλά και αδυναμίας φορτοεκφόρτωσης από τη παρούσα τεχνολογία (περιορισμός στο πλάτος του πλοίου). Επιπλέον η αύξηση του μεγέθους του πλοίου οδηγεί σε πιο αργούς ρυθμούς φορτοεκφόρτωσης, γεγονός που μειώνει την απόδοση των διεργασιών τόσο του λιμανιού αλλά και των πλοιοκτητών, με αποτέλεσμα να αυξάνεται ο χρόνος παραμονής του πλοίου στο λιμάνι.

Σύμφωνα με την βιβλιογραφία, έχουν γίνει αρκετές προτάσεις για τη βέλτιστη επίλυση των παραπάνω προβλημάτων. Το σύστημα που θεωρήθηκε πιο ελπιδοφόρο είναι το COFASTRANS, κατά το οποίο η φορτοεκφόρτωση γίνεται σε μία εσοχή ελλιμενισμού (indented berth) με τη χρήση νέων γερανών (Ship-to-Shore Portal Cranes, SSPC). Για τον λόγο αυτό, διερευνήθηκαν πιθανές αλλαγές στις κύριες διαστάσεις των μεγάλων πλοίων μεταφοράς εμπορευματοκιβωτίων ώστε να είναι συμβατά με το νέο σύστημα COFASTRANS και να ξεφορτώνουν και από τις δύο πλευρές. Η ανάλυση έγινε για 2 συμβατικής σχεδίασης πλοία (case study vessels) και προτάθηκαν 6 νέες σχεδιάσεις για το κάθε ένα.

Σε πρώτο στάδιο κρίθηκε αναγκαία η διερεύνηση των κριτηρίων αξιοπλοΐας, η οποία επετεύχθη με χρήση στατιστικών μεθόδων προκαταρτικής σχεδίασης. Βασική ήταν η διερεύνηση της καταλληλότητας αυτών για να εφαρμοστούν σε τέτοιου είδους και μεγέθους πλοία, λόγω της παλαιότητας των μεθόδων.

Επίσης ήταν αναγκαίος ο υπολογισμός των χρόνων φορτοεκφόρτωσης για όλες τις περιπτώσεις πλοίων. Λόγω του μεγάλου όγκου υπολογισμών, αναπτύχθηκε ένα εργαλείο για να μειωθεί ο υπολογιστικός χρόνος αλλά και να επαναληφθούν οι υπολογισμοί για όλα τα σενάρια.

Σημαντικό σημείο της μελέτης ήταν η οικονομική αξιολόγηση της κάθε περίπτωσης πλοίου μέσω του εισαγόμενου δείκτη FCT (Fuel Cost per TEU), ώστε να πάρει «σάρκα και οστά» η παραπάνω διαδικασία.

Τέλος έγινε αναλυτική αξιολόγηση των αποτελεσμάτων καθώς και προτάσεις για περαιτέρω βελτίωση της παραπάνω μελέτης αλλά και για μελλοντικές εφαρμογές.

Λέξεις Κλειδιά: εμπορευματοκιβώτια; Twenty-foot Equivalent Unit (TEU); πλοία μεταφοράς εμπορευματοκιβωτίων; κύριες διαστάσεις; προμελέτη/προκαταρτική σχεδίαση; εφοδιαστική αλυσίδα; Φορτοεκφόρτωση; παρούσα τεχνολογία φορτοεκφόρτωσης; Ship-to-Shore Gantry (SSG) cranes; COFASTRANS; Ship-to-Shore Portal Cranes (SSPC); Fuel Cost per TEU (FCT)

Nomenclature

14K:	14000 TEUs vessel
20K:	20000 TEUs vessel
ACT:	Amsterdam Container Terminal
AE:	Auxiliary Engine
AGV:	Automated Guided Vehicle
AP:	Aft Perpendicular of the vessel
ARMG:	Automated Rail Mounted Gantry Crane
ASC:	Automated Stacking Crane
Att. EEDI:	Attained EEDI ($grCO_2$/t-nm)
B:	Beam (m)
Bays:	Numerical coordinates of containers relating to the vessel's length
C_B:	Block coefficient
C_M:	Mid-ship section coefficient
C_P:	Prismatic coefficient
C_{WL}:	Water plane area coefficient
CAD:	Admiralty coefficient
COFASTRANS:	Container Vessel Fast Transshipment
CoG:	Center of Gravity
CRMG:	Cantilevers Rail Mounted Gantry Crane
CT:	Cycle time, the time needed for the trolley to make one circle of operation (sec)
c:	Corrected coefficient of displacement
DGPS:	Differential Global Positioning System
DWT:	Deadweight (t)
EEDI:	Energy Efficiency Design Index ($grCO_2$/t-nm)
EHP:	Effective Horse Power (kW)
EIV:	Estimated Index Value ($grCO_2$/t-nm)
FCT:	Fuel Cost per TEU ($/TEU)
FEU:	Forty-feet Equivalent Unit
FLA:	Full Load Arrival
FLD:	Full Load Departure
FP:	Forward Perpendicular of the vessel

GA: General Arrangement

GDP: Gross Domestic Product

GM: Metacentric height

HV: High Voltage

ILLC: International Load Line Convention

IMO: International Maritime Organization

ITTC: International Towing Tank Conference

L_{BP}: Length between perpendiculars (m)

LCG: Longitudinal Center of Gravity (m)

L_{OA}: Length overall (m)

LS: Lightship (t)

LSMGO: Low Sulphur Marine Gas Oil

L_{WL}: Waterline length (m)

ME: Main Engine

MEPC: Marine Environment Protection Committee

MRV: Monitoring-Reporting-Verification

MSC: Maritime Safety Committee

PTI: Power Take-In system

PTO: Power Take-Off system

QC: Quay Crane

Req. EEDI: Required EEDI (grCO_2/t-nm)

RMG: Rail Mounted Gantry crane

Rows: Numerical coordinates of containers relating to the vessel's beam

RTG: Rubber Tyred Gantry Cranes

SC: Straddle Carrier

SHI: Samsung Heavy Industries

SHP: Shaft Horse Power (kW)

SSG: Ship-to-Shore Gantry crane

SSPC: Ship-to-Shore Portal Crane

T: Draught (m)

T_{ST}: Starting draught of the operation (m)

T_{END}: Ending draught of the operation (m)

T_{ILLC}: Draught according to Load Line Convention, scantling (m)

TCG: Transverse Center of Gravity (m)

TEU: Twenty-feet Equivalent Unit

Tiers: Numerical coordinates of containers relating to the vessel's height

T&S: Trim and Stability Booklet

ULCV: Ultra Large Container Vessel

V or V_S: Service speed (kn)

VCG: Vertical Center of Gravity (m)

VLSFO: Very Low Sulphur Fuel Oil

γ: specific density of sea water (1.025 t/m^3 @ 15°C)

γ_{homo}: homogenous loading (t/TEU)

Δ: Displacement (t)

∇: Volume of Displacement (m^3)

km/h: Kilo-meters per hour

ft or ‘: Feet (1 ft=0.3048 m)

nm: nautical mile

hr: Hours

min: Minutes

sec: Seconds

kN: Kilo-Newton

kn: Knots (1 kn=0.5144 m/sec)

HP: Horse Power (1 HP=0.7457 kW)

kW: Kilo-Watts

kp: Kilo-ponds

t: tons

kWh: Kilo-Watts per hour

kJ/kg: Kilo-Joule per Kilo-gram

Chapter 1

Introduction

High efficiency has become an integral part of modern shipping. All the parties related to the shipping industry yearn to increase their profits. The key to this matter is saving time, as it is well described by the quote: “Time is Money”.

The major party of the container supply chain is the container shipping industry, especially the container vessels. The most efficient way of transfer regarding container ships has proved to be by sea, which is rightfully the way that most worldwide transported containers travel. The transportation of containers by the sea is distinguished in two groups of times; trip and port time. The trip time is the time needed for the vessel to cover a specific route and port time is the time that the vessel remains at port, including the operation of loading/unloading and possible delays due to the congestion of the terminal.

The “time saving” can be achieved by decreasing either trip, port or both times. According to present technology, the reduction of trip time seems to be an inefficient solution. In order to diminish the trip time, the vessels have to increase their service speed. Thus, the consumption and the fuel costs will increase. Another issue that has to be taken into account is the limitations in the emissions of the exhaust gases. These are measured by the Estimated Efficiency Design Index (EEDI), the Monitoring-Reporting-Verification (MRV) Regulation, Green Shipping Certificates etc. Therefore, the solution of reducing trip time is not optimal.

Justifiably, the attempts have focused on reducing port time. The necessity of reducing port time, in conjunction with the flaws of the present loading/unloading technology (e.g. congestion due to slow operation rates, vessel’s beam limitation due to the outreach of the cranes), indicate the fact that some changes must be made. Many proposed new concepts have been designed in order to find the optimal solution, such as: FastNet (Port Technology, 2011), GRID Project (GRID Logistics Inc., n.d.) or SuperDock (Ship-to-Rail System) (Alba & Risemberg, 2011) (Kim, Phan, & Woo, 2012), Ultra Large Floating Container Hub (ULFCH) (Nikolakakis, 2006), Gantry cranes using circulating trolleys (Han & Son, 2000) and Container Vessel Fast Transshipment (COFASTRANS) System (COFASTRANS, 2017) (Nevsimal, 2017). The most appealing one, is believed to be the COFASTRANS system, which is an indented berth concept with a new Ship-to-Shore Portal Crane (SSPC). On this basis, it was necessary to further study the effect of this system on the vessels, from the perspective of a ship owner.

The aim of the Thesis, was to investigate the possible changes in the main dimensions of the Ultra Large Container Vessels (ULCVs) in order to comply better with COFASTRANS system for loading/unloading from both sides of the vessel. For this to be done, some modifications of two case study vessels were made without changing their TEU capacity. For each case study vessel six alternative cases were proposed. The first goal was to make a preliminary feasibility study of all cases. Then, the main focus became the calculation of loading/unloading times, for conventional and SSPC concepts, so as to compare them. Last but not least, the techno-economic assessment of each crane was made in order to evaluate the investment.

Chapter 2

Worldwide Container Shipping

In this chapter, some general aspects of world container trade are examined. A discussion is made for the trademarks, the growth of container vessels and the restrictions of container ports and sea routes.

2.1 General Aspects

The needs of a rapidly growing world population can only be met by transporting goods and resources between countries. The international shipping industry has made this process more efficient and it has changed the shape of the world economy. This benefits consumers by creating choice, boosting economies and generating job positions. Costs for the consumer are minimized and efficiencies are improved and this in turn lowers the impact on the environment. The shipping industry enables the connection between countries, markets, businesses and people, allowing them to buy and sell goods on a reasonable scale (World Shipping Council, 2020). Furthermore, the international shipping industry is responsible for the carriage of around 90% of world trade (International Chamber of Shipping, 2019). The largest part of cargo being transported by the merchant fleet worldwide is nowadays containerized (with respect to the value), as seen in Figure 2.1, as the majority of manufactured and consumer products being shipped in containers, except in cases where the products are physically oversized or moved in sufficient volume to justify specific ship charters – for example iron and steel, cars, timber and semi-manufactures.

Figure 2.1: Value of World Seaborne Trade.

2.2 World Trades

Seaborne container trade has increased dramatically since its introduction over 50 years ago and until recently the global supply chain has worked well in a mature stability with well-balanced vessel and port dimensions. Apart from the global downturn correction, world container growth has been consistently positive, typically tracking or beating world Gross Domestic Product (GDP) and related trade growth, as seen in Figure 2.2.

In 2018, global containerized trade unfolded amid great uncertainty, emerging from the implications of the new International Maritime Organization (IMO) 2020 regulation imposing a Sulphur Cap on bunker fuels trade frictions, trends in China, weakness in consumer markets and unfavorable developments in the world economy. Together, these factors put a brake on containerized trade, with volumes expanding at a relatively much slower rate than in 2017.

Volumes as measured in 20-feet equivalent units (TEUs) increased, however the annual growth percentage decreased at 2.6% in 2018, down from 6% in 2017, bringing the total to 152 million TEUs (Figure 2.2). This range of growth is an dramatic change compared to the double-digit growth rates of the 2000s and less than half of the 5.8% average annual growth rate recorded over the past two decades (UNCTAD, 2019).

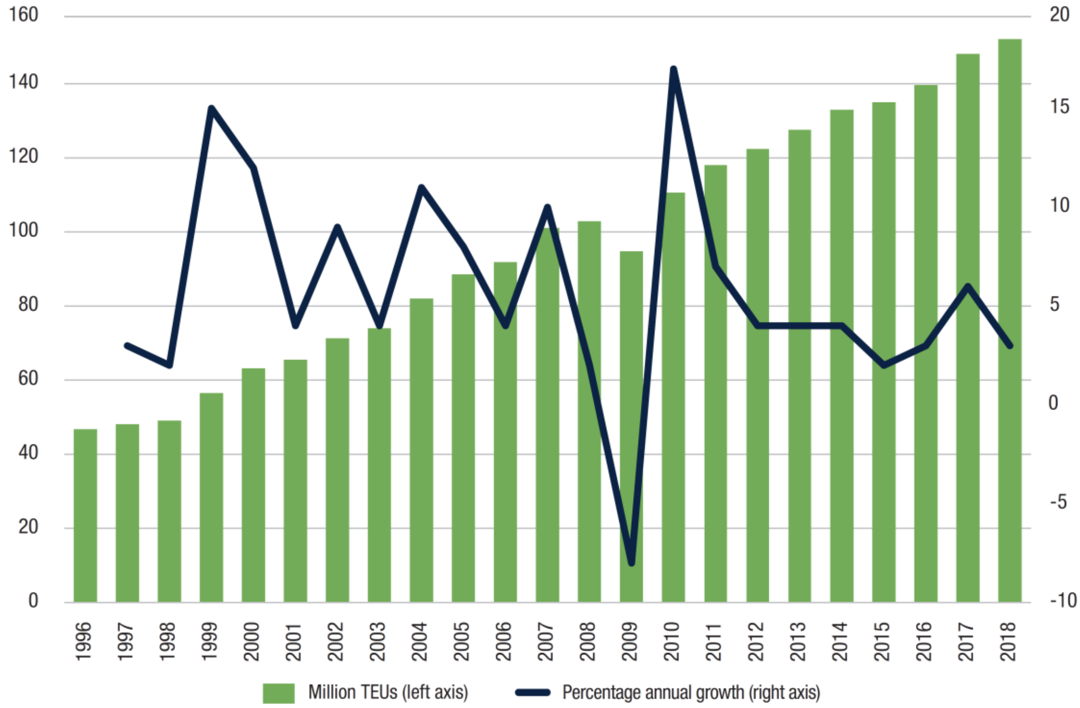

Figure 2.2: Global containerized trade, 1996-2018 (Million 20-foot equivalent units and annual percentage change). Source: (UNCTAD, 2019)

According to the research (UNCTAD, 2019), 40% of globalized containerized trade continues to be carried across the major East–West containerized trade arteries, namely Asia–Europe, the Trans-Pacific and the Transatlantic. However, the remaining percentage occurs in non-mainlane trade routes, such as intraregional flows. In 2018, trade continued to grow on the major East–West trade lanes. Trans-Pacific trade remained the busiest trade route, accounting for 28.2 million TEUs, followed by the Asia–Europe route (24.4 million TEUs) and the Transatlantic route (8.0 million TEUs). In 2017, the respective numbers of transferred TEUs were 26.8 million TEUs in the

Trans-Pacific route, 23.6 million TEUs in the Asia-Europe route and 7.6 million TEUs in the Transatlantic route. Parameters that have affected the 2018 trade were the additional tariffs on Chinese goods in the United States (Trans-Pacific route) and the ban on waste imports into China (eastbound volumes from Europe and westbound volumes on the Trans-Pacific routes). This value is not indicative for is the main trade route of ULCVs due to the fact that the results are influenced by small feeder vessels.

For 2020, a reduction in the total trades is expected due to the coronavirus pandemic. According to literature (Chambers, 2020), “the Sea-Intelligence suggests the box shortfall from the virus is up to 350000 TEUs per week, getting to the $350m figure based on average rate levels of around $1000 per TEU”. “Total of 21 sailings being blanked due to the coronavirus on the Transpacific, taking 198500 TEUs out of action.” “For Asia-Europe, 10 sailings have been blanked thanks to the virus, removing 151500 TEUs from the market”. However, Alphaliner warned that “the full impact of the Chinese coronavirus outbreak on container volumes will not be fully measured until ports announce their throughput numbers for the first quarter, but data collected on weekly container calls at key Chinese ports already shows a reduction of over 20% since 20 January”.

However, within the next few years it is anticipated that the world trade will continue to expand due to a rapid increase in population. This raises the question of whether the ports could handle the increasing number of imported and exported TEUs. It is believed that ports have constantly been required to invest in additional berthing and land areas and to employ increasingly sophisticated cargo handling equipment to meet demand.

2.3 Growth of Container Vessels

Since the beginning of containerization in the mid-1950s, container vessels undertook several waves of changes. An overview of the world container fleet shows the growth in the number and TEU capacity of vessels and an increase in vessel size in terms of all the primary parameters relevant to port design (overall length, draught, beam, TEU tiers, Deadweight, TEU capacity, handling performance in moves per hour, number of cranes applied at the same time). Figure 2.3 below shows the pattern of the historic progression of container vessel size.

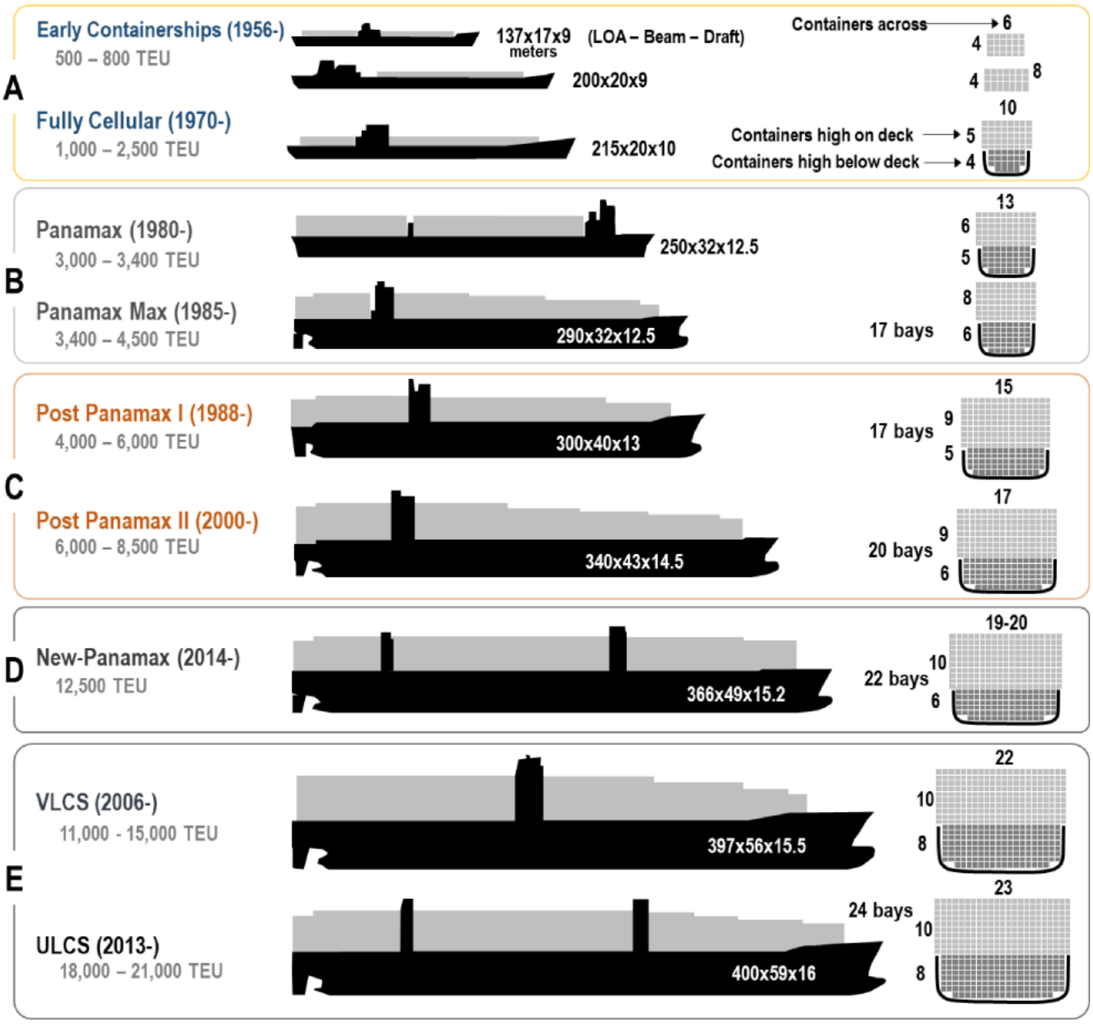

Figure 2.3: Evolution of Container Vessels. Source: (Rodrigue, 2017)

In Figure 2.3, all the dimensions are in meters. The magnitude “LOA” is a typical dimension of the overall length of the vessels. The loads displayed on deck represent maximal possible loads, which would involve a large share of empty containers. The loads are usually one to three container less in height. Containerships usually carry less containers because of weight restrictions, stability issues, weather conditions and lack of demand.

In the summer of 2019, the MSC - Mediterranean Shipping Company - announced that MSC Gülsün, the world’s largest container ship, has arrived in Europe after completing her landmark maiden voyage from the north of China. MSC Gülsün is the first of a new class of 23000+ TEU vessels (Series of 5 vessels). Built by Samsung Heavy Industries (SHI) in South Korea, she is almost 62m wide and 400m long and has a capacity of 23756 TEUs, in 24 rows across (MSC, 2019).

As to future possibilities, trend analysis suggests that container vessels will continue to get bigger, but it is unknown as to whether this will be in length, beam or draught. From ship owner’s scope, larger vessels make the operations more efficient. In order to meet their profit targets, the reduction of time for which the vessel remains at port, is necessary. The simultaneous trade and vessel growth lead the port operators to find solutions for a faster handling performance in order to keep vessel time in port to a minimum.

2.4 Container Ports, Sea Routes and Restrictions

Container ports play key role in the trade shipping lines. The center of the container supply chain consisted of the container terminals, which manage all the inbound and outbound containers both to the sea and to the shore. In simple terms, the port's role is like a key link in the container supply chain.

However, very few selected ports on the major Asia-Europe shipping route have port facilities and equipment able to accommodate Ultra Large Container Vessels (ULCVs) and efficiently handle their very large box exchanges. This fact, consequently, affects the trade route of these vessels. Figure 2.4 below is a density map and shows the current shipping routes of the largest container vessels.

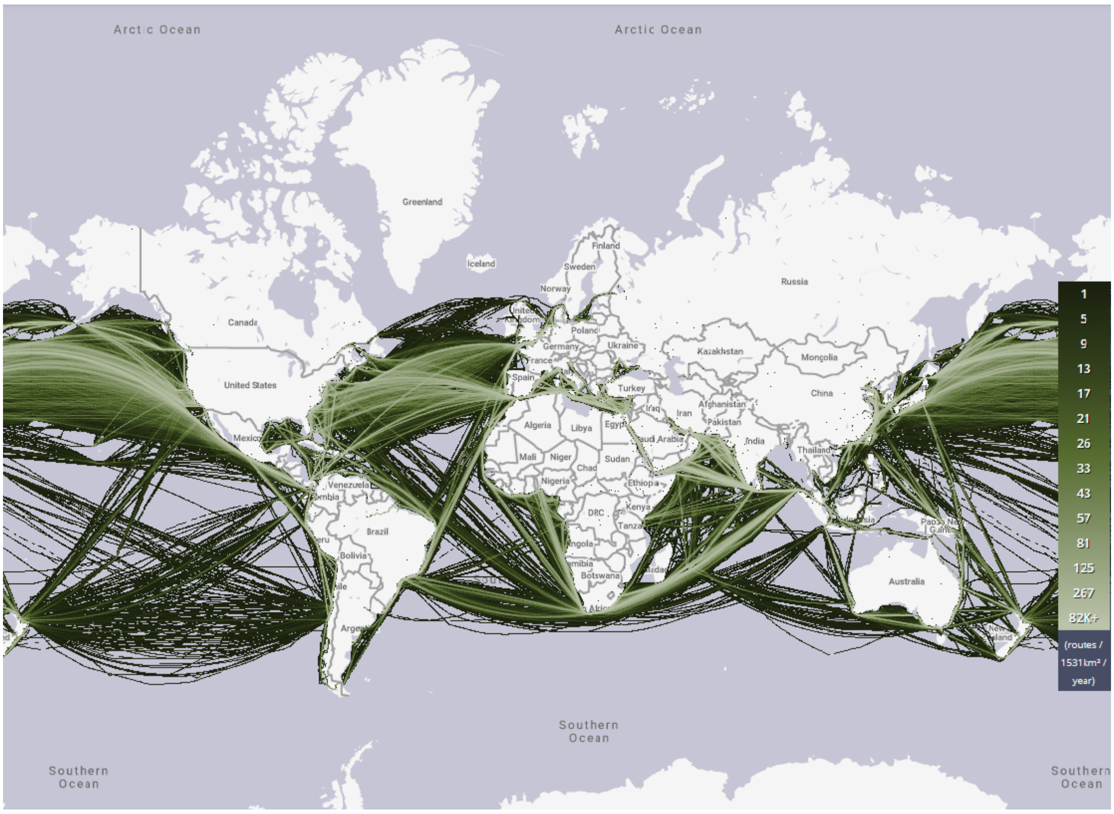

Figure 2.4: Density map of shipping routes of the largest container vessels. Source: (Marine Traffic, 2017)

Another parameter that affects the shipping routes of ULCVs are the sea route restrictions. Some of the major pinch points for these vessels on trading routes are: Panama Canal, Suez Canal, Malacca Straits, Arctic and North East Passage etc. Unfortunately, most ULSVs cannot pass from all the major sea routes passages due to nature and location limitations. These restrictions, sometimes affect the ship design of ULCVs.

Apart from passages restrictions, nature and location limitations are also observed in ports. The overall length (L_{OA}), the beam (B), the draught (T) and the air draught above sea level (H) play a key role to these restrictions. These dimensions are limited so as to avoid problems such as grounding, due to shallow waters or narrow passages, or collision with bridges, which are possibly located along the vessel's route and for safety reasons allow ships to turn and reverse their direction of travel (turning basin).

A research for possible nature restrictions both to ports and to sea route passages was conducted. The investigation sample consisted of 80 ports, containing some of the biggest ports of the world, and 7 major worldwide sea route passages. The sources were various and, usually, the necessary data was taken from the original web sites of port authorities. The results are listed in Table A.1 and Table A.2 of Appendix A.

According to this research, 48 ports have draught restriction over 14m (typical dimension for ULCVs), of which 23 are located in Asia, 16 in the United States and Canada, 8 in Europe and 1 in North Africa. In a few years, it is possible that some ports will be dredged to increase their demand. Furthermore, most of ULCVs can pass through Suez Canal, Malacca Straits and Neo-Panamax Canal.

This means that if the container vessels get bigger in order to achieve capacities over 23000 TEUs, then ports will have to be modified in order to enable loading/unloading such ships. This is an additional parameter that port operators have to take into account.

Chapter 3

Container Handling Systems

This chapter examines the evolution of container cranes and how they currently handle cargoes being loaded and unloaded from the world's largest transhipment vessels. Furthermore, it discusses terminal storage capabilities and how crane systems are used to transport containers within and through terminals using terminal operating systems. In addition, some new proposed concepts for faster handling operations are presented aiming to reduce the vessel time in port.

3.1 Present Technology

Container ships are nowadays loaded and unloaded at large container terminals. Figure 3.1 illustrates the loading and unloading process at a typical container terminal. This loading and unloading process can be divided into different sub processes, described below. When a ship arrives at the port, ship-to-shore gantry cranes (SSGs) or quay cranes (QCs) take the import containers off the ship's hold or off the deck. Next, the containers are transferred from the SSGs to vehicles that travel between the ship and the stack (container terminal vehicles). This stack consists of a number of lanes, where containers can be stored for a certain period. Equipment, like cranes or straddle carriers (SCs), serve the lanes. A straddle carrier can both transport containers and store them in the stack. It is also possible to use dedicated vehicles to transport containers. If a vehicle arrives at the stack, either it puts the load down or the stack crane (Rubber Tyred Gantry crane –RTG, or, Rail Mounted Gantry crane –RMG) takes the container off the vehicle and stores it in the stack. After a certain period, the containers are retrieved from the stack by cranes and transported by vehicles to transportation modes like barges, deep sea ships, trucks or trains. To load export containers onto a ship, these processes are also executed in reverse order. Most of the terminals make use of manned units, like straddle carriers, cranes and multi-trailer-systems. However, a few terminals, like some terminals in Rotterdam, are semi-automated. At such terminals Automated Guided Vehicles (AGVs) are used for the transportation of containers. Furthermore, the stacking process can also be done automatically by Automated Stacking Cranes (ASCs) (Vis, 2008).

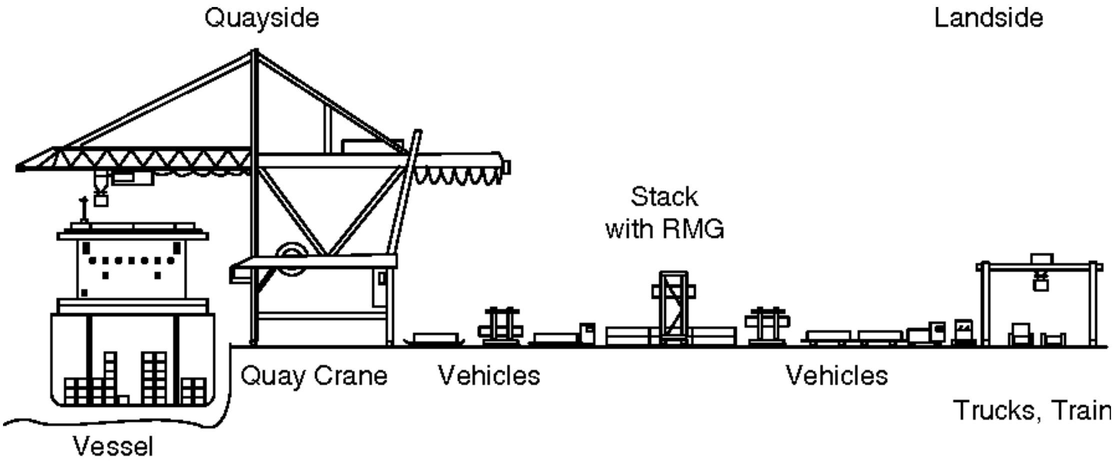

Figure 3.1: Process at a Typical Container Terminal. Source: (Steenken, Voβ, & Stahlbock, 2004)

3.1.1 Ship-to-Shore Gantry Cranes (SSG)

Ship-to-shore gantry cranes (SSG) are imposing, multi-story structures prominent at most container terminals, used to load intermodal containers on and off container ships. They operate along two rails (waterside and landside designations) space based (rail gauge) on the size of crane to be used. Lateral movement system is a combination of two sets of typically ten rail wheels. The lateral movement is controlled by a cabin along the landside wheel. During any lateral movement, lights and sirens operate to ensure safety of the crew operating adjacent to the crane. The wheels are mounted to the bottom of the vertical frame/bracing system.

The vertical frame and braces are a structurally designed system of beams assembled to support the boom, cabin, operating machinery, counter weights and the cargo being lifted. They display signage describing restrictions, requirements and identifiers. The crane boom is a horizontal beam that runs transversely to the berth. It spans from landside of the landside rail wheels to a length over the edge of the berth. The waterside span depends on the size of the ship that it can successfully load/unload. Beams also have the ability to be raised for storage purposes. The hook (hoist) is a device which moves vertically to raise and lower cargo as well as horizontally along the boom's length. For container cranes, a spreader is attached to span the container and lock it safely in place during movement.

SSGs are often used in pairs or teams of cranes in order to minimize the time required to load and unload vessels. As container ship size and beam have increased throughout the 20th Century, ship-to-shore gantry cranes and their implementation has become more complex in order to effectively load and unload vessels while maximizing profitability and minimizing time in port. One example are systems where specialized berths are built in order to accommodate one vessel at a time with ship-to-shore gantry cranes on both sides of the vessel. This allows for more cranes and double the workspace under the cranes to be used for transporting cargo off dock (Wikipedia, 2019).

Although, successive increases in vessel beam have meant that the SSG cranes, as seen in Figure 3.2, have correspondingly longer and higher booms (dimensions in meters), this has required progressive increases in the structures and weight of the cranes and also demands higher trolley speeds to maintain the overall throughput rates. With the present crane technology and berth arrangements, most ports find that six or seven cranes is the maximum number of cranes that can be operated efficiently on a single ship, while some ports are able to deploy eight or nine cranes only for a certain amount of time over the largest vessels.

	1970	1995	2002	2013	2018
Outreach	37	54	67	72	72
Backreach	15	20	25	25	
Lift Height +	25	38	41	52	55
Lift Height -	10	14	17	17	

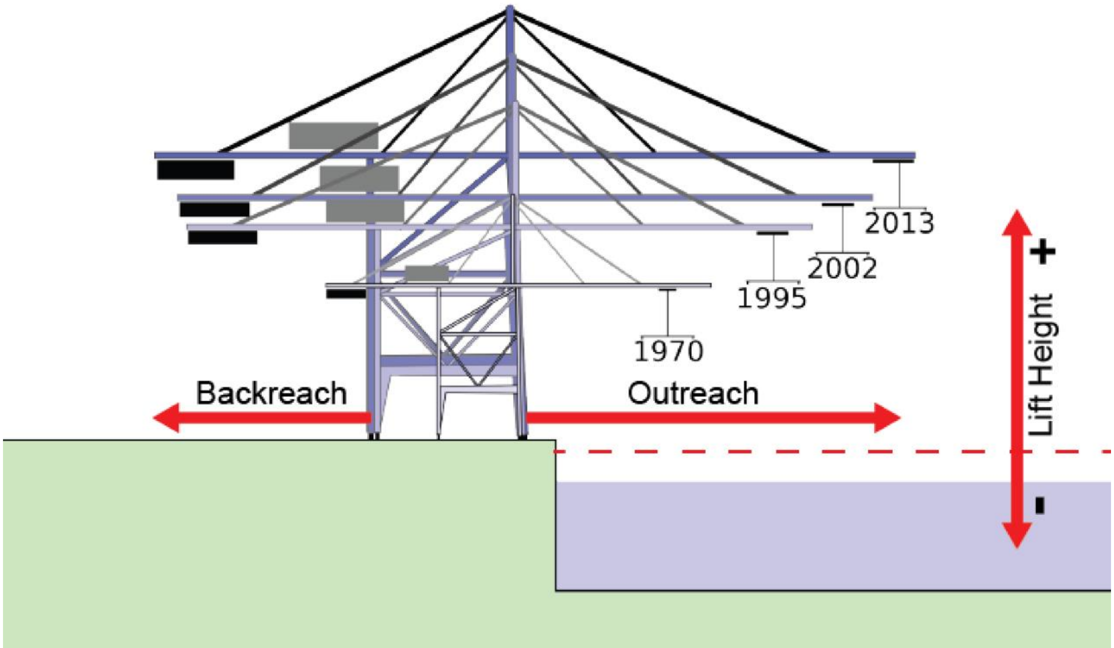

Figure 3.2: Evolution of Gantry Cranes. Source: (Rankine, Netherstreet, Perez Romero, & Palmer, 2018)

The dimensions in Figure 3.2 are measured in meters.

Gantry cranes are generally split into three generic types; Panamax (12-13 containers wide), Post-Panamax (18 containers wide) and Super-Post-Panamax (22 or more containers wide). However, the main dimensions of these cranes are determined in the following chapters.

Cranes consist of three major parts: the crane body, the trolley and the spreader. The trolley is the moving object of the crane which makes the trajectory from ship to shore and vice versa. The spreader is attached to the trolley and is the joint (or the crab) between the containers and the trolley.

But the original SSG concept is inherently inefficient in two respects: firstly, reaching out to pick up a heavy object using a cantilever means that additional weight has to be placed on the other side to prevent the crane from toppling over, adding to the crane's wheel loads and consequently the need for stronger foundations. Secondly, the further out the crane has to reach, the longer it will take to get there, making it slower in handling the bigger ships at a time when the industry is looking to reduce ship time in port.

3.1.2 Spreaders

The spreader is a device used for lifting containers and unitized cargo. The spreader used for containers has a locking mechanism at each corner that attaches to the four corners of the container. Container lift spreaders have developed from simple rectangular frames to hydraulic driven extendible frames able to lift a 40ft or twin 20ft containers in a single crane movement of two TEUs. There are many different types of spreaders. The most common are the twin lift spreaders (2 TEUs or 1 FEU), and the tandem ones (4 TEUs or 2 FEUs). A typical arrange of a twin lift spreader is shown in Figure 3.3.

Figure 3.3: Typical twin-lift spreader. Source: (PNGWAVE, 2020)

3.1.3 Storage Yard Cranes

The container storage arrangements within individual terminals very much depend upon the area of land available within the terminal, the local site conditions and preferences for particular operations.

Historically, the majority of major container terminals have used portal cranes in the form of either rubber tyred gantry cranes (RTGs) or sometimes rail mounted gantry cranes (RMGs) to span dense blocks of containers and terminal trailer loading lanes which have access to roadways between blocks.

RTG units have generally been preferred as they can span up to seven rows of containers, piled up to six high with a single lane loading roadway. The blocks are usually parallel to the quayside coping and about 250m long between perpendicular roadways. This allows trailers to move from the gate-railhead to a berth and vice versa.

The units usually require four pairs of wheels running along strengthened pavement lanes to support the vehicle and lifting loads, and present a plane running surface for trailers to move from the loading lane into the access roads between the RTG lanes. In the past, the RTG units have needed their own independent power source for their transmission and hoisting motors, which has given ports the flexibility to move units to high activity areas. Some units are now being supplied with high voltage (HV) electric power via trailing cables, which reduces pollution and improves their carbon footprint, but limits the ease with which the RTG units can be moved between stacks.

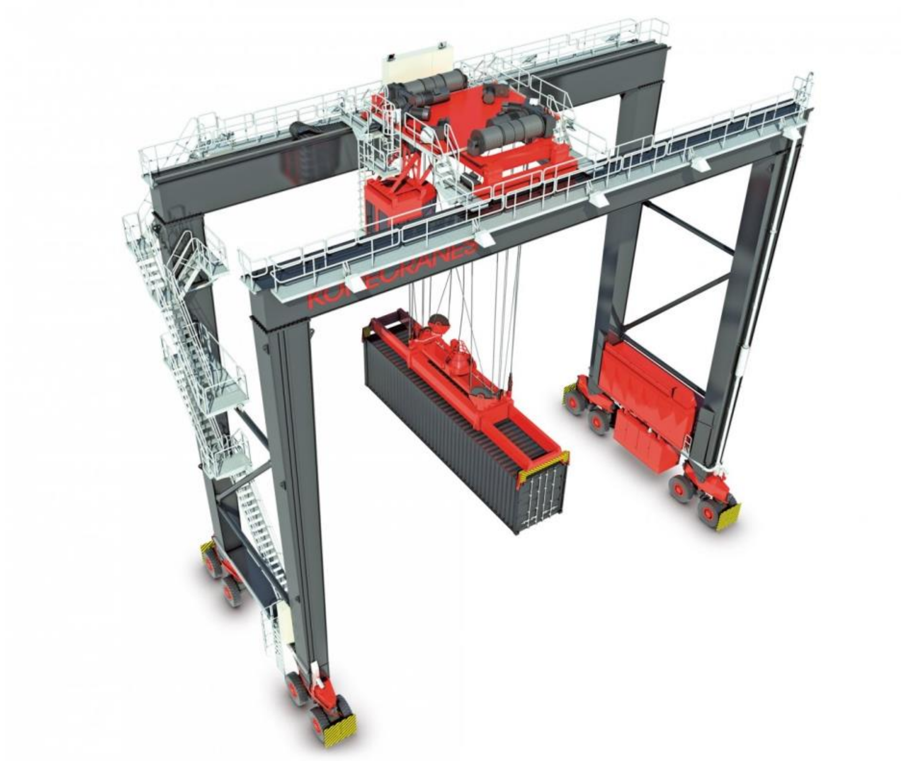

Figure 3.4: Typical RTG crane. Source: (KONECRANES, 2020)

Historically, the RMG units running on rail systems have been used to span rail siding loading areas. They generally require less maintenance than RTG units, can span many more rows of containers (up to 21 rows) and, if required, they can also provide cantilevers to discharge or load containers up to twenty meters 20m beyond the Cantilevers Rail Mounted Gantry (CRMG) cranes' rails. In the past, the rails have presented difficulties to trailer crossings and they offer no flexibility for repositioning units to other stacks. Therefore, they have seen only limited use in main container storage areas. However, recent terminals such as Euromax Rotterdam, Khalifa Abu Dhabi and London Gateway, which require high volumes of containers to be moved between their landside-gate/rail zone and their berth zone, are now providing multiple lines of groups of three numbers of 31m gauge RMG blocks, each spanning ten rows of containers and aligned perpendicularly to the cope line, separated by access roadways. Each of these blocks has two RMG units with no overhang, which are operated as a pair, with the one servicing loading bays and the other bringing boxes to the loading bay. The RMG stack heights vary from one over three in Delta Port to one over six in Abu Dhabi, but one over eight containers are now being offered by some manufacturers. The RMG units are readily adapted to fully automated (ARMG) operation and/or remotely operated (Driverless) operation to collect or discharge boxes to and from either the land or berth end of the stack.

Figure 3.5: Typical RMG crane. Source: (KONECRANES, 2020)

3.1.4 Container Terminal Vehicles

The usual means of moving containers around a terminal has been the standard terminal trailer which comprises of a demountable trailer unit drawn by a terminal tractor (prime mover). The allowable speed of these vehicles within the terminal varies between 15 and 40km/hr depending on the routes within the terminal and the distances travelled. Faster speeds are associated with high rates of pavement wear and most terminals strive to organize transportation by controlling the speed of the vehicles in order to minimize queueing at the cranes with varying levels of success. Various improvements have been developed over the years and some of them are outlined below.

Integrated tractor and trailer units with better manoeuvrability, reduced the overall weight and better distributed wheel loads achieving fuel consumption reduction.

Double stacked and coupled trailer systems drawn by a single prime mover, which increase the overall loading times for the trailer and decrease their speed but are only viable for efficient delivery to more remote stacking in some terminals.

Automated guided vehicles (AGV) using Differential Global Positioning System (DGPS), local positioning systems and proximity sensors have been developed and allow highly efficient transfers between berths and stacks. They have a generally stated straight line speed of 6m/sec, corner at three meters per second 3m/sec and can crab diagonally at one meter per second 1m/sec. One major benefit of AGVs is that they can reverse course rather than requiring a turning circle. However, separation of manual and automated system operating areas is required. Units can be diesel, hybrid or battery powered.

Straddle carriers deposit or pick-up containers from under the SSG and place them in single rows separated by 1.6m corridors in which the straddle carrier can move. Maximum stack height on the berth or yard is generally three boxes. Straddle carriers are particularly effective in non-rectangular stacking areas but cannot rival the stacking densities achieved with RMG and RTG units. The straddle carriers have eight rubber tyred wheels, which exert more load on the pavement than the trailers, but have maximum travel speeds at 30km/hr when empty and 26km/hr when carrying full load.

Shuttle-carriers are one over one or one over two straddle carriers which are faster versions of the typical straddle carrier and are designed to pick up and deliver boxes from the berth cranes to the automated stacking cranes (ASCs) in the new high volume terminals at London Gateway, Khalifa Port Container Terminal etc.

Figure 3.6: Straddle carrier (left) and AGV (right). Edited by Alexis Orfanidis. Source: (Turbosquid, 2017 & 2019)

3.1.5 Vessel Limitations

As mentioned above, the ship owners' tendency is to build larger vessels in order to transfer more containers and make their operation more efficient. There are three major problems that port operators will have to deal with:

- The further out the crane has to reach and pick up a heavy object (container), in the outreach direction, the more weight has to be placed on the other side (counter weight) to prevent the crane from toppling over due to high torque applied on this point. This means that since heavier cantilevers are required, the structure weight and the wheel load will be increased and consequently so will the construction and maintenance costs. An additional civil engineering work for the foundation of the rails will be necessary.
- The further out the crane has to reach the longer it will take to get there, making it slower to handle the bigger ships at a time when the industry is

looking to reduce ship time in port. To avoid this, more powerful crane engines are required. The engines, however, already work at their maximum load. This means that the trolley and the hoist speeds are at their maximum limit. Modifications in the whole crane structures would be needed, making the design more complex and heavier. The consequences will be the same as in the previous problem.

- Bigger vessels with bigger capacities of TEU will increase the transshipments rates in the container terminal. Ports would have the ability to handle faster rates by making the whole transshipment process faster. This would require, more container terminal vehicles, cranes and landside areas.

Especially for the quayside procedure, if the port operators cannot find a solution, then increasing the vessels beam will be an obstacle for naval architects. This limits the possible modifications in principal dimensions for making larger ships. The possible modifications in principal dimensions of vessels will be discussed further in the following chapters.

According to the literature, some new concepts were proposed for the quayside operations. Some of them are presented in the following section.

3.2 Proposed New Concepts

Some attempts have been made to change the status quo. A simple indented berth was operated successfully between 2006 and 2008 at the Ceres Paragon (latterly the Amsterdam Container Terminal (ACT)) (Young, 2012). But as conventional gantry cranes were used from both sides, the interference between cranes inevitably resulted in inefficient utilization. Furthermore, the berth was never able to demonstrate its full potential because it was accessible only through restricted-tidal locks and close to Rotterdam, which made it a less desirable destination (Rankine, Netherstreet, Perez Romero, & Palmer, 2018). Information about the port arrangement was presented in “PIANC 2002”, the 30th International Navigation Congress in Sydney on September 2002 (Ligteringen, Winkel Buiter, & Vermeer, 2002).

Research around this concept continued exploring various indented berth layouts for the largest ships at that time (Rankine, Developing a Container Vessel "Docking System", 1999).

Presumably in response to Maersk’s request for a step-change in container handling for the new larger vessels, APM Terminals developed, in 2006, a new concept called “FastNet” with narrower cranes indented to enable a greater number of individual cranes to work simultaneously on a vessel. The APM Terminals’ “FastNet” Crane concept was the winner of the “Innovation in Ship Operations” category of the 23rd Annual Seatrade Awards held at the Guild Hall in London on April 4th, in 2011 (Port Technology, 2011). According to the best of our knowledge, these cranes have never built, until today.

Another attempt was the GRID project or SuperDock concept, which derived from the need for an economically and environmentally superior container terminal at the ports of Los Angeles and Long Beach (Alba & Risemberg, 2011) (Kim, Phan, & Woo, 2012). The idea was a Ship-to-Rail System and turned the container terminal into a “vertical design” (GRID Logistics Inc., n.d.).

Other, not so appealing, attempts were “Ultra Large Floating Container Hub-ULFCH” (Nikolakakis, 2006) and “Gantry Cranes having Circulating Trolleys” (Han & Son, 2000).

Unfortunately, all the previously described projects were found to be complicated and have not been adopted. The most appealing concept, which takes into account all three major problems that were mentioned above, seems to be the “Container Vessel Fast Transshipment System-COFASTRANS”, which as regards the crane part was invented by Mr. Nevsimal-Weidenhoffer (COFASTRANS, 2017), who holds the patent of the new portal crane (International Patent WO 2017/071736A1, World International Property Organization, Publication Date 4 May 2017 (Nevsimal, 2017)). The COFASTRANS system provides faster handling operations both for the vessel and for the terminal. In addition, it gives the opportunity of increasing the beam of the vessels (New Crane Concept from Konecranes, 2018). The idea is described in the following Chapter.

Chapter 4

COFASTRANS System

In this chapter, the COFASTRANS system is described. The Ship to Shore Portal Cranes, the new terminal layouts and the provided answers to the major problems by COFASTRANS system are analyzed in the following sections.

4.1 General Description

COFASTRANS is a system for loading and unloading large container ships in container ports using a portal crane and indented berth, instead of the existing cantilever cranes and long straight-line berths. The objective is to substantially improve the efficiency of container transportation in terms of time, cost and environmental impact.

The containers are transferred to both sides of the vessel, cutting in half any congestion at the quayside. The new portal cranes have been designed so that each crane can line up and address two bays of containers simultaneously, with each bay being serviced by two trolleys. This can reduce the outreach distance in half and consequently the total operation time would decrease.

4.2 Ship to Shore Portal Cranes

In shipbuilding and maintenance yards it is common for large Goliath portal cranes to be used, as they have extremely high load carrying capacities across long spans at high levels and do not require for additional counter balance weights, that SSG designs require. These dockyard cranes typically have either a single lift beam with two lifting trolleys or a twin lift beam with three lifting points. They can span over 200m with lift capacities of up to 2000 tons, which is well over the 250t/beam envisaged for container terminals (COFASTRANS-Indented Berths Feasibility Study, 2015). The COFASTRANS crane concept uses the same basic structural form, which is referred as portal crane.

The concept of the Ship to Shore Portal Crane (SSPC) envisages placing two spanning beams with 2 trolleys on each beam over the indented berth to provide four independent lifting points per crane (refer Figure 4.1), each capable of undertaking single, twin or tandem lift spreader (i.e. single: 1 TEU, twin: 2 TEUs or 1 FEU, tandem: 4 TEUs or 2 FEUs side by side). The buffer to buffer length of the cranes will be less than 53m allowing a maximum of five SSPC units to be deployed over 400m long vessel (COFASTRANS-Indented Berths Feasibility Study, 2015). The number of cranes to be deployed over a vessel depends on the length of the ship and the crane availability of the container terminal. It is therefore considered that acceptable efficiency could be achieved by deploying only three or four SSPC units. The use of fourth SSPC unit is still under investigation due to economic reasons. However, in the present work, the use of both three and four SSPC units was studied. If all three SSPC units are used, this will result in the simultaneous operation of up to twelve spreaders over six bays of the vessel, which corresponds to the condition where six conventional cranes with six trolleys are deployed over six bays of the vessel. The two lifting beams are set about 30m apart so that each crane works upon two non-adjacent vessel bays at once.

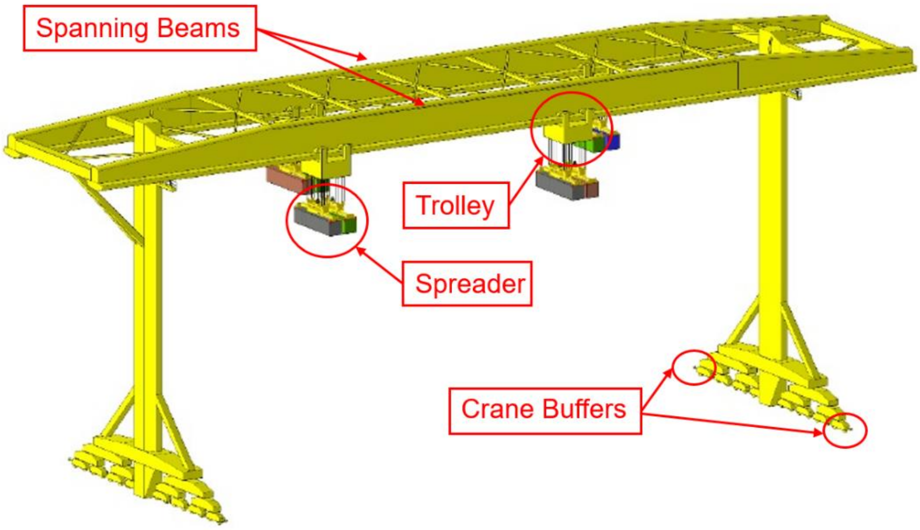

Figure 4.1: Ship to Shore Portal Crane. Source: (Rankine, Netherstreet, Perez Romero, & Palmer, 2018)

It is assumed that the cranes will complete the loading and unloading of each pair of 40ft bays before moving to the next adjacent bays and continue their operation. If dimensions of the funnel and bridge units are the same as the 40ft container bays, within the tolerance of the crane boom spacing, then the crane booms could operate simultaneously on the front and aft bays of these structures. The trolleys have the ability to move their hook ±0.75m in the vessel's longitudinal direction in order for them to operate on two non-adjacent bays, only if the distance between the two longitudinal centers of these bays is different than 30m. Typical positions of SSPC units along a vessel are illustrated in Figure 4.2. In this case 4 SSPC units are deployed along the vessel. Each arrow of each crane denotes the spanning beam.

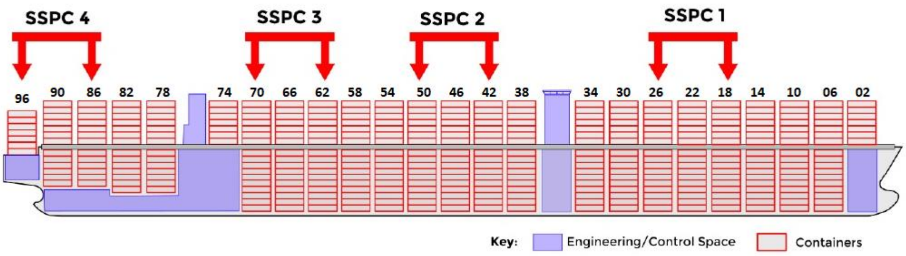

Figure 4.2: Typical positions of SSPC units along an ULCV.

It is likely that the SSPC cranes will be remotely operated with the drivers in the terminal's central control room rather than being fully automated. The vessels' loading/unloading procedures are very complex operations and they are based on a specific stowage plan. The stowage plan, nowadays, is based both on genetic algorithms and on human minds. The cranes should have the ability of adaptation in the various loading conditions and other factors, such as weather conditions etc. For this reason, the SSPC cranes will not be fully automated. With the remote operation of the crane the drivers will be safer, a fact that can lead to less workplace accidents.

An additional benefit of using a portal crane is that, due to the absence of the moment from the eccentric load on the SSG crane, the loads on each runway are reduced and almost equal. Furthermore, the heavily loaded crane rail beams on the jetty superstructure can be located well behind the quay cope line. This way the crane beam and runway construction costs are reduced and the very heavy crane rail sections that are required for the present generation of super post Panamax cranes are omitted. Additionally, the trolleys could work together either on the same side of the vessel or individually, depending on the configuration of the load. Trolleys will be fitted with proximity switches to ensure that they will not collide and the hooks can lift eccentrically by a suitable amount to take account of variability of vessel bay spacing. All of the mechanical elements and automated controllers available for SSG cranes can be deployed in order to be used on SSPC units.

The portal cranes can be slotted into existing terminals as well as into plans for new ports. In case of existing terminals, the only modifications needed have to do with port layouts for indented berths construction. At first, these changes seem to be costly, but both for ship owners and port operators this system would be an appealing solution due to higher efficiency of the transshipped containers and the reduction of vessel time at port that could be achieved.

4.3 Port Terminal Layouts

A COFASTRANS installation is an all-indented, multi-berth terminal or just the addition of a single new indented berth to augment and enhance the ship handling operations for the ULCVs adjacent to an existing terminal, with standard berths handling the smaller feeder vessels using standard SSG cranes. A module could be constructed on reclaimed or redeveloped land to include a single indented berth alongside the high-density container storage stacks alongside. Whatever the layout, the efficient delivery of cargoes to both sides of the vessel could reduce turnaround times. The basic advantage of the system is the creation of a zone around the ship and is totally focused on transferring containers as quickly as possible from ship to shore, or to another ship, and vice versa (Figure 4.3).

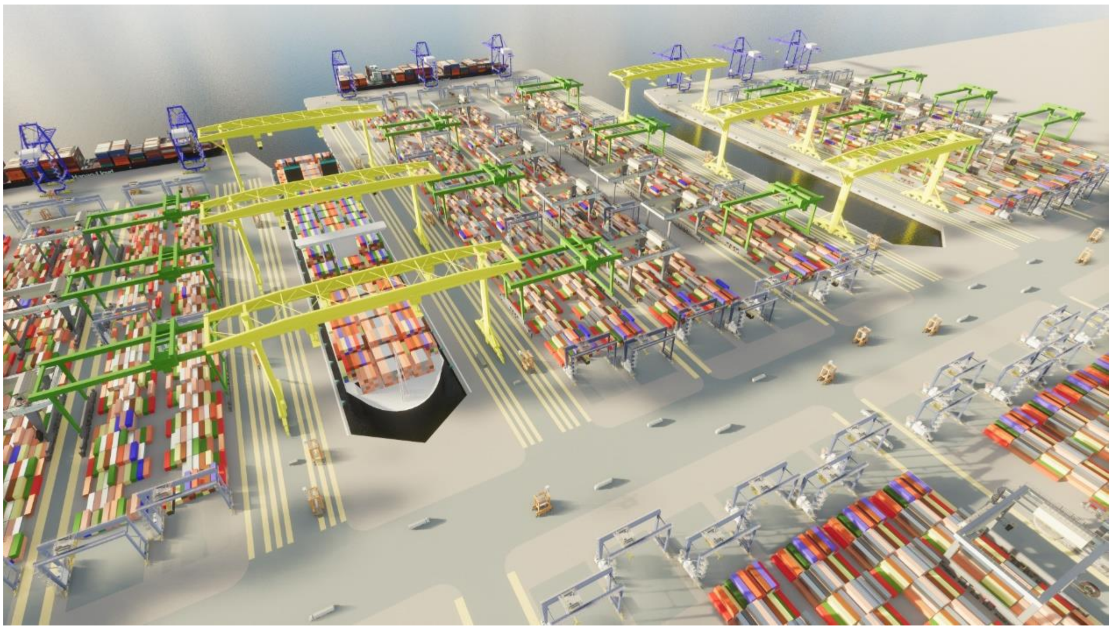

Figure 4.3: Quayside zone around and 2 Indented Berths Layout. Source: (Rankine, Netherstreet, Perez Romero, & Palmer, 2018)

Higher efficiencies into the terminal could be achieved by the combination of the new and the conventional system. This results in saving time and energy, as the carbon 'footprint' is decreased, due to the reduced moves of the containers.

Typically, the layout on a COFASTRANS terminal is more compact compared to an elongated conventional terminal, due to shorter distances that container terminal vehicles have to cover. With a conventional layout, an equivalent port expansion would involve taking a greater length of coastal strip, installing possibly heavier cranes, and moving containers greater distances between vessels and storage spaces. In portal cranes concept, the storage areas would be in each side of each crane in order to minimize the transportation time on shore. Containers could remain for a period of time to these stacks and then other container terminal vehicles would transfer them to another storage area to continue their journey.

Many different terminal layouts can be developed such as single indented berths, pair of indented berths and multiple ones. In all cases, the stacking areas could be slotted either parallel or perpendicular to the berth. The more efficient solution cannot be pre-defined and a preliminary analysis has to be made. Until now, some proposals have been made with a view to further optimization at a later stage. However, a further analysis concerns the port operators view, which is not the scope of this Thesis.

From the ship owner's point of view, essential parameters are the dimensions of the berth, the navigational services of the vessels, and the reduction of vessel time at port. The dimensions of the berth depend on the final designs of port layouts. Although, for any indented berth terminal, it would be necessary for the largest container vessels to safely and promptly berth in the constrained dock configuration. According to literature (Rankine, Netherstreet, Perez Romero, & Palmer, 2018), an initial assessment of requirements was based on information arising from the configuration of the Panama Canal lock entrances and modelling of the Ceres Paragon (ACT) indented berth. Rubber-tyred wheel fenders would be located along the length of the dock and a combination of large winches at the head and entrance of the dock and mules on quayside rails will be used to draw the vessel in and assist its departure. The vessels will enter the berth with bow in, to minimize damage risk to propellers and rudders. The dry-docking process will be helpful for this operation. Bunkering could be undertaken using a barges or vessels at the stern. Provisions could be delivered directly from ashore using the cranes of the vessel. All of these parameters can help reduce the remaining time of the vessel at port, but the question is by how much.

4.4 Possible Vessel Changes

As mentioned above, the ship design is limited due to natural restrictions. However, the ship owner's trends are to build larger vessels with bigger capacities in order to make their operations more efficient. A solution has to be found in order to satisfy their demands. It is possible that, the naval architects will be focused on changing the principal dimensions of the vessels. The magnitudes that affect the capacities of the vessels are the length, the beam, the draught and the height (air draught).

Increasing ship length to significantly greater than 400m may risk excessive longitudinal stresses due to bending and twisting in heavy and long wave conditions at sea.

There is a scope to increase maximum draught, which could add an additional tier below deck. However, a research was conducted for some of the biggest ports in the world and for major sea route passages (refer Section 2.2 and Appendix A), showed that a widely acceptable draught should be around 16m, which is a typical maximum depth for an ULCV. Dredging projects, mainly, in port canals can help in overcoming this obstacle. These works, however, require time and resources.

In addition, increasing the height of the vessels will cause stability problems and limitation of entrance to some ports or passages due to the acceptable height, set by the bridges along the route of the ship.

Until now the beam of the vessel has been limited (max. 60-62m) by the outreach of the ship to shore quayside cranes at the destination ports and is a bottleneck for the vessel designers. Crane manufacturers seem to be unable to build longer cranes in the outreach direction without making significant changes. These modifications will impact the weight, the size and the cost of the cranes. The operational time of the crane will be increased due to longer distances that the trolley will have to cover, resulting in slower rates of handling and a need for heavier cantilevers of the conventional cranes. At first, an increased beam appears to be an attractive option and it is believed that this would be the most efficient way to successfully enlarge these vast vessels even further.

It is clear that unless there is a quantum change in container system and ship design, ship size dimensional increments will become finite as the current technology that has been used and improved for the last 50 years has reached its cost and technical limits.

This problem has challenged port designers for many years and at last COFASTRANS system would provide an answer with a new ship-shore handling system that uses more efficient portal cranes, equipped with multiple hooks that simultaneously work over vessels from both sides, while they are docked within an indented berth.

An important consideration of the system is that whilst it accommodates a shift to even larger ULCV's, it can also allow for beamier but shallower draught vessels within many existing ports. However, this has to be examined.

The aim of this Thesis is to investigate this quantitative reduction of time for different ship designs and to determine how much this time is affected from the modification of the principal dimensions of the vessels. For this to be done, a comparison between new ship designs and the conventional ones was made. The research was conducted for one New-Panamax vessel (14000 TEUs or 14K) and for one ULCV (20000 TEUs or 20K). The scope of the analysis was to modify the main dimensions of the case studies vessels (14K and 20K) without changing the TEU capacity in order to achieve a comparison with similar parameters. It has to be mentioned that the maximum reduction of Depth (D) equals to two tiers, because of the Load Line Convention restrictions ($T_{DESIGN} \leq T_{ILLC}$) (MSC.143(77), 2003).

For both case study vessels, the modifications were classified in three cases, as follows:

Case 1. Increase of Beam (B), decrease of Depth (D), constant Length (L)
Case 2. Increase of Beam(B), constant Depth (D), decrease of Length (L)
Case 3. Increase of Beam(B), decrease Depth (D), decrease Length (L)

It has to be mentioned that the magnitude of length refers to the length between perpendiculars (L_{BP}).

All cases are classified in two more scenarios. The sub-scenarios of Case 1 are the following:

Case 1.1. Increase one row of Beam, decrease one tier of Depth, constant Length
Case 1.2. Increase two rows of Beam, decrease two tiers of Depth, constant Length

Case 2 is subdivided in:

Case 2.1. Increase one row of Beam, constant Depth, decrease one 40ft bay of Length
Case 2.2. Increase two rows of Beam, constant Depth, decrease two 40ft bays of Length

Case 3 is subdivided in:

Case 3.1. Increase two rows of Beam, decrease one tier of Depth, decrease one 40ft bay of Length
Case 3.2. Increase four rows of Beam, decrease two tiers of Depth, decrease two 40ft bays of Length (extreme scenario)

A preliminary study was made to check the feasibility and to calculate the ship resistance for all cases. The procedure of preliminary study and all the assumptions that were made, are described in Chapter 5. Furthermore, a software tool for calculating the loading/unloading times of the cranes was developed, in order to compare the various cases. The estimation of time method is depicted in Chapter 6.

Last but not least, the two proposed methodologies of Techno-Economic Assessment are described in Chapter 7. The results and a further discussion of them are presented in Chapters 8 and 9, respectively. Proposals for a future work or a further analysis are described in Chapter 10.

Chapter 5

Preliminary Study of Ultra Large Container Vessels

Traditionally, ship design can be divided into four main stages, namely:

a. Concept Design-Feasibility Study. In this design stage, the mission or else the ship owner's requirements are translated into technical ship characteristics (of naval architectural and marine engineering nature). This stage of ship design actually corresponds to a feasibility study. Preliminary estimations of the basic ship dimensions, such as length L, beam B, side depth D, draught T, block coefficient C_B, powering P_B etc. are made. However, alternative design solutions fulfilling the owner's requirements are explored with respect to the identification of the most inexpensive solution, but this is not necessarily achieved at this stage.
b. Preliminary Design. This stage is a more comprehensive elaboration of the various ship design steps partly addressed in the first stage. It involves the accurate determination of the ship's main characteristics, so as to satisfy the owner's requirements and to correspond to an optimal solution with respect to the economic criteria.
c. Contract Design. The objective of this stage is the completion of the necessary calculations and naval architectural drawings, as well as the drawing up of the technical specifications of the ship's building. All the above constitute integral of the formal shipbuilding contract between the ship owner and the appointed shipyard. This design stage involves a detailed description of the ship's hull form through the ship lines plan, the exact estimation of the powering for achieving the specified speed based on model tests in a towing tank, the theoretical or experimental analysis of the behavior of the designed ship in waves (seakeeping studies, in general not conducted for common type merchant ships), the analysis of the ship's maneuvering properties (not always performed, like with seakeeping), consideration of alternative propulsive systems (propeller–machine system), details of the ship's structural design, design of the ship's auxiliary/supply networks (electric, hydraulic, piping systems etc.) and finally, a more precise estimation of the individual ship weight components, of the ship's total weight and the corresponding centroids.
d. Detailed Design. In the last stage of the ship design procedure, a detailed design of all structural elements of the ship is produced, along with the setup of the technical specifications for the ship's construction and the fitting of the equipment. Recipients of this information are the yard's production units (panel–hull technicians, welders, fitters, machinists, riggers etc.), and the external suppliers of mechanical equipment and other outfitting.

The first two stages are often merged into the more general definition of preliminary design. Figure 5.1 sketches the course of the design of a ship, which is designed to service specific requirements or a mission (Mission), disposing certain functional (Function), form, space, weight (Form), technical performance (Performance) and economic characteristics (Economics).

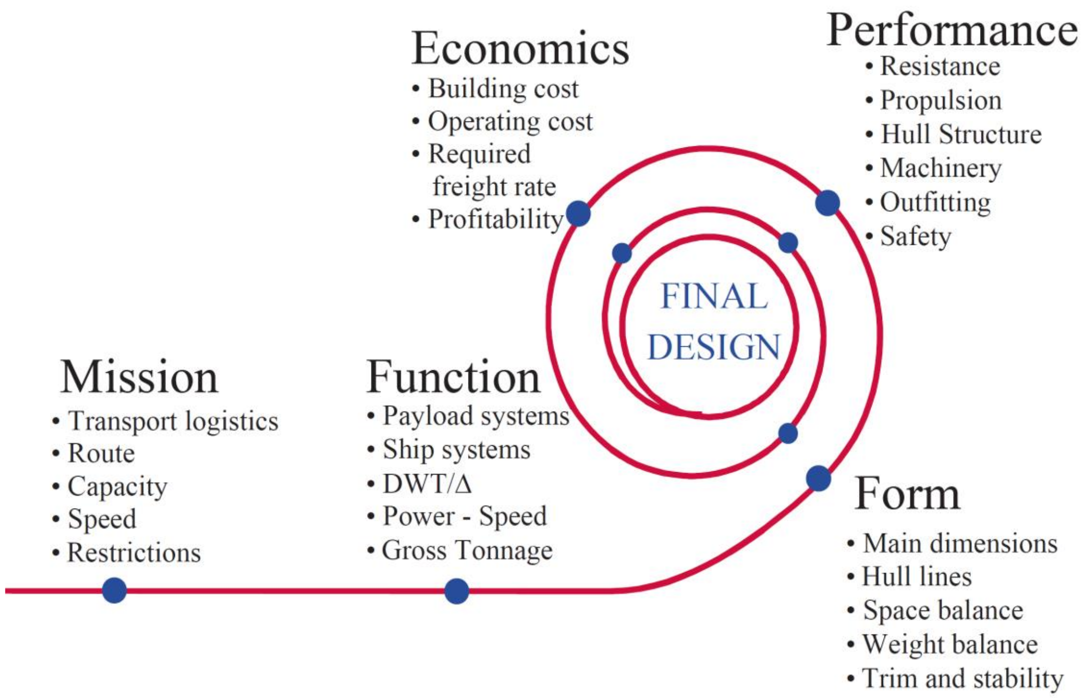

Figure 5.1: Ship Design procedure according to K. Lavender (2009) and Papanikolaou et. al (2009). Source: (Papanikolaou, 2014)

The preliminary ship design encompasses the following more detailed general objectives:

1. Selection of main ship dimensions
2. Development of the ship's hull form (wetted and above-water parts)
3. Specification of main machinery and propulsion system type and size (powering)
4. Estimation of auxiliary machinery type and powering
5. Control of floatability, stability, trim and freeboard (stability and load line regulations)
6. Design of general arrangement of main and auxiliary spaces (cargo spaces, machinery spaces and accommodation)
7. Specification of cargo-handling equipment
8. Design of main structural elements for longitudinal and transverse strength
9. Tonnage measurement (gross register tons)

For study purposes, all the above elements were determined, except the last four items (6-9). The aim of the Thesis was to investigate the possible changes of the main dimensions of the ULCVs. According to this, the excepted items were not considered essential to the objective of the study. However, these elements should be determined in the later design stages, especially, the design of main structural parts for longitudinal and transverse strength. Strength calculations were excluded from the procedure of preliminary design because it was considered that in the case of vessels that do not meet the strength limits, materials of higher tensile and greater thickness could be used. Such a thing would increase the structural cost; however, this is not within the objectives of the present study.

The preliminary design was based on the information of two case study vessels; 14000 (or 14K) TEUs (Case Study Vessel A) and 20000 (or 20K) TEUs (Case Study Vessel B). A more accurate description of the two case study vessels is shown in Chapter 8. However, a lot of necessary data of case study vessel B were missing and for this reason some assumptions were made. The whole procedure of preliminary design is almost identical for the two case study vessels. At points where the method differs, special reference is made.

As it was mentioned in Section 4.4, for each case study vessel, six alternative cases were made. The preliminary design was made for each scenario of each case study vessel, i.e. twelve times. In the following sections, the procedure and all the assumptions that were made are described. All the calculations were made in the environment of Microsoft Excel ©, which was developed by the author of the Thesis. The results for each case are presented in Chapter 8.

5.1 Main Dimensions and Form Coefficients

The Length (L), the Beam (B) and the Depth (D) are some of the principle particulars of a vessel. These magnitudes have been estimated according to the classification of the cases in Section 4.4. However, the subdivided cases that were chosen are listed, again, below:

- Case 1.1. Increase one row of Beam, decrease one tier of Depth, constant Length
- Case 1.2. Increase two rows of Beam, decrease two tiers of Depth, constant Length
- Case 2.1. Increase one row of Beam, constant Depth, decrease one 40ft bay of Length
- Case 2.2. Increase two rows of Beam, constant Depth, decrease two 40ft bays of Length
- Case 3.1. Increase two rows of Beam, decrease one tier of Depth, decrease one 40ft bay of Length
- Case 3.2. Increase four rows of Beam, decrease two tiers of Depth, decrease two 40ft bays of Length (extreme scenario)

Furthermore, the modification of the main dimensions was not considered to affect so much the block (C_B) and the water plane area (C_{WL}) coefficients. For this reason, these factors have been assumed equal to those of the case study vessel A. However, the C_B of case study vessel B was estimated by equation (5.1) (definition of block coefficient) and the C_{WL} has been assumed equal to that of case study vessel A.

$$C_B = \frac{\Delta}{c \cdot \gamma \cdot L \cdot B \cdot T} \tag{5.1}$$

where, C_B: block coefficient
Δ: displacement (t)
c: corrected coefficient of displacement
γ: specific density of sea water (1.025 t/m^3)
L: length (m)
B: beam (m)
T: draught (m)

The product $c \cdot \gamma$ depends on the type and the size of the vessel and on the density of sea water. For this reason, it was taken as 1.0254 t/m^3, and constant for all cases.

A regression equation based on graph by Jensen (1994) was used for the mid-ship section coefficient (C_M) estimation:

$$C_M = \frac{1}{1+(1-C_B)^{3.5}} \tag{5.2}$$

The prismatic coefficient (C_P) was defined as:

$$C_P = \frac{C_B}{C_M} \tag{5.3}$$

5.2 Propulsive Power

A first estimation of the installed power is needed for the engine selection. The installed power is calculated by the British Admiralty formula, which is depicted below:

$$P = \frac{\Delta^{2/3} \cdot V^3}{CAD} \tag{5.4}$$

where, P: installed power (HP)
V: service speed (kn)
CAD: Admiralty coefficient

For each proposed case, the Admiralty coefficient has been assumed constant with the case study vessels. However, to estimate the installed power, the determination of the new design vessels displacement is needed. The displacement is calculated by the following equation:

$$\Delta = LS + DWT \tag{5.5}$$

where, LS: Lightship (t)
DWT: Deadweight (t)

With the basic dimensions (L, B, D) known, the Lightship is estimated by the equation:

$$LS = w_{LS} \cdot L \cdot B \cdot D \tag{5.6}$$

where, “w_{LS}” is the weight factor of Lightship and remains constant for all cases.

The Deadweight was assumed constant due to the fact that the modifications of the main dimensions were made without changing the TEU capacity.

At this point, a first approximation of draught (T) can be made, according to the following equation:

$$T=\frac{\Delta}{c \cdot \gamma \cdot C_B \cdot L \cdot B} \tag{5.7}$$

In later design stages, a more accurate calculation of Lightship, displacement and draught was made. The engine was selected after the final calculation of these magnitudes. The first estimation of these magnitudes constitutes draft estimations in order to continue the calculations in the following design stages.

5.3 Lightship

The Lightship can be distinguished in: Hull weight (W_{HULL}), Outfit and Equipment weight (W_{OUT}) and Machinery weight (W_M).

$$LS=W_{HULL}+W_{OUT}+W_M \tag{5.8}$$

In the preliminary design, these weights are estimated by using statistical methods. A study was made in order to find the best fitted methods for ULCVs.

For the structural weight the following methods were examined: Schneekluth combined with Muller-Koster (Schneekluth & Bertram, 1998) (Papanikolaou, 2014), Watson (Watson, 1998) and Miller method (Miller, 1968). The Schneekluth method was developed for vessels with length varying from 100 to 250m and beam up to 32.25m (Panamax). The typical dimensions of ULCVs are greater than the application constrains of the method. For this reason, the Schneekluth method was rejected. Furthermore, in 1968, Miller proposed three formulas for calculating the hull, the outfitting and the machinery weight. The outfitting weight results for the case study vessels were negative. This means that the sample of the vessels was not indicative of the ULCV design. For this reason, the Miller method was also rejected. Satisfactory results were obtained from the Watson method. The method is described in sub-section 5.3.1.

For the equipment and outfitting weight the following methods were examined: the outfitting components method (Papanikolaou, 2014), the weight groups by Schneekluth (Papanikolaou, 2014), approximate formulas (Papanikolaou, 2014) and Miller method (Miller, 1968). The outfitting components method was rejected because no coefficients could be found, in literature, for containerships. The weight groups method developed by Schneekluth and the approximate formulas are described in sub-section 5.3.2. The mean value of all methods was the final result of the outfitting weight calculations.

For the machinery weight the following methods were examined: weight groups by Strohbusch (Papanikolaou, 2014), Watson-Gilfillan (Papanikolaou, 2014) and Miller method (Miller, 1968). These methods (except the Miller method) are described in sub-section 5.3.3. The mean value of all methods was the final result of machinery weight calculations.

All of these methods (W_{HULL}, W_{OUT}, W_M) were applied to the case study vessels. The calculations were based on statistical methods. This means that some corrections are needed in order to reach the actual Lightship value. For this to be done, an introduction of a divergence factor (ratio) between the calculated value and the actual one is needed. The ratio of calculated Lightship to actual Lightship of the case study vessels has been assumed to remain constant for each case (λ_{LS}=LScalc/LSactual). The actual Lightship of each case was estimated by the ratio λ_{LS} and the calculated Lightship.

With the actual Lightship of each case known, the final estimations of displacement and draught can be made by the repetition of equations (5.5) and (5.7) respectively. At this point, the engine can be selected.

5.3.1 Structural Weight

Hull weight or weight of the ship's structure (W_{HULL}), includes the steel weight of the main hull, the superstructures (even if part of the superstructure is not made from steel, for example, light weight superstructures from aluminum alloys), as well as of some heavy steel fittings (like masts or derricks, etc.). These heavy steel fittings could be included in the equipment and outfit weight (W_{OUT}) instead of the hull weight. There is a variety of hull weight calculations methods. The most appropriate one, which satisfies all the limitations of this size and kind of ships was considered to be the Watson method. The method is based on an assumption: The W_{HULL} can be calculated by the index E_N (Equipment Numerical) of the ship as defined by Lloyd's Register:

$$E_N=L\cdot(B+T)+0.8\cdot L\cdot(D-T)+0.85\cdot\sum_{i=1}^{N_1}h_{1i}\cdot l_{1i}+0.75\cdot\sum_{i=1}^{N_2}h_{2i}\cdot l_{2i} \qquad (5.9)$$

where, N_1, h_{1i}, l_{1i}: number, height and length of deckhouses[i]

N_2, h_{2i}, l_{2i}: number, height and length of superstructures[ii]

Using Figure 5.2, where the W_{HULL} is presented as a function of E_N, the corresponding weight for a standard block coefficient C_{B1}*, at the height 0.8D, equal to 0.70, can be calculated as follows:

$$(W_{HULL})^*=f(E_N),\ \text{Figure 5.2} \qquad (5.10)$$

Correction: For the ship's C_{B1}* (0.8D) ≠ 0.7, the following correction applies:

$$W_{HULL}=(W_{HULL})^*\cdot(1+0.05\cdot\left(C_{B1}^*-0.7\right)) \qquad (5.11)$$

Where the coefficient C_{B1}*(0.8D) can be estimated through the value of C_{B1}(T = D),

---

[i] By definition, the breadth of deckhouses can be up to 0.92·B

[ii] The breadth of superstructures is larger than 0.92·B according to the provisions of the International Tonnage Measurement regulation.

$$C^*_{B1}=C_{B1}+(1-C_{B1})\cdot(0.8\cdot D-T)/3\cdot T \qquad (5.12)$$

The C_{B1} (T=D) can be calculated from the following empirical equation:

$$C_{B1}=C_B\cdot\left(\frac{D}{T}\right)^{\frac{C_{WL}}{C_B}-1} \qquad (5.13)$$

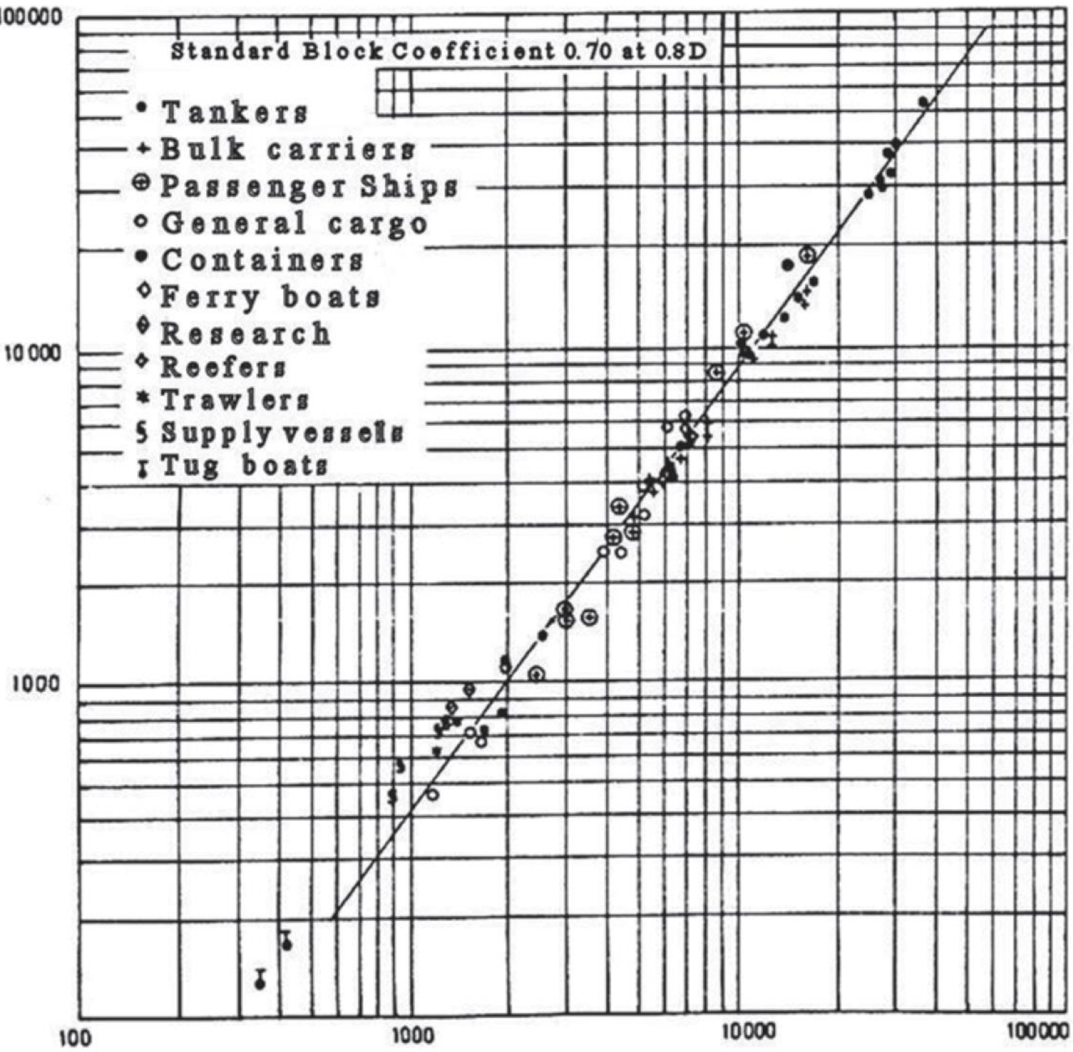

Figure 5.2: Steel weight versus outfitting index EN by Watson. Source: (Watson, 1998)

The line, shown in Figure 5.2, is a mean through most of the spots irrespective of ship type and has the formula $W_{ST}=0.33\cdot E_N^{1.36}$.

The method is valid for mild steel. ULCVs use high tensile steel and it is necessary to take into account this relation. According to literature (Watson, 1998), 1 ton of high tensile steel replaces 1.13 tons of mild steel. This conversion is based on high tensile steel with a yield stress of 315 N/mm^2 (Lloyds AH 32) as compared with mild steel of 245 N/mm^2.

5.3.2 *Weight of Equipment and Outfit*

Equipment and Outfit Weight (W_{OUT}) of accommodation and overall ship arrangements, generally includes the weight of all outfitting/equipment fitted to the "naked" ship hull, except the machinery equipment. The chosen calculation methods were: Approximate formulas for containerships and Weight groups developed by Schneekluth (Papanikolaou, 2014). The final outfit weight is the mean value of the results of these two methods.

For the first method, the following approximate formula was applied:

$$W_{OUT}=K_{OT}\cdot L\cdot B \quad (5.14)$$

where, K_{OT}= 0.34÷0.38 t/m^2, for containerships and depends on the vessel size.

It has to be noticed that for a larger area (bigger vessel) the factor K_{OT} is lower. In this case, it has been assumed that K_{OT}=0.34 t/m^2.

According to Schneekluth, the equipment and outfit weight is distinguished in four groups:

I. Hatch Covers
II. Cargo-handling equipment
III. Accommodation
IV. Other weights

The calculations were made for each weight group.

<u>Group I-Hatch Covers</u>: The weight of covers was calculated by Malzahn's formula. It has been assumed that this formula is valid for Piggy-Back hatch covers too. The equation is the following:

$$W_{HC}=\left(0.0533\cdot b_{HC}^{1.53}+\delta b_{HC}\cdot 0.065\right)\cdot l_{HC} \quad (5.15)$$

where, W_{HC}: weight of hatch covers (t)
l_{HC}: length of hatch covers (m)
b_{HC}: breadth of hatch covers (m)
δb_{HC}: difference in breadth beyond 12 meters (m)

The dimensions of the hatch covers are affected by the dimensions of the vessel. For instance, in case 1.1 the beam is increased by one row, so the breadth of the hatch cover should be increased by the width of a single container.

<u>Group II-Cargo handling equipment:</u> The case study vessels do not have cargo-handling systems. For containers on deck the weight of lashing equipment needs to be added. A mixed loading with TEU and FEU has been assumed. That means an additional weight of 0.043 t/TEU (Papanikolaou, 2014).

<u>Group III-Accommodation:</u> All the weights included in this group were calculated through the respective accommodation area. The specific weights for large cargo ships (the same was assumed for containerships) are from 180 to 200 kp/m^2. For this kind and size of ships, a specific weight of 190 kp/m^2 has been assumed.

<u>Group IV-Other weights:</u> The weight of this group was calculated by the following approximate formula:

$$W_{IV}=(L\cdot B\cdot D)^{2/3}\cdot C_1 \tag{5.16}$$

where, W_{IV} is given in tons and L, B, D in meters. It has been assumed that C_1=0.26.

5.3.3 Weight of Machinery Installation

The machinery weight (W_M) includes the weight of main engine, the weight of shaft and propeller and the weight of the rest of the mechanical components. The chosen calculation methods were: the Watson-Gilfillan formula and the Weight groups by Strohbusch (Papanikolaou, 2014). The final machinery weight is the mean value of the results of these two methods. The results depend on selected engine and therefore on service speed.

The Watson-Gilfillan formula is depicted below:

$$W_M=C_{MD}\cdot P_B^{0.89} \tag{5.17}$$

where, W_M: Machinery weight (t)

P_B: Break power of main engine (kW)

C_{MD}= 0.5 (low speed diesel engine)

According to Strohbusch, the coefficient of machinery weight for cargo ships (the same was assumed for containerships) varies from 85 to 90 kp/HP. It has been estimated that for the case study vessel the coefficient equals to 87.5 kp/HP. It has to be noticed that the power at the dominator refers to Shaft Horse Power (SHP).

5.4 Load Line

The calculation of Load Line is needed to verify that the estimated draught is acceptable. The calculations were made according to the referenced literature (MSC.143(77), 2003). According to Regulation 3, "the Length (L) shall be taken as 96% of the total length on a waterline at 85% of the least moulded depth measured from the top of the keel, or as the length from the fore side of the stem to the axis of the rudder stock on that waterline, if that be greater". In addition, "the depth for freeboard (D_f) is the moulded depth amidships, plus the freeboard deck thickness at side" (calculated by Mid-ship section). However, the containerships' stern profile has a stepped form. In this case, the moulded depth is calculated at the lowest part of the deck, which is below the upper deck. According to case study vessel A, the lowest part is 2.705m below the upper deck. This distance has been assumed constant in all cases and equal to the case study vessel A. In addition, the freeboard deck thickness at side has been assumed constant in all cases and equal to the case study vessel A.

According to Regulation 27, containerships are characterized as "Type B" ships. The freeboard (FB1) was estimated by Regulation 28, which refers to "Type B" ships and depends on ship Length. Freeboards at intermediate lengths of ship were obtained by linear interpolation. According to the Regulation, ships above 365m in length shall be dealt with by the Administration. However, it was not possible to find the necessary information from Administrators. For this reason, the freeboards were obtained by linear extrapolation. Some correction factors were inserted in the calculations.

5.4.1 Correction for ship types "B-60" and "B-100" (FB2)

This correction refers to ships which are characterized as "B-60" or "B-100". A Type B ship in which the reduction in freeboard has been increased up to 60% of the total difference between the values for basic Type A and Type B freeboards is called "Type B-60" vessel. The ship must meet one-compartment damage stability requirements (permeability 95%). Furthermore, a Type B ship in which the reduction in freeboard has been increased up to the total difference between the values for basic Type A and Type B freeboards, effectively making the ship a Type A ship, is called "Type B-100" vessel. This kind of ships must meet two-compartment damage stability requirements (permeability 95%). The case study vessels do not belong in any of these two categories. Thus, no correction was needed (FB2=0).

5.4.2 Correction for Hatch Covers (FB3)

According to Regulation 27, ships above 200m in length shall be dealt with the Administration. However, no information was found for this correction factor. For this reason, the factor was taken as zero (FB3=0).

5.4.3 Correction of ships "Type B" with Length under 100m (FB4)

The case study vessels are over 100m long. Thus, no correction was needed (FB4=0).

5.4.4 Correction for Block coefficient (FB5)

According to Regulation 30, the correction is made when the block coefficient at 0.85D ($C_B(0.85D)$) exceeds the value of "0.68". In this case, the specified freeboard from Regulation 28 shall be multiplied by the factor:

$$FB5=\frac{C_B(0.85D)+0.68}{1.36} \tag{5.18}$$

where, the $C_B(0.85D)$ was calculated by the empirical equation (5.13) for T=0.85D.

5.4.5 Correction for Depth (FB6)

According to Regulation 31, the correction is made when D_f exceeds the value of "L/15", then the freeboard shall be increased by,

$$FB6=(D_f-\frac{L}{15})\cdot R \tag{5.19}$$

where, R is a constant and equal to R=250, when the ship's Length is over 120m.

5.4.6 Correction for deckhouses and superstructures (FB7)

In each case, the examination of superstructure necessity is needed. According to Regulation 39, the bow height (F_b), defined as the vertical distance at the forward perpendicular (FP) between the waterline corresponding to the assigned summer freeboard and the designed trim and the top of the exposed deck at side, shall not be less than:

$$F_b=\left(6075\cdot\left(\frac{L}{100}\right)-1875\cdot\left(\frac{L}{100}\right)^2+200\cdot\left(\frac{L}{100}\right)^3\right)\cdot \left(2.08+0.609\cdot C_B-1.603\cdot C_{wf}-0.0129\cdot\left(\frac{L}{d_1}\right)\right) \tag{5.20}$$

where, F_b: minimum bow height (mm)

L: length for freeboard calculation, as defined in Regulation 3 (m)

B: moulded beam, as defined in Regulation 3 (m)

D_1: draught at 85% of the depth D (m)

C_B: Block coefficient

C_{wf}: waterplane area coefficient forward of L/2 (assumed equal to C_{WL})

In case that the minimum bow height (F_b) exceeds the actual bow height (F_r), then forecastle or sheer have to be added. The International Load Line Convention (ILLC) regulations state that if the minimum value of the bow height FP is achieved by consideration of a sheer, then the same height must extend over at least 15 % L from the FP. In addition, if the height is measured with respect to an existing forecastle, then it is appropriate for such a forecastle to extend over at least 7 % L aft of FP.

Furthermore, the examination of the relation between the breadth of the deckhouse and the ship's Beam is needed. If the breadth of the deckhouse is up to 92% of the ship's Beam, then the effective length of the structures will be estimated. The standard height (determined in Table 33.1, Regulation 33), the length and the breadth of the structures are essential magnitudes for the calculation. The effective length was calculated based on the following formulas:

$$l_E=\begin{cases} l\cdot\left(\frac{h}{h_s}\right)\cdot\left(\frac{b}{B}\right), & \text{when } \frac{h}{h_s}\leq 1 \\ l\cdot\left(\frac{b}{B}\right), & \text{when } \frac{h}{h_s}>1 \end{cases} \tag{5.21}$$

where, l_E: total effective length of structures (m)

l: length of structure (m)

h: height of structure (m)

h_S: standard height of structure (m)

b: breadth of structure (m)

According to Regulation 37, when the effective length of superstructures and trunks is 1L, the deduction of freeboard shall be 1070 millimeters for 122m ship's Length and above. When the effective length is less than 1L, the deduction shall be a percentage obtained from Table 37.1 (linear interpolation if needed). The correction factor of deckhouses and superstructures was calculated by the equation:

$$FB7=1070\cdot y \tag{5.22}$$

where, y: percentage of deduction

5.4.7 Correction for Sheer (FB8)

The freeboard is corrected for sheer according to Regulation 38. There are two kinds of sheer: the standard sheer profile (M_S) and the normal sheer (M_N), both measured in millimeters (mm). Usually, the containerships do not have sheer, due to the fact that a flat deck is needed for the transfer of containers. For this reason, the standard sheer profile has been assumed equal to zero (M_S=0), so the standard length of sheer (S_1) equals zero. The normal sheer was calculated by the equation:

$$M_N=12.5063\cdot\left(\frac{L}{3}+10\right) \tag{5.23}$$

The corrected factor was calculated by the equation:

$$FB8=(M_N-M_S)\cdot\left(0.75-\frac{S_1}{2L}\right) \tag{5.24}$$

where, the sheer and freeboard parameters are measured in millimeters (mm), and the length parameters in meters (m).

5.4.8 Summer Freeboard and Load Line Draught

All the freeboard factors were measured in millimeters (mm), except the FB5 term which is a multiplier and a dimensionless number. The total summer freeboard (FB_{SUMMER}) was estimated by the formula:

$$FB_{SUMMER}=(|FB1|-|FB2|+|FB3|+|FB4|)\cdot|FB5|+|FB6|-|FB7|+|FB8| \tag{5.25}$$

Consequently, the Load Line Draught (T_{ILLC}) was calculated by the equation:

$$T_{ILLC}=D_f-FB_{SUMMER} \tag{5.26}$$

5.5 Deadweight Analysis

During this stage, the analysis of the deadweight takes place. As the Trim and Stability Booklet of the case study vessel A was available, an overview of the various weight categories presents how weights like crew, stores, oil, fresh water and provisions are distributed throughout the ship. However, the Trim and Stability Booklet of the case study vessel B was not found. For this reason, the deadweight analysis was made only for case study vessel A.

As mentioned above, the objective of the Thesis is to investigate the possible changes of the main dimensions of a vessel without affecting the TEU capacity. For this reason, constant Deadweight (DWT) has been assumed. However, the distribution of weights, that constitute the DWT, is necessary for the calculations of initial stability (see Section 5.6). This enables a better estimation of the mass centers of the various DWT components, of the influence of individual weight elements on the arrangement of spaces of the vessel (e.g., tank spaces for fuel, ballast, etc.), as well as of the overall ship design and performance. The DWT is defined as follows:

$$DWT=W_{PL}+W_F+W_{PR}+W_P+W_{CR}+W_B \tag{5.27}$$

where, W_{PL}: payload (or cargo) weight (t)

W_F: weight of fuels, including the weight of lubricants (t)

W_{PR}: weight of provisions and water (t)

W_P: weight of passages and their baggage (t)

W_{CR}: weight of crew and their baggage (t)

W_B: weight of nonpermanent ballast (water), for a specified draught and satisfactory stability and trim.

For case study vessel A, the necessary information of these individual weights is listed in compartments tables of the Trim and Stability Booklet. The weight, the mass center and the free surface moment are provided in the compartment table. Each compartment table refers to a specific loading condition. The DWT analysis was made for the Full Load Departure (FLD) condition, which is achieved when the cargo and the consumables are in their maximum capacity.

The basic idea of the analysis was based on the introduction of a divergence factor, λ_{DWT}. This can be achieved, due to the similarity of the case study vessel with the proposed ones. The factor takes into account the main dimensions of the vessels and is estimated by:

$$\lambda_{DWT}=\frac{L_1 \cdot B_1 \cdot D_1}{L_0 \cdot B_0 \cdot D_0} \tag{5.28}$$

where, L_0, B_0, D_0: main dimensions of the case study vessel (m)

L_1, B_1, D_1: main dimensions of the proposed case vessel (m)

The desired results of the individual weights of the proposed cases vessels were obtained by multiplying the weights of the case study ship by the divergence factor, λ_{DWT}. The procedure's requested weight was the payload. According to the equation (5.27), all the individual weights are known, except the payload one. This provides the opportunity to estimate a distribution index (γ_{homo}), which describes how the cargo weight is distributed in the containers (t/TEU). This index refers to a homogeneous loading; all the containers transfer the same weight.

However, the weight calculations were verified by empirical methods used mostly in the early stages of ship design and are presented in the literature (Papanikolaou, 2014). For this purpose, some elements on which most of the related verification calculations were based have to be outlined.

5.5.1 Weight of fuels (W_F) (including the weight of lubricants)

The required fuel is calculated for a round trip from/to the departure/replenishment port (without refueling) by the following formula:

$$W_{F1}=C\cdot\left(P_{B,1}\cdot b_1\cdot t_1+\frac{P_{B,2}\cdot b_2\cdot t_2}{n_E}\right)10^{-6} \tag{5.29}$$

where, W_{F1}: weight of fuel (t)

$P_{B,1}$: required power of main engine (depending on speed and operating conditions) (kW)

$P_{B,2}$: average required power of electrical generators (kW)

t_1: time of a roundtrip voyage (hr) based on the service speed and operating range = range(nm)/service speed(kn)

t_2: operating time of electric generators (hr) = t_1 + time at port

b_1: specific consumption of the main engine (gr/kWh)

b_2: specific consumption of auxiliary engines for electric generators (gr/kWh)

n_E: average efficiency of electric generator units

C: margin reserve (C=1.4)

The source of all the above necessary data were taken from the engine manufacturers' project guides. The time parameter t_1 was considered constant with the case study vessel. The time at port was calculated. The procedure of calculation is described in Chapter 6.

The weight of the lubricants corresponds approximately to 3–5 % of the fuel weight (diesel engines). For this reason, an average of 4 % was taken.

$$W_{F2}=0.04\cdot W_{F1} \tag{5.30}$$

Consequently,

$$W_F=W_{F1}+W_{F2} \tag{5.31}$$

5.5.2 Provisions weights (W_{PR})

This weight group is distinguished in fresh water supply (drinking and cleaning) and food. The drinking water per person, per day was considered as 12 kg and the cleaning water as 200 kg per person, per day, due to bathtubs in accommodation.

The weight of supplies/food was estimated roughly at 16 kg per man, per day. These weights concern not only daily consumption but also the reserve for delays of voyage, deterioration of food, and delays of supply.

The number of crew members has been assumed constant in all cases.

5.5.3 Weight of Crew and Passenger effects (W_{CR}, W_P)

An approximate weight of 75 kg per person has been assumed. The luggage of the crew members was estimated as 60 kg per person due to their long stay on the vessel.

5.5.4 Weight of Ballast water (W_B)

According to the literature (Papanikolaou, 2014), it should be considered that for a well-designed cargo ship, in the design load condition, ballast water should not be necessary. Exceptions to the rule are the containerships, especially when in the full load/design condition they are expected to carry many containers on deck (causing a high center of ship's mass). This leads to a significant amount of ballast in the full load/design condition, to ensure adequate GM; consequently, for a given DWT, the overall payload capacity decreases. Recent containership design developments and ship design optimizations/innovations, however, look for minimum ballast (zero ballast ships). There is no existence of empirical formula. For this reason, this group weight was calculated with the divergence factor λ_{DWT}.

5.6 Initial Stability

One of the most important steps in the preliminary ship design stage is the verification/control of the ship's stability for the ship under consideration.

In the preliminary design stage it is sufficient to examine the intact[i] stability for small inclination angles (initial stability), which is essentially the control of the adequacy of the metacentric height (GM). The stability control is complemented in the next steps of the design by examining the ship's stability curves (stability for large inclination angles); the latter requires an accurate knowledge of the ship's hull geometry that is not available in the present stage of design. In later stages of ship design, the ship's damage[ii] stability also needs to be verified/examined against set damage stability criteria.

The metacentric height derives as the difference between the ship's form and weight stability:

$$GM = KM - KG \tag{5.32}$$

where, KG: the vertical position of the mass center of the vessel (m)

KM: the vertical position of the (transverse) metacenter (m), and calculated by:

$$KM = KB + BM_t \tag{5.33}$$

where, KB: the vertical position of the center of buoyancy (m)

BM_t: the vertical distance of metacenter from the initial center of buoyancy (transverse metacentric radius) (m)

There are no Regulations to limit the GM. However, high GM values ensure satisfactory stability and safety for the ship, preventing capsizing only if they are accompanied by a sufficient range of positive restoring arm curve for large inclination angles; it should be noted, that large GM values trigger intense roll motions (parametric rolling) and transverse accelerations on the ship's deck (and higher positions), in view of the relationship:

$$T_{roll} \propto B/\sqrt{GM} \tag{5.34}$$

---

[i] Intact stability: the stability of the ship assuming her buoyant hull intact.

[ii] Damage stability: the stability of the ship in case of loss of her watertight integrity.

where, T_{roll}: natural roll period of the ship (sec)

For large values of GM, that is, small roll period, the resultant transverse acceleration on the ship's deck (and higher positions) in resonance situation (i.e., for wave excitation period close to the ship's natural roll period), becomes particularly intense resulting in nausea or injuries of passengers and crew as well as the shift or damage of higher up stacked cargo. Thus, it is recommended that the GM values should not be unreasonably high, but certainly, in any case, regardless of the type and size of the ship, they should not be less than about 0.30–0.35m in departure and design loading condition.

The basic idea of initial stability calculation is to estimate the basic elements (KG, KB, KM) for the case study vessel and then transit to the proposed cases by correction factors. Due to the necessity of the weight factors that were described in Deadweight Analysis (Section 5.5), the initial stability procedure was made only for the case study vessel A. Furthermore, the analysis was made for both at Full Load Departure (FLD) and Full Load Arrival (FLA)[i] condition. The procedure is described below.

5.6.1 Calculation of vertical center of gravity (KG)

At this point, the KG of the vessel has to be determined. To achieve this, the KG of each weight group is needed. The weight groups are distinguished in Lightship, Cargo, Consumables and Constants. In order to calculate the vessel's KG, all the total transverse moments of the total weights are summed up and divided with the total of the weights. The same idea was used for the calculation of the vessel's longitudinal center of gravity (LCG). The procedure is, more clearly, presented in the following tables:

Table 5.1: Calculating KG and LCG of DWT.

Group (1)	**Weight (t) (2)**	**KG (m) (3)**	**M_T (tm) (4)=(2)·(3)**	**LCG (m) (5)**	**M_L (tm) (6)=(2)·(5)**
Cargo					
Consumables					
Constants					
Total=DWT	A	C=B/A	B	E=D/A	D

where, M_T: the transverse moment (tm)

M_L: the longitudinal moment (tm)

The elements of columns four (4) and six (6) are calculated as the product of the elements of columns two (2), three (3) and five (5) respectively. The numbers A, B and D are the totals of columns two (2), four (4) and six (6) respectively. With these numbers known, the numbers C and E are calculated.

[i] FLA: Cargo at maximum capacity, consumables at 10% capacity and constants at their normal values

Table 5.2: Calculating vessel's KG and LCG.

Group (1)	Weight (t) (2)	KG (m) (3)	M_T (tm) (4)=(2)·(3)	LCG (m) (5)	M_L (tm) (6)=(2)·(5)
DWT	A	C	B	E	D
LS					
Displacement	F	H=G/F	G	J=I/F	I

The idea of the calculation on Table 5.2 is similar to those of Table 5.1. The numbers H and J are the requested magnitudes (KG, LGG).

However, the KG (column 3) and the LCG (column 5) of the individual weight groups have to be estimated. For all the weight groups, except the cargo one, the estimations were made by the introduction of factors λ_{KG} and λ_{LCG}.

$$\lambda_{KG}=\frac{KG}{D} \tag{5.35}$$

$$\lambda_{LCG}=\frac{LCG}{L} \tag{5.36}$$

For each weight group, these factors were calculated for the case study vessel and were assumed to remain constant in the proposed cases.

Exceptions to this procedure were the cargo weights, due to the geometry nature of the containerships. The cargo's KG and LCG was calculated by the developed tool, which is described in Chapter 6. The shape of the vessels and the geometry of the containers provide the opportunity to calculate the mass center of the cargo's area by using simple equations.

5.6.2 Calculation of vertical center of buoyancy (KB)

There are many empirical formulas to estimate the vertical position of the center of buoyancy (KB). However, the non-compatibility with this kind and size of vessels have been considered. In order to achieve a more accurate estimation, the divergence factor λ_{KB} has been introduced.

$$\lambda_{KB}=\frac{KB}{T} \tag{5.37}$$

The factor was calculated for the case study vessel A and was assumed to remain constant in the proposed cases.

5.6.3 Calculation of transverse metacentric radius (BM)

The transverse metacentric radius (BM_T) is the vertical distance between the center of buoyancy and the metacenter. This distance is termed a radius because for small heel angles, the locus of successive centers of buoyancy approximates a circular arc, with the transverse metacenter as its center. Metacentric radius is equal to the moment of inertia of the waterplane about its longitudinal centerline (transverse moment of inertia, I_T) divided by the volume of displacement (∇):

$$BM_T=\frac{I_T}{\nabla} \tag{5.38}$$

If the waterplane shape can be accurately defined, the moment of inertia can be determined by numerical integration. However, at this design phase this was not possible.

For a rectangular waterplane, the transverse moment of inertia, measured in m^4 is calculated as:

$$I_T=\frac{L\cdot B^3}{12} \tag{5.39}$$

According to this, the transverse moment of inertia of most ships' waterplanes can be approximated by (Perumpalath, 2004):

$$I_T=C_{IT}\cdot\frac{L\cdot B^3}{12} \tag{5.40}$$

where, C_{IT}: the transverse inertia coefficient, which was calculated for the case study vessel and was assumed to remain constant in the proposed cases.

The volume of displacement was calculated by the equation:

$$\nabla=C_B\cdot L\cdot B\cdot T \tag{5.41}$$

With all the necessary magnitudes known, the vertical position of the (transverse) metacenter (KM) is calculated by using the equation (5.33) and the metacentric height from the equation (5.32).

5.7 Resistance

Ship resistance is defined as the force required to tow the ship in calm water at a constant speed. For this reason, resistance is a very essential parameter for the engine and service speed selection of the vessel.

There are many methods calculating resistance in design stages. The most accurate one is by model experiments. In order to minimize the range of experimental runs the Computational Fluid Dynamics (CFD) simulation is made. However, this method can be applied in later design stages. At the preliminary design stage, there are various statistical methods and systematic series of resistance calculations providing satisfactory results. An example of an applicable statistical method for containerships is the Holtrop and Mennen’s Method. Furthermore applicable systematic series for containerships are:: Lap-Keller, BSRA, FORMDATA (Schneekluth & Bertram, 1998).

The Lap-Keller method does not take into account the influence of bulb and can be applied for a specific range of input values:

$$0.4 \leq \sqrt{\frac{V}{C_P \cdot L_{BP}}} \leq 1.5 \tag{5.42}$$

where, V: vessel's service speed (m/sec)

C_P: prismatic coefficient

L_{BP}: length between perpendiculars (m)

The investigation cases have bulbous bow and do not feature this limitation. For this reason, the Lap-Keller was rejected.

The BSRA method was developed for reference vessels and the final result is expressed by the introduction of correction factors. The method is applied to vessels with beam to draught ratio (B/T) from 2.1 to 3.2 (Ventura). All the proposed cases have greater beam to draught ratios. For this reason, the BSRA method was also rejected.

The FORMDATA combines many methods, and it was not considered suitable for this size and kind of vessels. Hence, it was rejected too.

Moreover, the systematic series are not easily programmed due to the use of factors from diagrams. For study's purposes, the ship resistance calculations were made twelve times. That was an additional reason for the rejection of the systematic series.

On the other hand, Holtrop and Mennen's method is arguably one of the most popular statistical method to estimate resistance and powering of displacement type ships and it can be applied at the preliminary study. Furthermore, the method is the only early design estimate for resistance and propulsion that has adopted the International Towing Tank Conference (ITTC) form factor approach. Since the use of a form factor affects the estimate of the residuary resistance (in this case, wave resistance), the method should not be used without a form factor. It is based on the regression analysis of a vast range of model tests and trial data which give it a wide applicability. Resistance is calculated as a dimensional force. The method also provides formulas to estimate the hull–propeller interaction parameters thrust deduction (t), effective wake fraction (w) and relative rotative efficiency (n_R).

5.7.1 Holtrop and Mennen's Method

In the late 1970s and early 1980s, J. Holtrop and G.G.J. Mennen developed a resistance and propulsion prediction method based on the regression analysis of model tests and trial data of Maritime Research Institute of Netherlands (MARIN), the model basin in Wageningen (Holtrop, A statistical power prediction method, 1978) (Holtrop, An approximate power prediction method, 1982).

The method can be applied in specific ranges of Froude number (Fr), prismatic coefficient (C_P) and length to beam ratio (L/B) respectively. Reasonable estimates can be expected for cases that fit the following conditions (Birk, 2019):

$$Fr \leq 0.45 \tag{5.43}$$

$$0.55 \leq C_P \leq 0.85 \tag{5.44}$$

$$3.9 \leq \frac{L}{B} \leq 9.5 \tag{5.45}$$

However, a greater divergence was expected due to the fact that the present hull forms of Large container vessels are observed with several changes compared to the models used in the Holtrop and Mennen's tests. For this reason, it was considered that the calculations of the hull-propeller interaction were not accurate for these designs, hence they were excluded from the procedure.

According to the method, the total resistance of a ship has been subdivided into (Holtrop, An approximate power prediction method, 1982):

$$R_{Total}=R_F \cdot (1+k)+R_{App}+R_W+R_B+R_{TR}+R_A+R_{AA} \tag{5.46}$$

where, R_F: frictional resistance according to the ITTC 1957 friction formula (kN)

- 1+k: form factor describing the viscous resistance of the hull form in relation to R_F
- R_{App}: resistance of appendages (kN)
- R_W: wave-making and wave-breaking resistance (kN)
- R_B: additional pressure resistance of bulbous bow near the water surface (kN)
- R_{TR}: additional pressure resistance of immersed transom stern (kN)
- R_A: model-ship correlation resistance (kN)
- R_{AA}: air resistance (kN)

Resistance components were computed as functions of Froude (Fr) and Reynolds (Re) numbers for the design speed. The Froude and Reynolds numbers were calculated as:

$$Fr=\frac{V}{\sqrt{g \cdot L}} \tag{5.47}$$

$$Re=\frac{V \cdot L}{v} \tag{5.48}$$

where, V: vessel's speed (m/sec)

- g: acceleration due to gravity (m/sec^2)
- L: vessel's length (m)
- v: kinematic viscosity (m^2/sec)

Input to Holtrop and Mennen's method consists of principal dimensions and a few basic hull form parameters. The necessary parameters are listed in the following table:

Table 5.3: Required input parameters for Holtrop and Mennen's method. Source: (Birk, 2019)

Parameter	Symbol	Units	Remarks
Length in waterline	L_{WL}	m	
Molded beam	B	m	
Molded mean draught	T	m	Typically: $T=0.5\cdot(T_F+T_A)$
Molded draught at aft perpendicular	T_A	m	
Molded draught at forward perpendicular	T_F	m	
Volume of displacement (moulded)	∇	m^3	alternatively use the block coefficient as $C_B=\nabla/(B\cdot T\cdot L\cdot_{WL})$
Prismatic Coefficient (based on L_{WL})	C_P	-	Or use $C_P=C_B/C_M$
Mid-ship section Coefficient	C_M	-	
Waterplane area Coefficient	C_{WL}	-	
Longitudinal center of buoyancy	lcb	%	positive forward; with respect to $L_{WL}/2$ in percent of L_{WL}
Transverse area of ship and cargo above waterline	A_{VT}	m^2	projected in direction of vessel's speed
Immersed transom area	A_T	m^2	
Transverse area of bulbous bow	A_{BT}	m^2	measured at forward perpendicular
Height of center of A_{BT} above keel	h_B	m	has to be smaller than $0.6\cdot T$
Stern shape parameter	C_{stern}	-	
Wetted Surface (hull)	S	m^2	
Wetted surface of appendages	S_{app}	m^2	Bilge keels, rudder, etc.
Half angle of waterline entrance	i_e	degrees	
Diameter of bow thruster tunnel	d_{TH}	m	

In early design stages some input parameters were unknown. They initially derived from design formulas or from some assumptions that were made.

The waterline length has been considered equal to the length between perpendiculars (L_{BP}). The longitudinal center of buoyancy was not yet known, and it has been assumed to be located in the same position with the longitudinal center of gravity, which was calculated from the initial stability. The wetted area of the hull was calculated by the proposed formula of the method (Holtrop, An approximate power prediction method, 1982):

$$S=L\cdot(2T+B)\cdot\sqrt{C_M}\left(0.453+0.4425\cdot C_B-0.2862\cdot C_M-0.003467\cdot\frac{B}{T}+0.3696\cdot C_{WL}\right)+2.38\cdot\frac{A_{BT}}{C_B} \quad (5.49)$$

Except for the input parameters, some constants were used for the calculation of the total resistance. These constants were summarized and listed below:

Table 5.4: Constants for Holtrop and Mennen's method.

Constants	Symbol	Unit	Remarks
Acceleration due to gravity	g	m/sec^2	g=9.80665 m/sec^2
Density of sea water at 15°C	ρ	t/m^3	ρ=1.025 t/m^3
Density of air	ρ_{air}	t/m^3	$\rho_{air}=1.225\cdot10^{-3}$ t/m^3
Kinematic Viscosity of sea water at 15°C	v	m^2/sec	v=1.18831·10^{-6} m^2/sec

5.7.1.1 Frictional Resistance (R_F)

The frictional resistance R_F was calculated on the basis of the ITTC 1957 model–ship correlation line coefficient C_F as the resistance of a flat plate with wetted surface S.

$$R_F=\frac{1}{2}\cdot\rho\cdot V^2\cdot S\cdot C_F \quad (5.50)$$

where, V: vessel's speed (m/sec)
C_F: friction coefficient, calculated by

$$C_F=\frac{0.075}{[\log_{10}(Re)-2]^2} \quad (5.51)$$

For the form factor of the hull the following prediction formula was used (Holtrop, A statistical power prediction method, 1978):

$$1+k=0.93+0.487118\cdot c_{14}\left(\frac{B}{L}\right)^{1.06806}\left(\frac{T}{L}\right)^{0.46106}\left(\frac{L}{L_R}\right)^{0.121563}\left(\frac{L^3}{\nabla}\right)^{0.36486}(1-C_P)^{-0.604247} \quad (5.52)$$

where, L_R: run length (m)
c_{14}: coefficient which accounts the stern shape

The run length (L_R) was defined as (Holtrop, A statistical power prediction method, 1978):

$$L_R = L \cdot \left(1 - C_P + \frac{0.06 \cdot C_P \cdot lcb}{4 \cdot C_P - 1}\right) \tag{5.53}$$

The coefficient c_{14} depends on the stern shape coefficient (C_{stern}) for which the following tentative figures can be given:

Aft body shape	C_{stern}
pram with gondola	−25
V-shaped sections	−10
normal sections	0
U-shaped sections	+10

Figure 5. 3: Influence of the aft body shape. Source: (Birk, 2019)

$$c_{14} = 1 + 0.011 \cdot C_{stern} \tag{5.54}$$

The aft body shape of container vessels, commonly, is consisted of normal sections. For this reason, the stern shape coefficient was considered as zero (C_{stern}=0).

5.7.1.2 Appendages Resistance (R_{App})

Appendages mostly affect the viscous resistance. Form factors of appendages must be taken into account for a reasonable estimation. In the figure below, tentative k_2 values are given for streamlined flow-oriented appendages.

Appendage	k_{2i} value
rudder behind skeg	0.2–0.5
rudder behind stern	0.5
twin screw rudder (slender)	1.5
twin screw rudder (thick)	2.5
shaft brackets	2.0–4.0
skeg	0.5–1.0
strut bossing	2.0–3.0
hull bossing	1.0
exposed shafts (angle with buttocks about 10 degrees)	1.0
(angle with buttocks about 20 degrees)	4.0
stabilizer fins	1.8
dome	1.7
bilge keels	0.4

Figure 5.4: Form factors of various appendages. Source: (Birk, 2019)

The equivalent 1+k_2 value for a combination of appendages was determined from (Holtrop, An approximate power prediction method, 1982) as:

$$(1+k_2)_{eq}=\frac{\sum(1+k_2)\cdot S_{app}}{\sum S_{app}} \quad (5.55)$$

The resistance due to a bow thruster tunnel opening was computed according to (Holtrop, An approximate power prediction method, 1982) as:

$$R_{TH}=\rho\cdot V^2\cdot\pi\cdot d_{th}{}^2\cdot C_{BTO} \quad (5.56)$$

where, d_{th}: tunnel diameter (m)

The drag coefficient C_{BTO} for the thruster tunnel takes values between 0.003 and 0.012. The smaller values are for thrusters which are in the cylindrical part of the bulbous bow.

The appendage resistance was calculated as the sum of thruster resistance and all considered appendages (Birk, 2019):

$$R_{App}=\frac{1}{2}\cdot\rho\cdot V^2\cdot(1+k_2)_{eq}\cdot C_F\sum S_{app}+\sum R_{TH} \quad (5.57)$$

For the purpose of the study, only rudder (k_2=0.5) and bilge keels (k_2=0.4) were taken into account. The wetted surface of such kind of appendages was estimated by the roughly calculation of 2.5% of the total wetted surface of the vessel (Politis, 2019). Furthermore, the higher figures of bow thruster opening coefficient (C_{BTO}) were taken into account.

5.7.1.3 Wave Resistance (R_W)

Wave resistance is a function of the Froude number. For the estimation of R_W, Holtrop subdivided the range of Froude numbers into three sections (Holtrop, A statistical power prediction method, 1978):

$$R_W(Fr)=\begin{cases} R_{Wa}(Fr), \ \text{if } Fr \le 0.4 \\ \text{interpolation}, \ \text{if } 0.4 < Fr \le 0.55 \\ R_{Wb}(Fr), \ \text{if } 0.55 < Fr \end{cases} \tag{5.58}$$

Reasonable values of Froude numbers of container vessels are less than 0.4. For this reason, the following description of wave resistance calculation refers to $R_{Wa}(Fr)$ magnitude.

$$R_{Wa}(Fr)=c_1 \cdot c_2 \cdot c_5 \cdot \nabla \cdot \rho \cdot g \cdot \exp\{m_1 \cdot Fr^d + m_4 \cdot \cos(\lambda \cdot Fr^{-2})\} \tag{5.59}$$

with:

$$c_1=2223105 \cdot c_7^{3.78613} \left(\frac{T}{B}\right)^{1.07961} (90-i_e)^{-1.37565} \tag{5.60}$$

$$c_7=\begin{cases} 0.229577 \cdot \left(\frac{B}{L}\right)^{0.33333}, \ \text{when } \frac{B}{L}<0.11 \\ \frac{B}{L}, \ \text{when } 0.11 \le \frac{B}{L} \le 0.25 \\ 0.5-0.0625 \cdot \frac{L}{B}, \ \text{when } \frac{B}{L}<0.25 \end{cases} \tag{5.61}$$

$$c_2=\exp\{-1.89 \cdot \sqrt{c_3}\} \tag{5.62}$$

$$c_3=0.56 \cdot \frac{A_{BT}^{1.5}}{B \cdot T \cdot (0.31 \cdot \sqrt{A_{BT}}+T_F-h_B)} \tag{5.63}$$

$$c_5=1-0.8 \cdot \frac{A_T}{B \cdot T \cdot C_M} \tag{5.64}$$

Expressions c_2 and c_3 are parameters which account for the reduction of the wave resistance due to the action of bulbous bow, where h_B is the vertical position of the center of the transverse area (A_{BT}) above the keel line. h_B has been roughly estimated as: $h_B=0.6 \cdot T_F$. Similarly, c_5 expresses the influence of a transom stern on the wave resistance. In the expression A_T represents the immersed part of the transverse area of the transom at zero speed.

The transverse area A_{BT} above keel line and the immersed part of the transverse area of the transverse (A_T) has been assumed equal to those of case study vessel for each proposed case.

In the formula for the wave resistance, Fr is the Froude number based on the waterline length L_{WL}. The other parameters were determined from:

$$\lambda=\begin{cases}1.446\cdot C_P-0.03\cdot\frac{L}{B}, \text{ when } \frac{L}{B}\leq 12\\ 1.446\cdot C_P-0.36, \text{ when } \frac{L}{B}>12\end{cases} \tag{5.65}$$

$$m_1=0.0140407\cdot\frac{L}{T}-1.75254\cdot\left(\frac{\nabla^{\frac{1}{3}}}{L}\right)-4.79323\cdot\frac{B}{L}-c_{16} \tag{5.66}$$

$$c_{16}=\begin{cases}8.07981\cdot C_P-13.8673\cdot C_P^2+6.984388\cdot C_P^3, \text{ when } C_P\leq 0.8\\ 1.73014-0.7067\cdot C_P, \text{ when } C_P>0.8\end{cases} \tag{5.67}$$

$$m_4=c_{15}\cdot 0.4\cdot\exp\{-0.034\cdot Fr^{-3.29}\} \tag{5.68}$$

$$c_{15}=\begin{cases}-1.69385, \text{ when } \frac{L^3}{\nabla}<512\\ -1.69385+\frac{\left(\frac{L}{\nabla^{\frac{1}{3}}}-8\right)}{2.36}, \text{ when } 512\leq\frac{L^3}{\nabla}\leq 1726.91\\ 0, \text{ when } 1726.91<\frac{L^3}{\nabla}\end{cases} \tag{5.69}$$

$$d=-0.9 \tag{5.70}$$

The half angle of entrance i_e is the angle of the water at the bow in degrees with reference to the center plane but neglecting the local shape at the stern, and it was estimated from the following formula:

$$i_e=1+89\cdot\exp\{-\left(\frac{L}{B}\right)^{0.80856}(1-C_{WL})^{0.30484}(1-C_P-0.0225\cdot lcb)^{0.6367}\left(\frac{L_R}{B}\right)^{0.34574}\left(100\frac{\nabla}{L^3}\right)^{0.16302}\} \tag{5.71}$$

The half angle of entrance sometimes can result in negative values.

5.7.1.4 Additional pressure resistance of bulbous bow near the water surface (R_B)

The additional resistance due to the presence of a bulbous bow near the surface was determined from (Holtrop, An approximate power prediction method, 1982):

$$R_B=0.11\cdot \exp\{-3\cdot P_B^{-2}\}\frac{Fr_i^3\cdot A_{BT}^{1.5}\cdot \rho\cdot g}{1+Fr_i^2} \quad (5.72)$$

where, PB: measure for the emergence of the bow and given by:

$$P_B=\frac{0.56\cdot\sqrt{A_{BT}}}{T_F-1.5\cdot h_B} \quad (5.73)$$

Fri: Froude number based on the bulbous bow immersion, given by:

$$Fr_i=\frac{V}{\sqrt{g\cdot(T_F-h_B-0.25\cdot\sqrt{A_{BT}})+0.15\cdot U^2}} \quad (5.74)$$

5.7.1.5 Additional pressure resistance of immersed transom stern (R_{TR})

In a similar way, the additional pressure resistance due to the immersed transom was determined (Holtrop, An approximate power prediction method, 1982) as:

$$R_{TR}=\frac{1}{2}\cdot\rho\cdot V^2\cdot A_T\cdot c_6 \quad (5.75)$$

The coefficient c_6 has been related to the Froude number based on the transom immersion:

$$c_6=\begin{cases}0.2\cdot(1-0.2\cdot Fr_T)\text{, when } Fr_T<5\\ 0\text{, when } Fr_T\geq 5\end{cases} \quad (5.76)$$

The Froude number based on the transom immersion is given by:

$$Fr_T=\frac{V}{\sqrt{2\cdot g\cdot A_T/(B+B\cdot C_{WL})}} \quad (5.77)$$

5.7.1.6 Model-ship correlation resistance (R_A)

The correlation allowance considered here includes effects of roughness and additional phenomena not captured in other resistance components. Note that correlation allowance and roughness effects have been separated in the current ITTC performance prediction procedure. First, the additional coefficient c_4, was given by:

$$c_4=\begin{cases}\frac{T_F}{L}, \text{ when } \frac{T_F}{L}\leq 0.04\\ 0.04, \text{ when } \frac{T_F}{L}>0.04\end{cases} \tag{5.78}$$

Then, the correlation allowance coefficient follows in the equation below:

$$C_A=0.00546\cdot(L_{WL}+100)^{0.16}-0.002+0.003\sqrt{\frac{L_{WL}}{7.5}}\cdot C_B^4\cdot c_2\cdot(0.04-c_4) \tag{5.79}$$

Holtrop (1988) states that with modern hull coatings, values of C_A may be achieved that are $0.1\cdot 10^{-3}$ lower than predicted. However, this will not make a significant difference for early design estimations. The effect of surface roughness higher than the standard value of k_S= 150 μm may be estimated by an addition to C_A.

$$\Delta C_A=\begin{cases}0, \text{ if } k_S=150\mu m\\ \frac{0.105\cdot k_S^{1/3}-0.005579}{L^{1/3}}, \text{ if } k_S>150\mu m\end{cases} \tag{5.80}$$

It is noted that the magnitudes k_S and L_{WL} have to be entered in meters to obtain correct results. The correlation resistance was, then, given by (Birk, 2019):

$$R_A=\frac{1}{2}\cdot\rho\cdot V^2\cdot(C_A+\Delta C_A)\cdot[S+\sum S_{app}] \tag{5.81}$$

5.7.1.7 Air Resistance (R_{AA})

The wind forces and moments acting on the ship hull, are estimated by the use of the empirical formulas proposed by Blendermann (Blendermann, Die Windkräfte am Schiff, 1986):

$$X_w=0.5\cdot\rho_{air}\cdot C_x\cdot A_{VT}\cdot V_{res}^2 \tag{5.82}$$

$$Y_w=0.5\cdot\rho_{air}\cdot C_Y\cdot A_{VL}\cdot V_{res}^2 \tag{5.83}$$

$$K_w=0.5\cdot\rho_{air}\cdot C_K\cdot({A_{VL}}^2/L)\cdot V_{res}^2 \tag{5.84}$$

$$N_w=0.5\cdot\rho_{air}\cdot C_N\cdot A_{VL}\cdot L\cdot V_{res}^2 \tag{5.85}$$

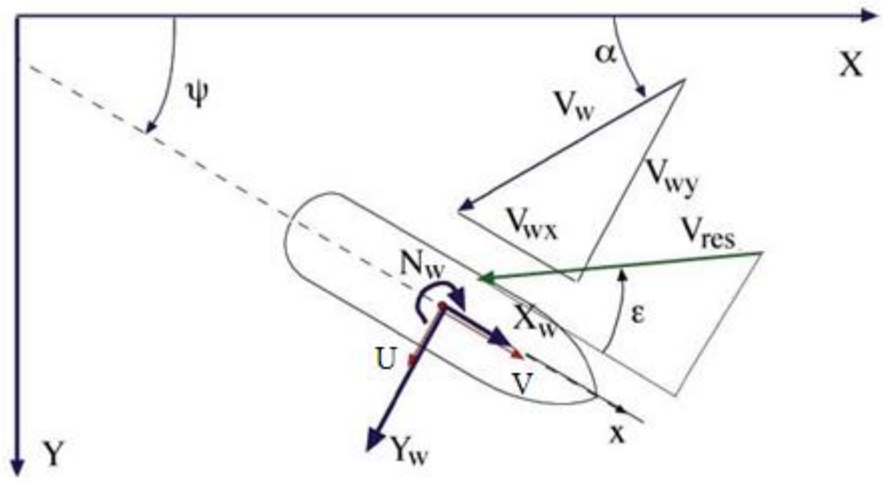

Figure 5.5: Air velocity components and aerodynamic force/ moment vectors acting on the ship.

where, V_{res}: the resultant wind velocity acting on the ship (m/sec), and given by:

$$V_{res}=\sqrt{(V_{wx}+V)^2+\left(V_{wy}+U\right)^2} \tag{5.86}$$

A_{VT}: Transverse area of ship and cargo above waterline (m^2) and approximated by:

$$A_{VT}=(D\text{-}T)\cdot B+(con_h\cdot tiers_d)\cdot B \tag{5.87}$$

Where D is the depth of the vessel (m), T is the molded draught (m), B is the molded beam (m), con_h is the height of a single container (con_h=2.591m) and $tiers_d$ is the maximum number of above deck container tiers.

A_{VL}: Longitudinal area of ship and cargo above waterline (m^2)

C_X, C_Y, C_K, C_N: dimensionless coefficients which are functions of above water ship's profile

These coefficients are obtained from published, model experimental data for each specific vessel type; e.g., they were given by Blendermann (Blendermann, Parameter identification of wind loads on ships, 1994) in tabulated form as a function of the relative wind angle for various ship types.

For the calculation of the total resistance only the impact of the longitudinal force of wind (X_W) was examined. Moreover, it has been considered that the angle of wind equals to zero degrees (head wind) and affects only the surge direction. The resultant wind velocity acting on the ship was determined as:

$$V_{res}=|V_{wx}-V| \tag{5.88}$$

For study purposes, it has been assumed that the wind was characterized with Beaufort Number 2 (B=2), so this results to $V_{wx}=0.836\cdot B^{1.5}=0.836\cdot 21.5$ m/sec=2.36m/sec.

The C_X coefficient was calculated according to the following diagram, which was published by Blendermann.

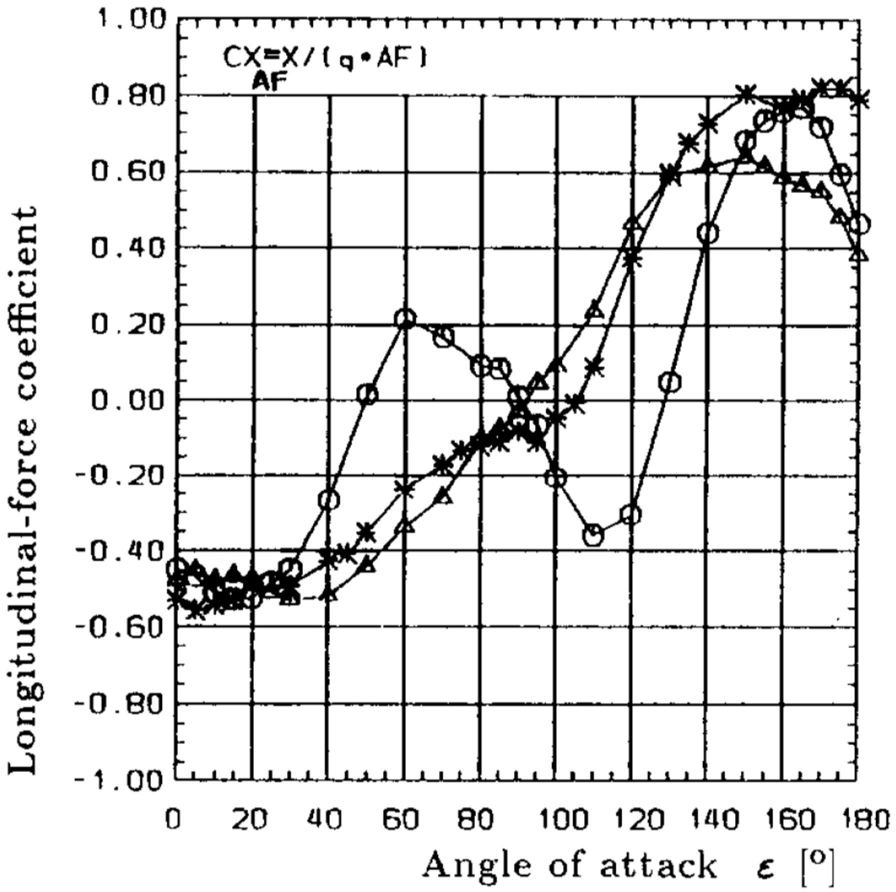

Figure 5.6: Relation between longitudinal force coefficient and angle of attack. Source: (Blendermann, Parameter identification of wind loads on ships, 1994)

Negative values of C_X coefficient indicate that the X_W force is in the opposite direction than the one shown, shown in Figure 5.5. For head wind, the C_X coefficient is equal to C_X=-0.5.

5.7.1.8 Propulsion Calculation

As mentioned above, the hull-propeller interaction was not accurate for these designs and they were excluded from the procedure. An approximate calculation of propulsive power was made by introducing a divergence factor λ_{SHP}. First, the Effective Horse Power (EHP), measured in kilowatts (kW), was determined as:

$$EHP=0.735499\cdot\frac{R_T\cdot V}{75} \qquad (5.89)$$

where, R_T: total resistance (kp)

The Shaft Horse Power (SHP) is related to the Effective Horse Power (EHP) by the equation:

$$\frac{EHP}{SHP} = \text{P.C. (Propulsive Coefficient)} \tag{5.90}$$

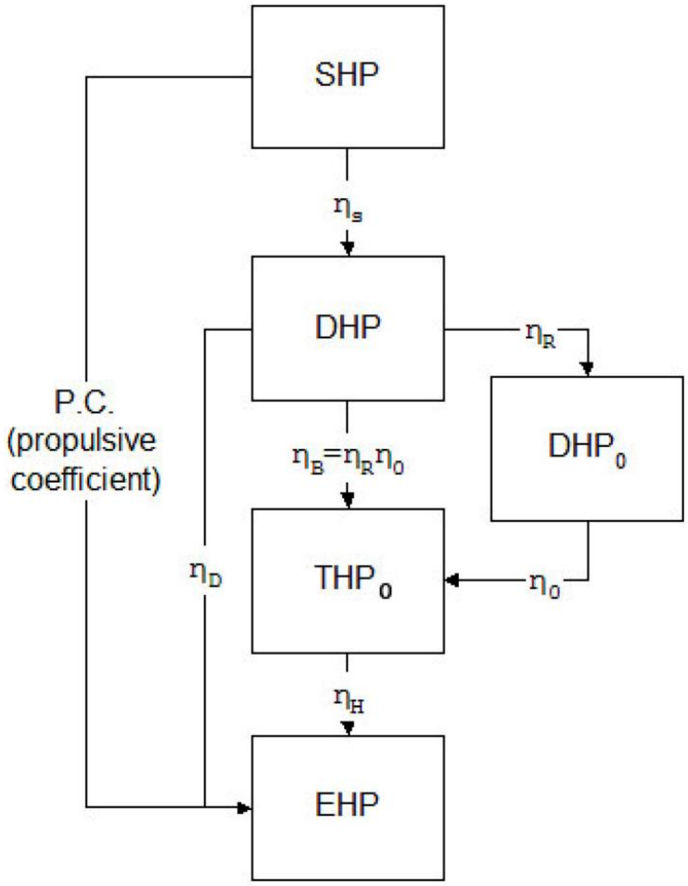

Figure 5.7: Flow Chart of propulsion power. Source: (Politis, 2019)

To simplify the calculations, a 65% efficiency of the propulsive system (P.C.=0.65) was chosen. Then, the divergence factor was included in the calculations. This factor was estimated for the case study vessels and remained constant for all proposed cases. The factor λ_{SHP} was determined as:

$$\lambda_{SHP} = \frac{SHP_{real}}{SHP_{calc}} \tag{5.91}$$

For each case study vessel, the parameter SHP_{real} refers to the Max Continuous Rating (MCR). For the proposed cases, the SHP_{real} is the requested magnitude.

For the sake of completeness of the Thesis, the SHP_{real} calculation methodology is described below (without the assumption of P.C.).

First, the propeller properties have to be chosen for each case (Propeller Diameter, Pitch, number of blades, expanded ratio). A reasonable assumption would be, the proposed cases to have the same propeller with the case study vessel. Then, the hull–propeller interaction parameters, thrust deduction (t), effective wake fraction (w), and relative rotative efficiency (η_R) have to be estimated, either using the Holtrop and Mennen's method or empirical formulas. With total resistance and thrust deduction known, the thrust force can be calculated (T) by:

$$T=\frac{R_T}{1-t} \tag{5.92}$$

According to the relevant literature (Politis, 2019), at Table 10, page 4-315, column 4, with the propeller diameter (D), pitch ratio(P/D), number of blades(z), expanded ratio (A_E/A_O), ship speed (V) and thrust force (T) known, the factor C can be calculated by:

$$C=\frac{T}{\rho\cdot V^2\cdot D^2} \tag{5.93}$$

The parabola $k_T=CJ^2$ can be plotted on the corresponding Wagenigen B-series propeller diagram and the intersection with the k_T-J curve of the propeller can be detected. The dimensional thrust coefficient (k_T), the dimensional torque coefficient (k_Q) and the dimensional advance coefficient (J) can be calculated from the same diagram. Consequently, all the necessary data for the calculation of Propulsive coefficient are known:

$$P.C.=n_H\cdot n_o\cdot n_R\cdot n_S \tag{5.94}$$

where, η_H: hull efficiency, given by:

$$\eta_H=\frac{1-t}{1-w} \tag{5.95}$$

η_o: open water efficiency, given by:

$$\eta_O=\frac{J\cdot k_T}{2\cdot\pi\cdot k_Q} \tag{5.96}$$

η_R: relative rotative efficiency (calculated above)
η_S: shaft efficiency (assumed 98%)

5.8 EEDI

The ship "Energy Efficiency Design Index (EEDI)" has been formulated by the IMO Marine Environment Protection Committee (MEPC) as a measure of the CO_2 emission performance of ships. The EEDI requires a specified energy efficiency that could be primarily expressed by fuel consumption per capacity mile (e.g. ton mile) for different ship types and size. With the level being tightened over time, the EEDI stimulates continued technical development of all the components influencing the energy efficiency of a ship. The EEDI factor of a particular ship is calculated based on her characteristics at the building stage, incorporating parameters including ship capacity, engine power and fuel consumption. The indented application of this index was to stimulate innovation and technical development of all elements influencing the energy efficiency of a ship from its design phase. For each new ship the attained EEDI shall be considered as follows:

$$\text{Attained EEDI} \leq \text{Required EEDI}$$

where,

Attained EEDI: The actual EEDI of the ship, as calculated by the shipyard and verified by a recognized organization ($grCO_2$/t-nm)

Required EEDI: The regulatory limit of the ship's EEDI, which the actual EEDI must not exceed ($grCO_2$/t-nm)

5.8.1 Required EEDI calculation

The reference EEDI (reference line value - RLV) and the reduction factor X are established for each ship type and are used for the determination of the required EEDI. A reference line is established as a curve representing an average index value fitted on a set of individual index values for a defined group of ships. The IMO's MEPC has calculated EEDI reference lines, which denote the maximum allowable EEDI values that newly constructed ships constructed, can have, in order to be issued an International Energy Efficiency Certificate. The reference line values – RLV of a container carrier was calculated as follows (Borkowski et.al, 2012):

$$RLV = a \cdot b^{-c} \tag{5.97}$$

where, a and c: constants agreed for each ship type and included in the regulation

b: ship capacity (t)

The parameters "a" and "c" were determined from the following table of the regulation.

Table 5.5: Parameters a and c for Reference EEDI. Source: (Bazari, 2016)

Ship Type	a	c
Bulk Carrier	961.79	0.477
Gas Carrier	1120.00	0.456
Tanker	1218.80	0.488
Container Vessel	174.22	0.201
General Cargo Ship	107.48	0.216
Refrigerated Cargo Carrier	227.01	0.244
Combination Carrier	1219.00	0.488

The next step was to establish the reduction factor (X) for the ship. This is dependent on year of ship built and is specified within the regulation. The following table shows the reduction factors for typical containerships.

Table 5.6: Reduction factors (in percentage) for the EEDI relative to the EEDI Reference Line. Source: (MEPC.1-Circ.866, 2017)

Ship Type	Size	Phase 0 1Jan2013 - 31Dec2014	Phase 1 1Jan2015 - 31Dec2019	Phase 2 1Jan2020 - 31Dec2024	Phase 3 1Jan2025 and onwards
Container vessel	15000 DWT and above	0	10	20	30
	10000-15000 DWT	n/a	0-10	0-20	0-30

The proposed cases are examined to operate in the next years. The 30% reduction was chosen for the required EEDI calculation.

Having established the Reference EEDI and X, the Required EEDI was calculated from the following equation:

$$\text{Required EEDI}=\left(1-\frac{X}{100}\right)\cdot RLV \tag{5.98}$$

5.8.2 Attained EEDI calculation

The Attained EEDI is the actual value of EEDI for a ship and represents the amount of CO_2 generated by her while doing one ton-mile of transport work. The value was calculated based on the following formula (Bazari, 2016):

$$\text{Attained EEDI}=\frac{\left(\prod_{j=1}^{n} f_j\right)\cdot\left(\sum_{i=1}^{nME} P_{ME(i)}\cdot C_{FME(i)}\cdot SFC_{ME(i)}\right)+\left(P_{AE}\cdot C_{FAE}\cdot SFC_{AE}\right)}{f_i\cdot f_c\cdot DWT\cdot f_w\cdot V}+$$
$$+\frac{\left(\left(\prod_{j=1}^{n} f_j \sum_{i=1}^{nPTI} P_{PTI(i)}-\sum_{i=1}^{neff} f_{eff(i)}\cdot P_{AEeff(i)}\right)C_{FAE}SFC_{AE}\right)-\left(\sum_{i=1}^{neff} f_{eff(i)}P_{eff(i)}C_{FME}SFC_{ME}\right)}{f_i\cdot f_c\cdot(70\%DWT)\cdot f_w\cdot V} \tag{5.99}$$

where, f_j: Correction factor for ship specific design features (e.g. ice-class ships)

n_{ME}: Number of main engines

P_{ME}: Ship propulsion power that is 75% of main engine Maximum Continuous Rating (MCR) or shaft motor (where applicable); also taking into account the shaft generator. This will be influenced by alternative propulsion configurations (kW)

C_{FME}: Carbon factor for fuel for main engines ($grCO_2$/grfuel)

SFC_{ME}: Specific fuel consumption for main engines as per NOx certification values (gr/kWh)

P_{AE}: Ship auxiliary power requirements at normal sea going conditions (kW)

CF_{AE}: Carbon factor for fuel for auxiliary engines ($grCO_2$/grfuel)

SFC_{AE}: Specific fuel consumption for auxiliary engines as per NO_x certification values (gr/kWh)

n_{PTI}: Number of power take-in systems (e.g. shaft motors)

P_{PTI}: 75% of installed power for each power take-in system (kW)

n_{eff}: Number of innovative technologies

f_{eff}: Correction factor for availability of innovative technologies

P_{AEeff}: Auxiliary power reduction due to use of innovative electric power generation technologies (kW)

P_{eff}: 75% of installed power for each innovative technology that contributes to propulsion (kW)

f_i: Correction factor for capacity of ships with technical elements that influence ship capacity

f_c: Correction factor for capacity of ships with alternative cargo types that impact the deadweight-capacity relationship

DWT: For containerships, 70% of the deadweight (DWT) should be used as capacity (t)

f_w: Correction factor for speed reduction due to representative sea conditions

V: Reference ship speed attained at propulsion power equal to P_{ME} and under calm sea and deep-water operation at summer load line draught (kn)

The items that primarily influence EEDI are (Bazari, 2016):

- Main engine and energy needed for propulsion; this represented by the first term in the nominator of the formula.
- Auxiliary power requirements of the ship; this is represented by the second term in the nominator.
- Any innovative power (electric) generation devices on board, such as electricity from waste heat recovery or solar power. These are represented by the third term in the nominator.
- Innovative technologies that provide mechanical power for ship propulsion such as wind power (sails, kites, etc.). This is the last term in the nominator.
- In the denominator of the formula, ship capacity and ship speed are represented and together they give the value of transport work.

No innovative power generators or innovative technologies were found for the case study vessels. For this reason, the third and the fourth nominators of the formula were excluded from the calculation. According to MEPC 1-Circ. 866, if no necessity of correction factors is granted, they should be assumed to be one (1.0). It has been assumed that the auxiliary engines' power is equal to the 50% of the ones installed. Furthermore, the carbon content factors (C_F) were determined according to MEPC 1-Circ.866, and they correspond to the fuel used. For Very Low Sulphur Fuel Oil (VLSFO) and Low Sulphur Marine Gas Oil (LSMGO), the carbon content factor is, respectively, as follows (MEPC.1-Circ.866, 2017):

- C_F(VLSFO)= 3.114 gr-CO_2/gr-Fuel
- C_F(LSMGO)= 3.206 gr-CO_2/gr-Fuel

5.8.3 *Estimated Index Value (EIV) calculation*

An estimated index value (EIV) for each ship was calculated using several constant assumptions, namely:

- the carbon emission factor for all engines and dependent to fuel oil grade, i.e. C_F = 3.1144 grCO_2/grfuel – for RM heavy fuel oil,
- the specific fuel consumption for main engine types, i.e. SFC = 190 gr/kWh,
- the main engine power – $P_{ME(i)}$ is 75% of the total installed power (MCR),
- the specific fuel consumption for all auxiliary engines, i.e. SFC = 215 gr/kWh,
- the auxiliary engine power – $P_{AE(i)}$ is 50% of the total installed auxiliary power.

For containerships, 70% of the deadweight (70% DWT) is used as capacity for calculating the estimated index value (EIV) for each containership as follows (MEPC.1-Circ.866, 2017):

$$EIV = 3.1144 \cdot \frac{190 \cdot \sum_{i=1}^{nME} P_{MEi} + 215 \cdot P_{AE}}{(70\%DWT) \cdot V} \tag{5.100}$$

Chapter 6

Calculation of Loading/Unloading Times

A very essential point of the Thesis was to examine whether new proposed designs are gaining in port time. This gain was quantified in order to follow the extensive techno-economic analysis, which is described in Chapter 7. The objective of this Chapter is to present the procedure and time calculation for the loading/unloading of a large container vessel using conventional ship to shore gantry cranes (SSG) and the new concept ship to shore portal cranes (SSPC) (Nevsimal, 2017). The following sections present all necessary data and assumptions taken into account, as well as the procedure for calculating the loading/unloading time of the vessel. The calculations have been incorporated in an algorithm (tool) in order to make the calculations faster and automatically. The user manual of the tool is shown in "Appendix B". The methodology is generic and can be applied to any ship. The whole procedure was made for both case study vessels A and B. Some of the necessary data for the case study vessel B were missing. For this reason, additional assumptions were made according to case study vessel A. Specific references of these assumptions are mentioned in Chapter 8. The methodology is identical for both case study vessels.

6.1 General Calculations

A first round of calculations is made after the insertion of the necessary vessel data. In Table 6.1 the main and the specific data needed for the calculations are shown (see also Figure 6.1 and Figure 6.2). These data are input values in the algorithm.

Table 6.1: Main and specified data of the vessel for calculations.

Category	Magnitude
Main Data	Beam at amidships (B)
	Length overall (L_{OA})
	Depth (D)
	Double bottom height (h_{DB})
	Height of hatch covers (h_{HC})
	Air draught from keel (H)
Specific Data	TEU transverse spacing (s)
	Draught at the beginning of operation-full load (T_{ST})
	Draught at the end of operation-ballast condition (T_{END})
	Number of 40ft bays ($Bays_n$)
	Maximum number of above deck container rows ($rows_d$)
	Maximum number of below deck container rows ($rows_h$)
	Maximum number of above deck container tiers ($tiers_d$)
	Maximum number of below deck container tiers ($tiers_h$)

where,

- TEU transverse spacing (s) is the transverse distance between the (geometric) centers of two adjacent containers (Figure 6.1). The below deck containers are not located side by side in the transverse direction, but in cell guides. The width of these cell guides has to be taken into account. The above deck containers are also not located side by side; instead they are grouped. Thus, their average transverse spacing has to be taken into account. It has been assumed that the transverse spacing in case of both above deck and below deck TEU is the same. The transverse distance is calculated by taking into account the width of the container and the width of the cell guides.
- Draught at the beginning of operation-full load (T_{st}) is the draught when operation starts (Figure 6.2). During the procedure the vessel's draught changes. An average draught has to be taken into account. For the purpose of this study, an entire unloading/loading of the vessel has been considered.
- Draught at the end of operation-ballast condition (T_{end}). It is needed for calculating the average draught. The chosen scenario was the ballast condition with 100% Ballast (Figure 6.2).
- Number of 40ft bays ($Bays_n$) is the number of 40ft bays along the ship. This magnitude is needed for entering data information for every 40ft bay of the vessel. It has also been assumed that all deck TEU along the ship are above the hatch covers. This is not true for the first two tiers of the aft bay of the present case study vessel.
- Maximum number of above deck and below deck container rows ($rows_d$, $rows_h$) and maximum number of above deck and below deck container tiers ($tiers_d$, $tiers_h$) are essential magnitudes for the algorithm's calculations (Figure 6.2).

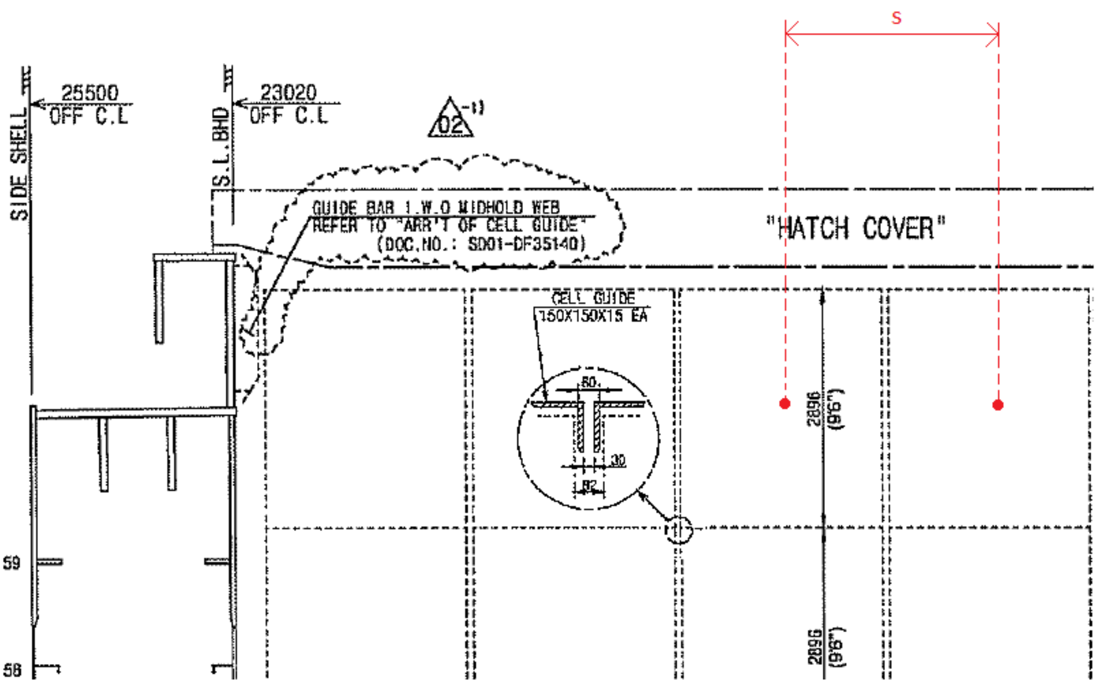

Figure 6.1: Typical transverse section of holds and basic geometric data of cell guides.

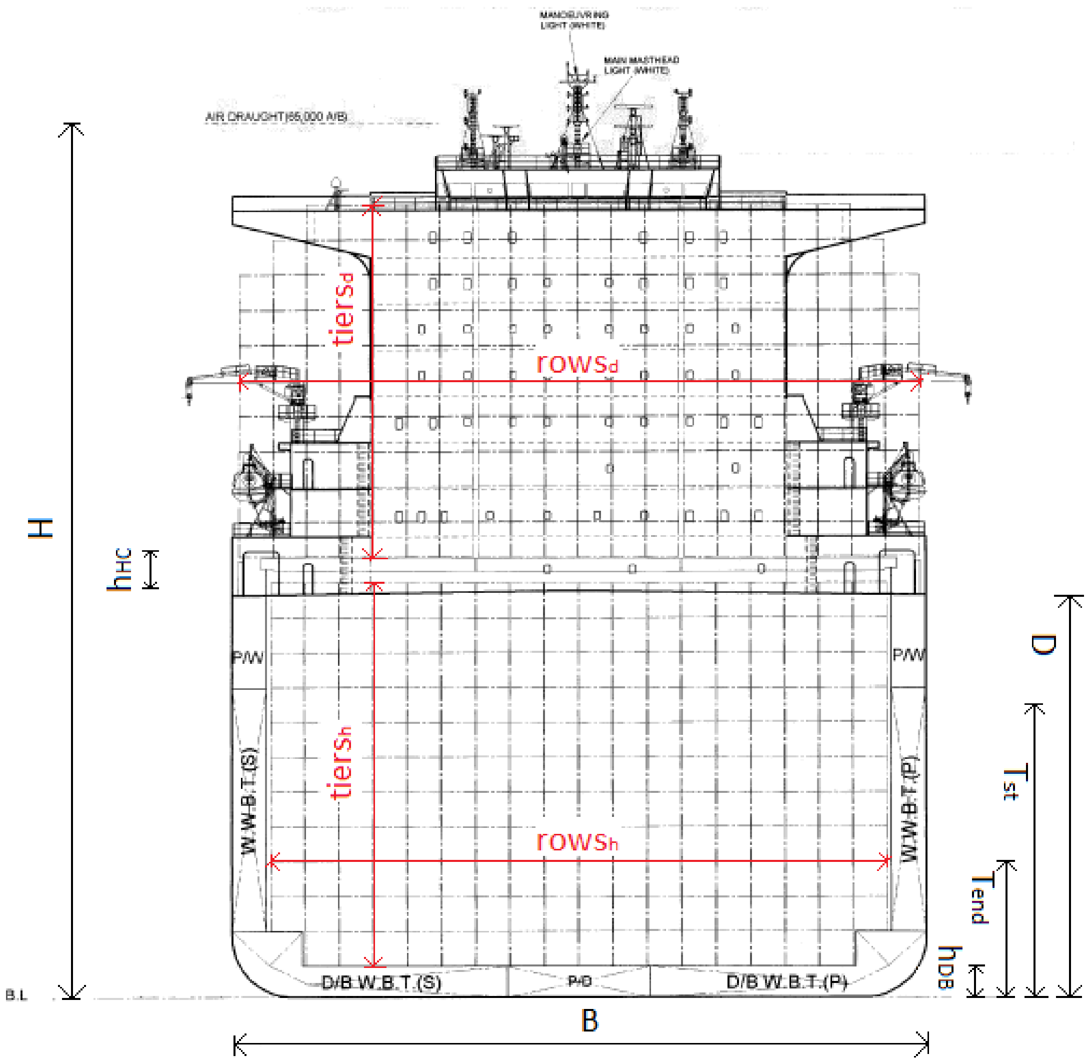

Figure 6.2: Typical Mid-Section and basic geometric data of a ULCV.

The dimensions of the containers have been considered as following:

Table 6.2: Typical dimensions of a container (20ft and 40ft).

Container Height (con_h)	2.591 m
Container Width (con_w)	2.438 m

Based on the above data, some basic additional geometric magnitudes for each bay are initially calculated. For an accurate calculation of the loading/unloading time of a vessel, it is necessary to estimate the cycle time of each bay. The cycle time of each bay is the time needed for the trolley to make one move (one cycle) of operation. For the calculation of the cycle time, an estimation of the average position of the TEU in each bay is needed. This was achieved by separating the TEUs of each bay to those above deck and those below deck and calculating the center of gravity (CoG) of each one of these two groups of TEUs, for each bay.

For implementing this analysis into the algorithm, the bay plan of each bay is needed. The definition of this bay plan was done by creating two tables, one for the above deck TEUs having "tiers$_d$" lines and "rows$_d$" columns, and one for the below deck

TEUs having "tiers_h" lines and "rows_h" columns (Figure 6.3). Then, the allocation of TEU in each bay was done by assigning the value "1" at the places where TEU exists, and the value "0" at empty (or non-existent) places.

A representative example can be seen in Figure 6.3. On the left, the bay plan of bay No. 2 of case study vessel A is depicted, whereas on the right its computer implementation can also be seen. All cells with the value of "1" (colored yellow in Figure 6.3) indicate the existence of a TEU and, therefore, the yellow area is the bay plan of this specific bay.

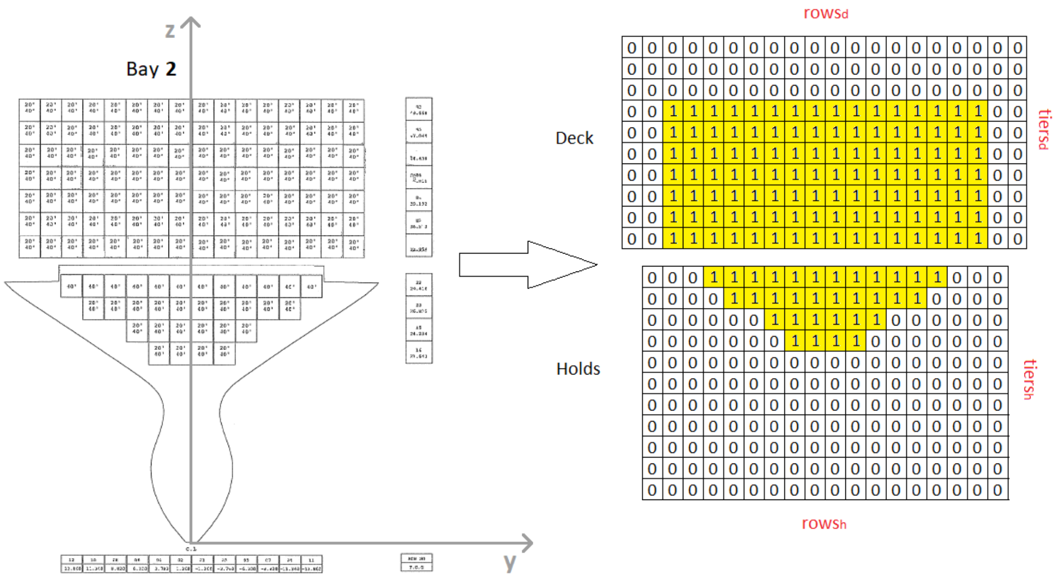

Figure 6.3: Transfer of bay plan information to the computer for further calculations.

Based on the information included in the Trim and Stability Booklet of case study vessel A, this data entry procedure has to be done for each 40ft bay separately. An advantage of the tool is that the entry procedure is done only once for each vessel. In case of two 20ft bays which are comprising one 40ft bay and they are slightly different from each other, data entry is carried out for the aft most 20ft bay. After the data entry, the algorithm scans the table and identifies the cells having value "1" acquiring in this way information about the position of each TEU in the bay, and calculating the vertical and transverse coordinates of the CoG of each one of them. For the case study vessel B, the Trim and Stability Booklet was missing. In this case, the above deck bay plan was made according to the various vessel's images on the internet. On the other hand, the below deck bay plan was made according to the corresponding bay plan of the case study vessel A.

For the purposes of this study, an orthogonal coordinate system was defined on the ship, having its origin at the intersection of the aft perpendicular with the base line of the ship, axis x in the longitudinal direction (positive forward), axis y in the transverse direction (positive port) and axis z in the vertical direction (positive upwards, Figure 6.3). Moreover, the numbering of lines (tiers) starts from the top and increases downwards, whereas the numbering of columns (rows) starts from starboard and increases towards the port side of the ship. Thus, the transverse and vertical coordinates (y_n, z_n) of the n^{th} TEU in each bay were calculated from the following equations:

Above deck:

$$y_n = \left(j - \frac{rows_d}{2} - 0.5\right) \cdot s \cdot M(i,j) \tag{6.1}$$

where, y_n: y-coordinate of CoG of n^{th} container (m)
s: transverse spacing of TEU (m)
$rows_d$: maximum number of above deck container rows
j: row (column) number of n^{th} container
i: tier (line) number of n^{th} container
$M(i,j)$: cell value at line i and column j (value 0 or 1)

$$z_n = \left\{D + h_{HC} + con_h \cdot [(tiers_d - i) + 0.5]\right\} \cdot M(i,j) \tag{6.2}$$

where, z_n: z-coordinate of CoG of n^{th} container (m)
D: depth (m)
h_{HC}: height of hatch covers including hatch coamings (m)
con_h: container height (=2.591m)
$tiers_d$: maximum number of above deck container tiers

Below deck:

$$y_n = \left(j - \frac{rows_h}{2} - 0.5\right) \cdot s \cdot M(i,j) \tag{6.3}$$

where, $rows_h$: maximum number of below deck container rows

$$z_n = [h_{DB} + con_h \cdot ((tiers_h - i) + 0.5)] \cdot M(i,j) \tag{6.4}$$

where, h_{DB}: double bottom height (m)
$tiers_h$: maximum number of below deck container tiers

Having calculated the coordinates of the CoG of each TEU in every bay of the ship, the coordinates of the CoG of the whole batch of TEUs in each bay were estimated from the following equations:

$$TCG_c = \frac{\sum A_n \cdot y_n}{\sum A_n} \tag{6.5}$$

$$VCG_c = \frac{\sum A_n \cdot z_n}{\sum A_n} \qquad (6.6)$$

where, TCG_C: y-coordinate of CoG of all TEUs in the bay (m)
VCG_C: z-coordinate of CoG of all TEUs in the bay (m)
A_n: cross section area of each container (m^2)
y_n: y-coordinate of CoG of each TEU (m)
z_n: z-coordinate of CoG of each TEU (m)

The bay coordinates' calculations are different for the conventional cranes (SSG) concept and for the portal cranes (SSPC) one. In the case of the SSG concept, the crane loads/unloads the whole bay, thus the transverse coordinate of the whole batch of TEUs in a bay will be zero (CoG lies on the central longitudinal plane of symmetry of the ship), due to the symmetry of the bay. On the other hand, in the case of the SSPC concept, TEUs are loaded/unloaded from both sides of the ship, thus the calculations of the coordinates of the CoG of the whole batch of TEUs in a bay are made for one half of the bay (either the one on the starboard side or the one on the port side). The determination of CoG is not only used for the calculation of loading/unloading time of a vessel. It is also used for the estimation of the metacentric height – GM (see sub-section 5.6.1).

In the following sections, the procedure of running calculations by the algorithm for the SSG concept and the SSPC one are described.

6.2 Operation of conventional cranes (SSG)

In this section, the loading/unloading procedure in the case of conventional cranes is described. Figure 6.4 depicts the desired trajectory (Hamalainen, A., Baharova, & Virkkunen, 1995) of the trolley and the hoist and the basic geometric and technical characteristics of the SSG concept. The illustrated vessel shown in Figure 6.4 represents a typical Mid-ship section of a ULCV.

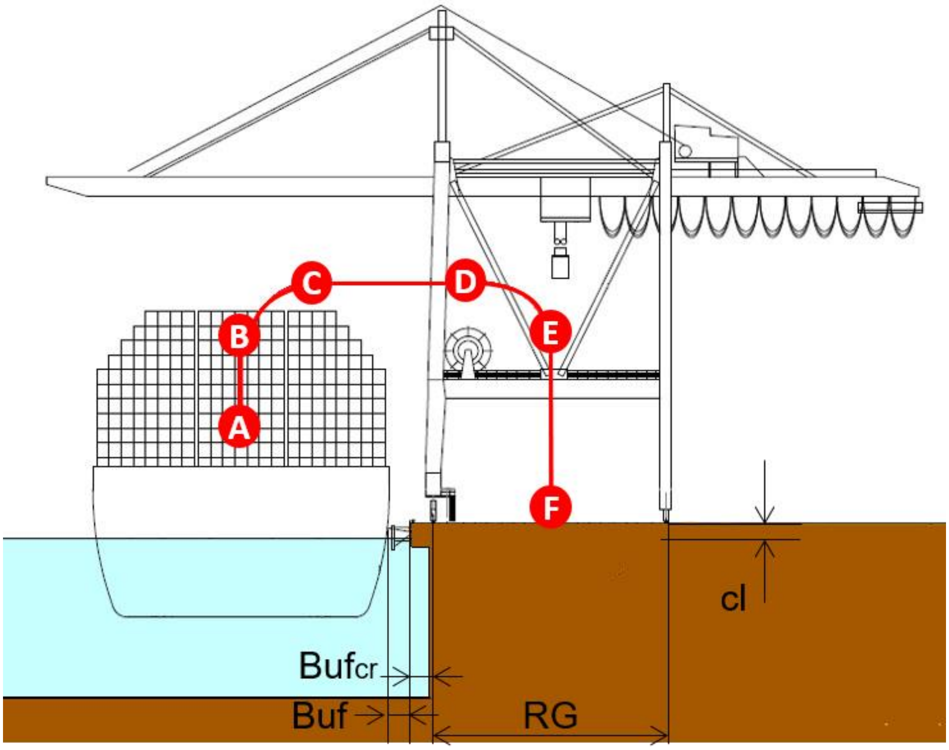

Figure 6.4: Typical hoist path in case of conventional cranes (SSG). Source: (COFASTRANS-Indented Berths Feasibility Study, 2015)

The operation is divided in the unloading and loading cycle. The major differences of these two cycles is that in the unloading cycle the hoist starts from position A (see Figure 6.4) and in this position the spreader is loaded with TEU. On the other hand, in the loading cycle the hoist starts from position F (see Figure 6.4) and in this position the spreader is loaded with TEU. More details are presented below in the following sections.

For the sake of simplicity some assumptions were made. The assumptions are listed and described below:

- An entire loading/unloading of the vessels has been assumed in order to make similar comparisons of the various cases of vessels. The factor of the proper stowage plan of the vessel is eliminated and no TEU re-handles are required.
- The simultaneous vertical hoist movement and horizontal trolley travel were taken into account, in order to minimize the cycle time needed for loading/unloading.
- The time required for unloading is different from the time required for loading due to different position of the control points of the trajectories. Calculations were made for both.
- The points of the trajectory correspond to the movement of the spreader (see Figure 6.5).

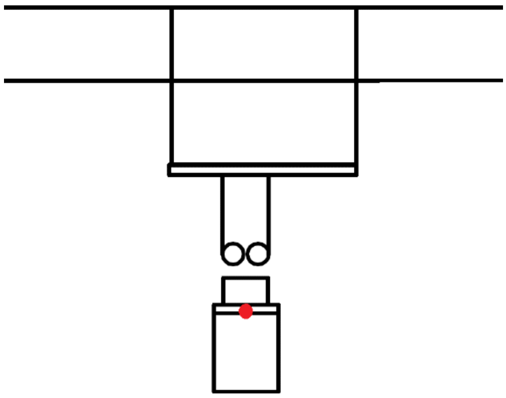

Figure 6.5: Definition of trajectory's point.

- The different number of TEUs per bay (e.g. smaller number of TEUs near the stern and the bow than at amidships) was taken into account. This is the reason why general calculations were developed (see Section 6).
- During unloading, the ship's draught at the start of the procedure is larger than the draught at the end. The mean value of these two draughts was taken into account in the calculations. The opposite happens in the case of loading. The starting and the ending draught of the vessel are critical input values to the algorithm (Table 6.1).
- The TEUs, when unloaded from the ship and transferred to the port, are put on the quay and not on some truck. This can be easily modified, depending on the actual scenario. For this to be done, changes need to be made in the algorithm's code.
- The results may not be very realistic, due to various delay factors that are involved. These factors are neutralized for the different ship cases, due to the comparison of the results. The algorithm makes a rough approximation of the operational time.
- When the TEUs are transferred, there is a time delay due to the swaying of the spreader wire ropes. This time was not taken into account.
- When loading/unloading the below deck TEUs there is a remarkable delay time of placing the spreader into the cell guides, due to flippers "hitting". This means that the below deck TEUs' operations are significantly longer than the above deck TEUs'. This time was not taken into account.
- The time required for docking the TEUs to the spreader (dwell time, Dt) was taken equal to 15 sec.
- The time required for the cranes to move along the quay was taken into account.
- The spreader has the capacity to transfer four TEUs in one move (tandem lift) and the following transfer index was considered (COFASTRANS-Indented Berths Feasibility Study, 2015):

$$ex=3.2\frac{TEU}{move} \qquad (6.7)$$

- The positioning time, in case of using tandem lift spreader, is slower than using a twin lift spreader (1.6 TEU/move). This time was not taken into account.
- Table 6.3 presents typical geometric and technical characteristics of conventional cranes.

Table 6.3: Typical geometric and technical characteristics of SSG crane.

Geometric Characteristics			
Name	**Value**	**Reference**	
Rail Gauge (RG)	30.5 m	(COFASTRANS-Indented Berths Feasibility Study, 2015)	
Buffer (Buf)	2.3 m	(COFASTRANS-Indented Berths Feasibility Study, 2015)	
Distance between Buffer and seaside rail of crane (Buf_{cr})	3.0 m	(COFASTRANS-Indented Berths Feasibility Study, 2015)	
Vertical distance between sea and quay level (cl)	5.0 mCD	Assumed	
Technical Characteristics			
Name	**Value**	**Acceleration Time**	**Reference**
Hoist speed, when spreader is empty of containers (u_1)	180m/min	4.0sec	(Nevsimal-Weidenhoffer & Oja, 2018)
Hoist speed, when spreader is loaded with containers (u_2)	90m/min	2.0sec	(Nevsimal-Weidenhoffer & Oja, 2018)
Trolley transit speed (u_3)	250m/min	5.0sec	(Nevsimal-Weidenhoffer & Oja, 2018)
Gantry speed (u_4)	45m/min	5.0sec	(COFASTRANS-Indented Berths Feasibility Study, 2015) and personal communication with Mr. Oja

- The acceleration time equals to the deceleration one.
- The algorithm was developed for the case when the acceleration time of the loaded spreader's hoist, t_2, is smaller or equal to the acceleration time of the trolley, t_3 ($t_2 \leq t_3$). This is a typical relation between these two acceleration times. The opposite one is not often observed. However, if the algorithm was developed to satisfy the opposite relation of the two-acceleration time, the procedure would have been more complex and would not have a serious impact on the results. The aim was to compare the operational times of the various design vessels' cases and not to calculate the accurate operational time.
- The method was developed for vessels of typical size and for cranes of typical hoist and trolley speeds.

During the loading/unloading procedure, the trolley is carrying out moves of different length in the crane outreach and backreach direction. For this reason, some average distances of trolley movements had to be calculated, based on the geometric characteristics of the ship and the quay. These average distances are analytically presented in the following sections.

The operation time depends largely on the time required by the trolley to move (Figure 6.6). Initially, it was necessary to define the trajectory of the hoist for each operation.

6.2.1.1 Unloading Cycle

The operation was divided in two phases; the ship to berth phase (Figure 6.6, up) and the berth to ship phase (Figure 6.6, down). For the ship to berth phase (Figure 6.6, up), the sequence of the hoist movement consists of five stages (Hamalainen, A., Baharova, & Virkkunen, 1995). The initial time at starting point A is t_A ($t_A = 0$). In the upwards stage A-B, the load is lifted from the initial level z_A to level z_B, that is above any possible obstacles in the vicinity. It is assumed that the load arrives at B with its maximum lifting speed u_2^{max}. During the so-called diagonal acceleration movement B-C, the load is lifted up to level z_C above any obstacles along the rest of the path. The hoist speed (vertical) is decelerated and the trolley speed (horizontal) is accelerated. The composition of speeds, curves the trajectory. It is assumed that at point C the trolley has not reached its maximum speed. Furthermore, from point C to point D the trolley moves at maximum speed u_3^{max}. Stage D-E is called the diagonal deceleration movement, because the trolley speed decreases from u_3^{max} to zero, while the load is coming down to level z_E. After point D, there is a simultaneous movement of the trolley (horizontal) and hoist (vertical). During the diagonal deceleration and before point E, it is assumed that the hoist speed has gained its maximum speed u_2^{max}. Then the load is lowered from E to F. At some point before point F, the hoist speed decreases from u_2^{max} to zero. A dwell time (Dt) is taken into account at point F.

For the berth to ship phase (Figure 6.6, down), the trajectory is similar, but the control points are in different positions. The hoist now has no TEU, so the hoist speed increases to u_1^{max}. A dwell time (Dt) is taken into account at point A.

The whole unloading cycle (ship to berth and then berth to ship) consists of steps A-B-C-D-E-F-G-H-I-J-A.

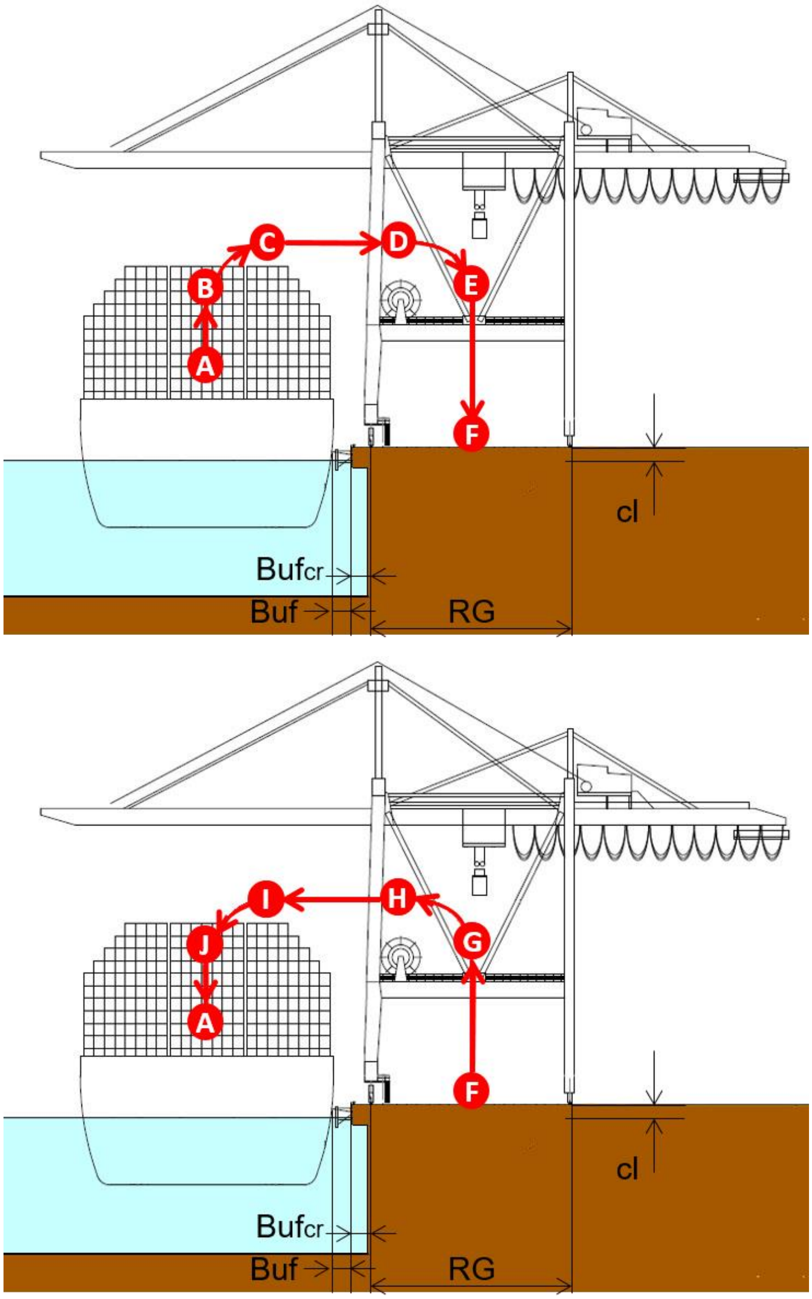

Figure 6.6 : Ship to berth (up) and berth to ship (down) hoist trajectories of unloading with conventional cranes (SSG). Source: (COFASTRANS-Indented Berths Feasibility Study, 2015)

It was observed that the path of unloading above deck TEUs is different from that for below deck TEUs, due to the different nature of obstacles present in the hoist trajectory. Therefore, the trajectories of these two cases are different and are calculated bellow separately (see Table 6.4 and Table 6.5, respectively).

<u>Above deck:</u>

The calculation of the cycle time depends on the position of the trajectory control points. The coordinates of these control points for each separate 40ft bay, were calculated as follows:

Table 6.4: Coordinates of control points for the above deck TEU, in the case of unloading using SSG cranes.

Point	Y-coordinate	
A	$y_A=TCG_c^{deck}$	(6.8)
B	$y_B=y_A$	(6.9)
C	$y_C=y_B+\frac{1}{2}\cdot a_3\cdot(t_2)^2$	(6.10)
D	$y_D=y_F-\frac{1}{2}\cdot a_3\cdot(t_3)^2$	(6.11)
E	$y_E=y_F$	(6.12)
F	$y_F=\frac{B}{2}+\frac{RG}{2}+Buf_{cr}+Buf$	(6.13)
G	$y_G=y_F$	(6.14)
H	$y_H=\begin{cases} y_F-\frac{1}{2}\cdot a_3\cdot(t_1)^2, \text{ when } t_1\le t_3 \\ y_F-\frac{1}{2}\cdot a_3\cdot(t_3)^2-u_3\cdot(t_1-t_3), \text{ when } t_3<t_1 \end{cases}$	(6.15)
I	$y_I=\begin{cases} y_J+\frac{1}{2}\cdot a_3\cdot(t_x)^2, \text{ when } t_x\le t_3 \text{ and } d_{JA}<\left(0.5\cdot a_1\cdot(t_1)^2\right) \\ y_J+\frac{1}{2}\cdot a_3\cdot(t_3)^2, \text{ when } t_3\le t_1 \text{ and } d_{JA}\ge\left(0.5\cdot a_1\cdot(t_1)^2\right) \\ y_J+\frac{1}{2}\cdot a_3\cdot(t_1)^2, \text{ when } t_1<t_3 \text{ and } d_{JA}\ge\left(0.5\cdot a_1\cdot(t_1)^2\right) \\ y_J+\frac{1}{2}\cdot a_3\cdot(t_3)^2, \text{ when } t_3\le t_x<t_1 \text{ and } d_{JA}<\left(0.5\cdot a_1\cdot(t_1)^2\right) \end{cases}$	(6.16)
J	$y_J=y_A$	(6.17)
	Z-coordinate	
A	$z_A=VCG_c^{deck}+\frac{con_h}{2}$	(6.18)
B	$z_B=z_A+con_h+0.5$	(6.19)
C	$z_C=z_B+\frac{1}{2}\cdot a_2\cdot(t_2)^2$	(6.20)
D	$z_D=z_C$	(6.21)
E	$z_E=z_D-\frac{1}{2}\cdot a_2\cdot(t_2)^2-u_2\cdot(t_3-t_2)$	(6.22)
F	$z_F=\frac{T_{st}+T_{end}}{2}+con_h+cl$	(6.23)
G	$z_G=z_H-\frac{1}{2}\cdot a_1\cdot(t_1)^2$	(6.24)
H	$z_H=z_I$	(6.25)
I	$z_I=\begin{cases} z_J+\frac{1}{2}\cdot a_1\cdot(t_x)^2, \text{ when } t_x\le t_3 \text{ and } d_{JA}<\left(0.5\cdot a_1\cdot(t_1)^2\right) \\ z_J+\frac{1}{2}\cdot a_1\cdot(t_3)^2, \text{ when } t_3\le t_1 \text{ and } d_{JA}\ge\left(0.5\cdot a_1\cdot(t_1)^2\right) \\ z_J+\frac{1}{2}\cdot a_1\cdot(t_1)^2, \text{ when } t_1<t_3 \text{ and } d_{JA}\ge\left(0.5\cdot a_1\cdot(t_1)^2\right) \\ z_J+\frac{1}{2}\cdot a_1\cdot((t_x)^2-(t_3)^2), \text{ when } t_3\le t_x<t_1 \text{ and } d_{JA}<\left(0.5\cdot a_1\cdot(t_1)^2\right) \end{cases}$	(6.26)
J	$z_J=z_A+1.0$	(6.27)

Note: The values of 0.5m and 1.0m at the z-coordinates of points B and J, respectively, are taken for safety reasons.

where, TCG_C^{deck}: Transverse center of gravity for the whole batch of above deck containers of the specific 40ft bay (y-coordinate, m)

RG: Rail gauge (m)

Buf_{cr}: Distance between buffer and seaside rail of crane (m)

Buf: Buffer (m)

B: Beam at amidships (m)

VCG_C^{deck}: Vertical center of gravity for the whole batch of above deck containers of the specific 40ft bay (z-coordinate, m)

con_h: Container's height (m)

T_{st}: Draught at the beginning of operation-full load (m)

T_{end}: Draught at the end of operation-ballast condition (m)

cl: Vertical distance between sea and quay level (mCD)

d_{JA}: Vertical distance from point J to point A (m)

t_x: Time needed to travel distance d_{JA}, when $d_{JA} < 0.5a_1(t_1)^2$ (sec)

a_1: Acceleration hoist speed when hoist has no TEU (m/sec^2)

a_2: Acceleration hoist speed when hoist is loaded with TEU (m/sec^2)

a_3: Acceleration trolley speed (m/sec^2)

t_1: Acceleration time, when hoist has no TEU (sec)

t_2: Acceleration time, when hoist is loaded with TEU (sec)

t_3: Acceleration trolley time (sec)

u_1: Hoist speed when spreader has no TEU (m/sec)

u_2: Hoist speed when spreader is loaded with TEU (m/sec)

u_3: Trolley speed (m/sec)

Note: Obviously, time t_x is equal or smaller than time t_1. It is considered that the trolley speed, in case of $t_1 \leq t_3$, starts decreasing from maximum speed u_3^{max} before point I. At point I, the simultaneous move of hoist and trolley starts.

<u>Below deck:</u>

For the below deck TEU, the coordinates of the most control points for each separate 40ft bay are the same with Table 6.4. The points with different parametric coordinates were calculated as follows:

Table 6.5: Coordinates of control points for the below deck TEU, in the case of unloading using SSG cranes.

Point	Y- coordinate	
A	$y_A = TCG_c^{holds}$	(6.28)
	Z-coordinate	
A	$z_A = VCG_c^{holds} + \frac{con_h}{2}$	(6.29)
B	$z_B = D + h_{HC} + con_h$	(6.30)
J	$z_J = D + h_{HC}$	(6.31)

where, TCG_C^{holds}: Transverse center of gravity for the whole batch of below deck containers of the specific 40ft bay (y-coordinate, m)

D: Depth (m)

h_{HC}: Height of hatch covers (m)

VCG_C^{holds}: Vertical center of gravity for the whole batch of below deck containers of the specific 40ft bay (z-coordinate, m)

The other magnitudes have been defined in the previous table.

The cycle time was calculated separately for the above deck TEUs and for those below deck. Having calculated the various distances, in which the trolley and the hoist have to travel, the unloading cycle time was calculated as follows:

$$CT = T_{AB} + T_{BC} + T_{CD} + T_{DE} + T_{EF} + Dt_1 + T_{FG} + T_{GH} + T_{HI} + T_{IJ} + T_{JA} + Dt_2 \qquad (6.32)$$

where, CT: estimated cycle time, time needed for one move (sec)

T_{AB}: time needed to cover distance from point A to point B (sec)

T_{BC}: time needed to cover distance from point B to point C (sec)

T_{CD}: time needed to cover distance from point C to point D (sec)

T_{DE}: time needed to cover distance from point D to point E (sec)

T_{EF}: time needed to cover distance from point E to point F (sec)

Dt_1: dwelling time due to unloading the containers from spreader to berth (sec)

T_{FG}: time needed to cover distance from point F to point G (sec)

T_{GH}: time needed to cover distance from point G to point H (sec)

T_{HI}: time needed to cover distance from point H to point I (sec)

T_{IJ}: time needed to cover distance from point I to point J (sec)

T_{JA}: time needed to cover distance from point J to point A (sec)

Dt_2: dwelling time due to loading the containers from ship to spreader (sec)

Notes:

- Times T_{CD} and T_{HI} depend on the trolley speed u_3
- Times T_{FG}, T_{GH}, T_{IJ} and T_{JA} depend on the hoist speed u_1, with empty spreader.
- Times T_{AB}, T_{BC}, T_{DE} and T_{EF} depend on the hoist speed u_2, with loaded spreader.

The number of moves needed to unload each bay are based on the exchange index (ex, see Section 6.2). The index depends on the type of the spreader (tandem or twin).

$$m=\frac{cap}{ex} \tag{6.33}$$

where, m: number of moves needed to unload each bay
cap: capacity of bay (TEU)
ex: the number of TEUs exchanged in one move (3.2 TEU/move)

Consequently, the total calculation of unloading time for the mth bay was calculated as:

$$T_{unl}^{m} = \frac{CT_{unl}^{m\_deck} \cdot m_{unl}^{m\_deck}}{3600} + \frac{CT_{unl}^{m\_holds} \cdot m_{unl}^{m\_holds}}{3600} \tag{6.34}$$

where, T_{unl}^{m}: Unloading time of mth bay (hr)
$CT_{unl}^{m\_deck}$: Above Deck TEU unloading cycle time of mth bay (sec)
$m_{unl}^{m\_deck}$: Moves needed to unload above deck containers in mth bay
$CT_{unl}^{m\_holds}$: Below Deck TEU unloading cycle time of mth bay (sec)
$m_{unl}^{m\_holds}$: Moves needed to unload below deck containers in mth bay

The total unloading time of the vessel depends on the number of deployed cranes along the ship. Six cranes are commonly used in most of the major terminals worldwide (Rankine, Netherstreet, Perez Romero, & Palmer, 2018). The configuration plan of the operation is needed. The optimum configuration plan could not be constructed automatically. The aim of the optimum configuration plan is to minimize the time for which cranes remain idle.

With the unloading time of mth bay (T_{unl}^{m}) known the total unloading time of the vessel (T_{unl}) can be calculated. The operators have to build the cranes' configuration plan of the operation. In conventional cranes concept the configuration plan is simple due to the fact that the SSG cranes operate in adjacent bays. Each crane, unloads a group of bays. The total unloading time of each crane equals to the sum of the total unloading times of the bays included in the specific group. In the total unloading time of each crane is included the time needed for the crane to move from one bay to the next one (depends on the gantry speed – u_4). The maximum unloading time of the cranes is the total unloading time of the vessel.

6.2.1.2 Loading Cycle

In the previous section, the unloading cycle process was described. The procedure for the loading cycle is slightly different. The trajectory of the hoist in the case of loading is the same as that in the case of unloading presented above (see sub-section 6.2.1.1) and depicted in Figure 6.6. The loading cycle is F-G-H-I-J-A-B-C-D-E-F. The hoist path is similar to the one in the case of unloading, but the control points are in a different position. The differences in the coordinates of the trajectory control points between the loading and the unloading cycles occur due to the different hoist speeds when loaded and when unloaded, in conjunction with the different parts of the trajectory where the hoist is considered loaded or unloaded, in the two cycles.

Above deck:

The coordinates of the trajectory control points for each separate 40ft bay, are depicted in the following table, in the case of above deck TEU.

Table 6.6: Coordinates of control points for the above deck TEU, in the case of loading using SSG cranes.

Point	Y-coordinate	
A	$y_A=TCG_c^{deck}$	(6.35)
B	$y_B=y_A$	(6.36)
C	$y_C = \begin{cases} y_B+\frac{1}{2}\cdot a_3\cdot(t_x)^2, \text{ when } t_x \le t_3 \text{ and } d_{AB} < \left(0.5\cdot a_1\cdot(t_1)^2\right) \\ y_B+\frac{1}{2}\cdot a_3\cdot(t_3)^2+u_3\cdot(t_1\text{-}t_3), \text{ when } t_3 \le t_1 \text{ and } d_{AB} \ge \left(0.5\cdot a_1\cdot(t_1)^2\right) \\ y_B+\frac{1}{2}\cdot a_3\cdot(t_1)^2, \text{ when } t_1 < t_3 \text{ and } d_{AB} \ge \left(0.5\cdot a_1\cdot(t_1)^2\right) \\ y_B+\frac{1}{2}\cdot a_3(t_3)^2+u_3\cdot(t_x\text{-}t_3), \text{ when } t_3 \le t_x < t_1 \text{ and } d_{AB} < \left(0.5\cdot a_1\cdot(t_1)^2\right) \end{cases}$	(6.37)
D	$y_D=y_F-\frac{1}{2}\cdot a_3\cdot(t_3)^2$	(6.38)
E	$y_E=y_F$	(6.39)
F	$y_F=\frac{B}{2}+\frac{RG}{2}+Buf_{cr}+Buf$	(6.40)
G	$y_G=y_F$	(6.41)
H	$y_H=y_F-\frac{1}{2}\cdot a_3\cdot(t_2)^2$	(6.42)
I	$y_I=y_J+\frac{1}{2}\cdot a_3\cdot(t_2)^2$	(6.43)
J	$y_J=y_A$	(6.44)
	Z-coordinate	
A	$z_A=VCG_c^{deck}+\frac{con_h}{2}$	(6.45)
B	$z_B=z_A+1.0$	(6.46)
C	$z_C=\begin{cases} z_B+\frac{1}{2}\cdot a_1\cdot(t_x)^2, \text{ when } t_x \le t_3 \text{ and } d_{AB} < \left(0.5\cdot a_1\cdot(t_1)^2\right) \\ z_B+\frac{1}{2}\cdot a_1\cdot(t_1)^2, \text{ when } t_3 \le t_1 \text{ and } d_{AB} \ge \left(0.5\cdot a_1\cdot(t_1)^2\right) \\ z_B+\frac{1}{2}\cdot a_1\cdot(t_1)^2, \text{when } t_1 < t_3 \text{ and } d_{AB} \ge \left(0.5\cdot a_1\cdot(t_1)^2\right) \\ z_B+\frac{1}{2}\cdot a_1\cdot(t_x)^2, \text{ when } t_3 \le t_x < t_1 \text{ and } d_{AB} < \left(0.5\cdot a_1\cdot(t_1)^2\right) \end{cases}$	(6.47)
D	$z_D=z_C$	(6.48)
E	$z_E=\begin{cases} z_D-\frac{1}{2}\cdot a_1\cdot(t_1)^2-u_1\cdot(t_3\text{-}t_1), \text{ when } t_1 \le t_3 \\ z_D-\frac{1}{2}\cdot a_1\cdot(t_3)^2, \text{ when } t_3 < t_1 \end{cases}$	(6.49)
F	$z_F=\frac{T_{st}+T_{end}}{2}+con_h+cl$	(6.50)
G	$z_G=z_H-\frac{1}{2}\cdot a_2\cdot(t_2)^2$	(6.51)
H	$z_H=z_I$	(6.52)
I	$z_I=z_J+\frac{1}{2}\cdot a_2\cdot(t_2)^2$	(6.53)
J	$z_J=z_A+con_h+0.5$	(6.54)

Note: The values of 0.5m and 1.0m at the z-coordinates of points J and B, respectively, are taken for safety reasons.

Where the various magnitudes have been defined in the previous section.

Below deck:

For the below deck TEU, the coordinates of most control points for each separate 40ft bay are the same with Table 6.6. The points with different parametric coordinates were calculated as follows:

Table 6.7: Coordinates of control points for the below deck TEU, in the case of loading using SSG cranes.

Point	Y-coordinate	
A	$y_A = TCG_c^{holds}$	(6.55)
	Z-coordinate	
A	$z_A = VCG_c^{holds} + \frac{con_h}{2}$	(6.56)
B	$z_B = D + h_{HC}$	(6.57)
J	$z_J = D + h_{HC} + con_h$	(6.58)

Where the various magnitudes have been defined in the previous section. From this point and onwards, the procedure is identical to the one which was described in the unloading cycle (see sub-section 6.2.1.1).

6.3 Operation of new concept cranes (SSPC)

Figure 6.7 depicts all the moves of the trolley and the hoist of a new-concept ship to shore portal crane (SSPC) for loading/unloading the vessel. In the following, all assumptions made are listed and described. They are mostly similar or identical to those made for conventional cranes. For reasons of clarity all assumptions are listed below.

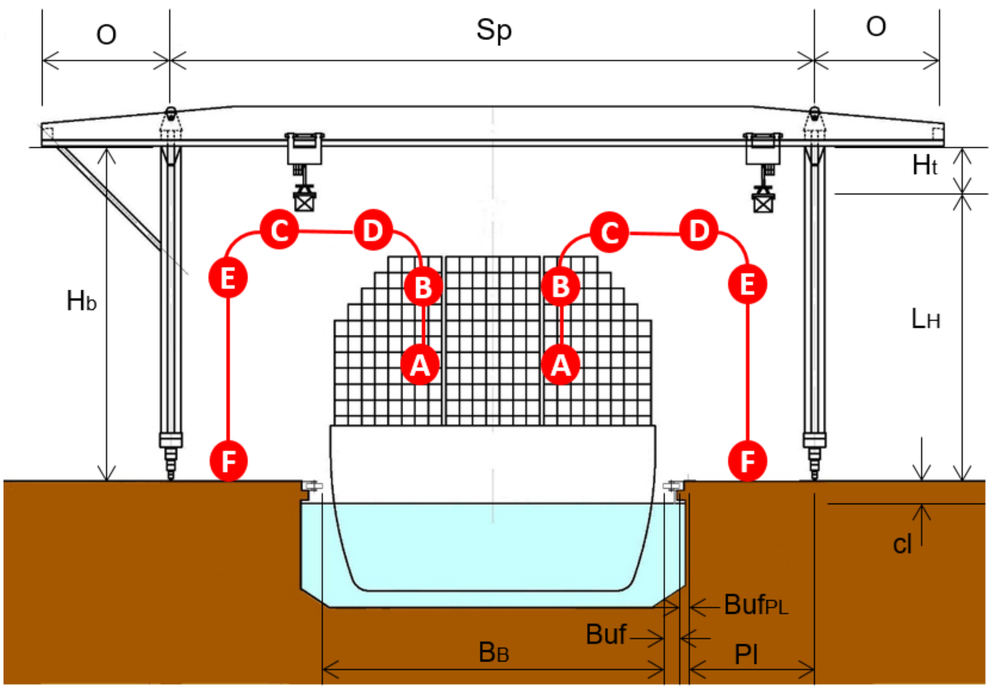

Figure 6.7: Indented Berth Layout. Source: (COFASTRANS-Indented Berths Feasibility Study, 2015)

- An entire loading/unloading of the vessels has been assumed in order to make similar comparisons of the various cases of vessels. The factor of the proper stowage plan of the vessel is eliminated and no TEU re-handles are required.
- The simultaneous vertical hoist movement and horizontal trolley travel were taken into account, in order to minimize the cycle time needed for loading/unloading.
- The time required for unloading is different from the time required for loading due to different position of the control points of the trajectories. Calculations were made for both.
- The points of the trajectory correspond to the movement of the spreader. (see Figure 6.5).
- Both trolleys of both beams of the crane are working continuously for loading or unloading the ship. This cannot happen in some cases depending on the arrangement of the TEU bays along the ship and one beam of the crane may remain idle for some time, while the other beam is working.
- The different number of TEUs per bay (e.g. smaller number of TEUs near the stern and the bow than at amidships) was taken into account. This is the reason why general calculations were developed (see Section 6).
- During unloading, the ship's draught at the start of the procedure is larger than the draught at the end. The mean value of these two draughts was taken into account in the calculations. The opposite happens in the case of loading. The starting and the ending draught of the vessel are critical input values to the algorithm (Table 6.1).
- The TEUs, when unloaded from the ship and transferred to the port, are put on the quay and not on some truck. This can be easily modified, depending on the actual scenario. For this to be done, changes need to be made in the algorithm's code.
- The results may not be very realistic, due to various delay factors that are involved. These factors are neutralized for the different ship cases, due to the comparison of the results. The algorithm makes a rough approximation of the operational time.
- The longitudinal distance between the centers of two adjacent 40ft bays is, in general, different in each vessel. At the beginning of the operation, there is a time delay for the trolley to adjust its position along the longitudinal direction of the ship. The trolleys have the ability to move their hook ±0.75m in the vessel's longitudinal direction (COFASTRANS-Indented Berths Feasibility Study, 2015). The acquired time for this longitudinal movement of the trolley was not taken into consideration.
- The buffers' width equals to the buffers' width in SSG concept ($Buf+Buf_{cr}=Buf+Buf_{PL}$) in order to make similar comparisons.
- When the TEUs are transferred, there is a time delay due to the swaying of the spreader wire ropes. This time was not taken into account.

- When loading/unloading the below deck TEUs there is a remarkable delay time of placing the spreader into the cell guides, due to flippers “hitting”. This means that the below deck TEU’s operations are significantly longer than the above deck TEU’s. This time was not taken into account.
- The time required for docking the TEUs to the spreader (dwell time, Dt) was taken equal to 15 sec.
- The time required for the cranes to move along the quay was taken into account.
- The spreader has the capacity to transfer four TEUs in one move (tandem lift). The equation 6.7 shows the transfer index for tandem lift operation.
- The positioning time, in case of using tandem lift spreader, is slower than using a twin lift spreader (1.6 TEU/move). This time was not taken into account.
- The algorithm runs the calculations for both starboard and port side of the vessel. The bay plan is divided into two halves; the starboard and the port side one. If the number of rows is an even number, then the same cycle time is expected. In case of odd number of rows, the port side trolley undertakes to unload the remaining row. For this reason, the cycle time of the two trolleys is different. In this case, the output of the algorithm is the maximum time.
- The acceleration time equals to the deceleration one.
- The algorithm was developed for the case when the acceleration time of the loaded spreader’s hoist, t_2, is smaller or equal to the acceleration time of the trolley, t_3 ($t_2 \leq t_3$) (see Table 6.8).
- The method was developed for vessels of typical size and for cranes of typical hoist and trolley speeds.

There are two types of berths and consequently two types of portal cranes. The basic geometric and technical characteristics of the two types of portal cranes and indented berths are proposed in the corresponding literature (COFASTRANS-Indented Berths Feasibility Study, 2015). In Table 6.8, all the initially proposed characteristics are listed. Some of these characteristics should change so that cranes and berths would be able to comply with new generation, larger ships. For the study purposes, some of the basic characteristics have been changed. The modified characteristics are listed in Table 6.9.

As mentioned above, there are two types of portal cranes; Type A and Type B. Type B are wider than Type A, in order to operate in wider vessels. Type A are able to operate in most of the present ULCVs. Vessels need some clearance to enter in indented berths. For instance, the MSC Gülsün series cannot enter in SSPC Type A berth. For this reason, Type B were also designed so as to operate in new generation, wider vessels.

Table 6.8: Geometric and Technical Characteristics of SSPC units and Indented Berths.

<table>
<tr><th colspan="5">Geometric Characteristics</th></tr>
<tr><th colspan="2">Name</th><th>Value</th><th colspan="2">Reference</th></tr>
<tr><td colspan="2">Height of crane beam above sea level (H_b)</td><td>66.0m</td><td colspan="2">(COFASTRANS-Indented Berths Feasibility Study, 2015) Subsequent research has shown that it could extend up to 70m.</td></tr>
<tr><td colspan="2">Height of trolley (H_t)</td><td>10.0m</td><td colspan="2">Assumed</td></tr>
<tr><td colspan="2">Vertical distance between sea and quay level or clearance (cl)</td><td>5.0mCD</td><td colspan="2">Assumed</td></tr>
<tr><td colspan="2">Maximum lifting height of the crane above quay level (L_H)</td><td>51.0m</td><td colspan="2">Calculated[i]</td></tr>
<tr><td colspan="2">Length of platform (Pl)</td><td>23.0m</td><td colspan="2">(Rankine, Netherstreet, Perez Romero, & Palmer, 2018)</td></tr>
<tr><td colspan="2">Buffer (Buf)</td><td>2.3m</td><td colspan="2">(Rankine, Netherstreet, Perez Romero, & Palmer, 2018)</td></tr>
<tr><td colspan="2">Distance between buffer and platform (Buf_{PL})</td><td>3.0m</td><td colspan="2">(Rankine, Netherstreet, Perez Romero, & Palmer, 2018)</td></tr>
<tr><td rowspan="3">SSPC Type A</td><td>Span (Sp)</td><td>117.0m</td><td colspan="2">(Rankine, Netherstreet, Perez Romero, & Palmer, 2018)</td></tr>
<tr><td>Width of berth (B_B)</td><td>62.0m</td><td colspan="2">(Rankine, Netherstreet, Perez Romero, & Palmer, 2018)</td></tr>
<tr><td>Overhangs (O)</td><td>18.5m</td><td colspan="2">(COFASTRANS-Indented Berths Feasibility Study, 2015)</td></tr>
<tr><td rowspan="3">SSPC Type B</td><td>Span (Sp)</td><td>127.0m</td><td colspan="2">(COFASTRANS-Indented Berths Feasibility Study, 2015)</td></tr>
<tr><td>Width of berth (B_B)</td><td>72.0m</td><td colspan="2">(COFASTRANS-Indented Berths Feasibility Study, 2015)</td></tr>
<tr><td>Overhangs (O)</td><td>23.5m</td><td colspan="2">(COFASTRANS-Indented Berths Feasibility Study, 2015)</td></tr>
<tr><th colspan="5">Technical Characteristics</th></tr>
<tr><th colspan="2">Name</th><th>Value</th><th>Acceleration Time</th><th>Reference</th></tr>
<tr><td colspan="2">Hoist speed, when spreader is empty of containers (u_1)</td><td>180m/min</td><td>4.0sec</td><td>(Nevsimal-Weidenhoffer & Oja, 2018)</td></tr>
<tr><td colspan="2">Hoist speed, when spreader is loaded with containers (u_2)</td><td>90m/min</td><td>2.0sec</td><td>(Nevsimal-Weidenhoffer & Oja, 2018)</td></tr>
<tr><td colspan="2">Trolley transit speed (u_3)</td><td>125m/min</td><td>4.0sec</td><td>(Nevsimal-Weidenhoffer & Oja, 2018)</td></tr>
<tr><td colspan="2">Gantry speed (u_4)</td><td>30m/min</td><td>5.5sec</td><td>(Nevsimal-Weidenhoffer & Oja, 2018)</td></tr>
</table>

The width of spanning beam equals to the sum of widths of berth, buffers and platforms. Initially, the SSG buffers are larger than the SSPC ones. However, same buffers in the two concepts were assumed. For this reason, the spans' widths are larger in Table 6.9 than the initially proposed (Table 6.8). Moreover, for SSPC Type Ba wider berth was proposed in order to operate in the extreme scenario of the case study vessel B (Case 3.2). However, a strength analysis of the proposed cranes should be made in later design stages.

[i] The maximum lifting height of the crane above the quay level is calculated by the equation:

$$L_H=H_b-H_t-cl$$

Table 6.9: Modified Geometric characteristics for COFASTRANS concept.

Geometric Characteristics			
Name		Value	Reference
SSPC Type A	Span (Sp)	118.6m	Assumed
	Width of berth (B_B)	62m	Assumed
	Overhangs (O)	Not calculated	-
SSPC Type B	Span (Sp)	130.6m	Assumed
	Width of berth (B_B)	74m	Assumed
	Overhangs (O)	Not calculated	-

6.3.1.1 Unloading Cycle

The unloading time depends largely on the time required by the trolley to move (Figure 6.8). The idea is the same as the one described in the previous section (see sub-section 6.2.1.1) about the SSG crane concept. The difference lies in the different geometric characteristics of the two types of cranes. The unloading cycle carried out by each trolley of the SSPC is A-B-C-D-E-F-G-H-I-J-A.

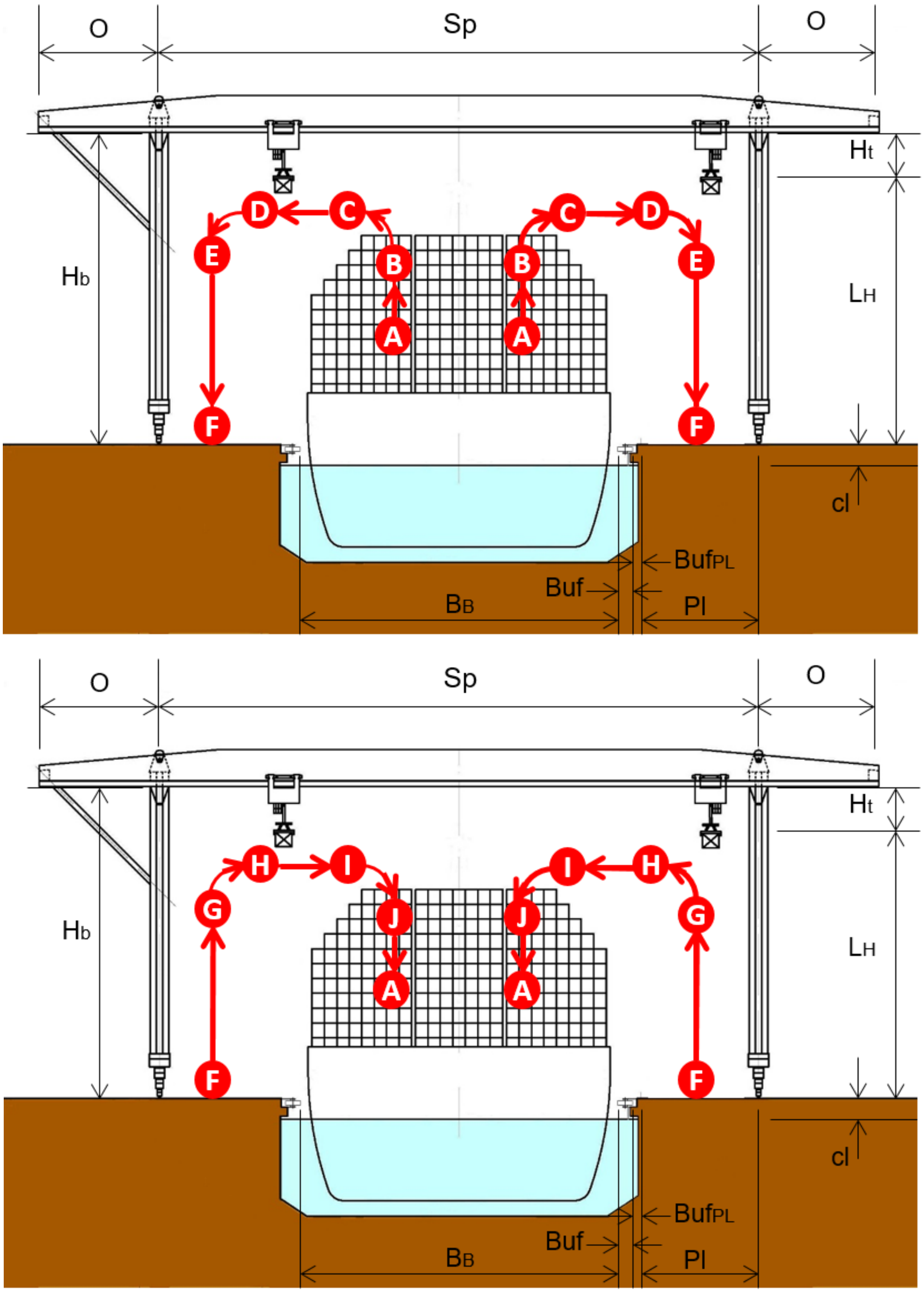

Figure 6.8: Ship to berth (up) and berth to ship (down) hoist trajectories of unloading with SSPC.

Due to the parametric nature of the trajectory's control points, the geometric difference between the two concepts is undertaken only in point F. However, in order to be thorough, all the coordinates of the points are presented.

<u>Above deck:</u>

Table 6.10: Coordinates of control points for the above deck TEU, in the case of unloading using SSPC units.

Point	Y-coordinate	
A	$y_A=TCG_c^{deck}$	(6.59)
B	$y_B=y_A$	(6.60)
C	$y_C=y_B+\frac{1}{2}\cdot a_3\cdot(t_2)^2$	(6.61)
D	$y_D=y_F-\frac{1}{2}\cdot a_3\cdot(t_3)^2$	(6.62)
E	$y_E=y_F$	(6.63)
F	$y_F=\frac{B}{2}+\frac{PL}{2}+Buf_{PL}+Buf+\frac{B_B-B}{2}$	(6.64)
G	$y_G=y_F$	(6.65)
H	$y_H=\begin{cases} y_F-\frac{1}{2}\cdot a_3\cdot(t_1)^2, \text{ when } t_1\le t_3 \\ y_F-\frac{1}{2}\cdot a_3\cdot(t_3)^2-u_3\cdot(t_1-t_3), \text{ when } t_3<t_1 \end{cases}$	(6.66)
I	$y_I=\begin{cases} y_J+\frac{1}{2}\cdot a_3\cdot(t_x)^2, \text{ when } t_x\le t_3 \text{ and } d_{JA}<\left(0.5\cdot a_1\cdot(t_1)^2\right) \\ y_J+\frac{1}{2}\cdot a_3\cdot(t_3)^2, \text{ when } t_3\le t_1 \text{ and } d_{JA}\ge\left(0.5\cdot a_1\cdot(t_1)^2\right) \\ y_J+\frac{1}{2}\cdot a_3\cdot(t_1)^2, \text{ when } t_1<t_3 \text{ and } d_{JA}\ge\left(0.5\cdot a_1\cdot(t_1)^2\right) \\ y_J+\frac{1}{2}\cdot a_3\cdot(t_3)^2, \text{ when } t_3\le t_x<t_1 \text{ and } d_{JA}<\left(0.5\cdot a_1\cdot(t_1)^2\right) \end{cases}$	(6.67)
J	$y_J=y_A$	(6.68)
	Z-coordinate	
A	$z_A=VCG_c^{deck}+\frac{con_h}{2}$	(6.69)
B	$z_B=z_A+con_h+0.5$	(6.70)
C	$z_C=z_B+\frac{1}{2}\cdot a_2\cdot(t_2)^2$	(6.71)
D	$z_D=z_C$	(6.72)
E	$z_E=z_D-\frac{1}{2}\cdot a_2\cdot(t_2)^2-u_2\cdot(t_3-t_2)$	(6.73)
F	$z_F=\frac{T_{st}+T_{end}}{2}+con_h+cl$	(6.74)
G	$z_G=z_H-\frac{1}{2}\cdot a_1\cdot(t_1)^2$	(6.75)
H	$z_H=z_I$	(6.76)
I	$z_I=\begin{cases} z_J+\frac{1}{2}\cdot a_1\cdot(t_x)^2, \text{ when } t_x\le t_3 \text{ and } d_{JA}<\left(0.5\cdot a_1\cdot(t_1)^2\right) \\ z_J+\frac{1}{2}\cdot a_1\cdot(t_3)^2, \text{ when } t_3\le t_1 \text{ and } d_{JA}\ge\left(0.5\cdot a_1\cdot(t_1)^2\right) \\ z_J+\frac{1}{2}\cdot a_1\cdot(t_1)^2, \text{ when } t_1<t_3 \text{ and } d_{JA}\ge\left(0.5\cdot a_1\cdot(t_1)^2\right) \\ z_J+\frac{1}{2}a_1\cdot((t_x)^2-(t_3)^2), \text{ when } t_3\le t_x<t_1 \text{ and } d_{JA}<\left(0.5\cdot a_1\cdot(t_1)^2\right) \end{cases}$	(6.77)
J	$z_J=z_A+1.0$	(6.78)

Note: The values of 0.5m and 1.0m at the z-coordinates of points B and J, respectively, are taken for safety reasons.

where, PL: the platform's length (m)

Buf_{PL}: the distance between the platform and the buffer (m)

B_B: the width of the berth (m)

All the other magnitudes have been described in the previous sections.

Below deck:

The coordinates of most control points are the same as the ones in Table 6.10. The modified ones are depicted in the following table:

Table 6.11: Coordinates of control points for the below deck TEU, in the case of unloading using SSPC units.

Point	Y- coordinate	
A	$y_A=TCG_c^{holds}$	(6.79)
	Z-coordinate	
A	$z_A=VCG_c^{holds}+\frac{con_h}{2}$	(6.80)
B	$z_B=D+h_{HC}+con_h$	(6.81)
J	$z_J=D+h_{HC}$	(6.82)

The remaining calculations are the same with those described in sub-section 6.2.1.1. The only difference is in the number of the SSPC units used for the operation. For this study, calculations were made for three and four cranes deployed along the vessel. In this case, the configuration plan is more complex due to the fact that the cranes operate in two non-adjacent bays (see Figure 4.2).

6.3.1.2 Loading Cycle

The idea is the same as that described in the previous section (see sub-section 6.2.1.2) about the SSG crane concept. The difference lies in the different geometric characteristics of the two types of cranes. The loading cycle carried out by each trolley of the SSPC is F-G-H-I-J-A-B-C-D-E-F.

Above deck:

The coordinates of the trajectory control points for each separate 40ft bay, are depicted in the following table, in the case of above deck TEU.

Table 6.12: Coordinates of control points for the above deck TEU, in the case of loading using SSPC units.

Point	Y-coordinate	
A	$y_A = TCG_c^{deck}$	(6.83)
B	$y_B = y_A$	(6.84)
C	$y_C = \begin{cases} y_B + \frac{1}{2} \cdot a_3 \cdot (t_x)^2, \text{ when } t_x \le t_3 \text{ and } d_{AB} < \left(0.5 \cdot a_1 \cdot (t_1)^2\right) \\ y_B + \frac{1}{2} \cdot a_3 \cdot (t_3)^2 + u_3 \cdot (t_1 - t_3), \text{ when } t_3 \le t_1 \text{ and } d_{AB} \ge \left(0.5 \cdot a_1 \cdot (t_1)^2\right) \\ y_B + \frac{1}{2} \cdot a_3 \cdot (t_1)^2, \text{ when } t_1 < t_3 \text{ and } d_{AB} \ge \left(0.5 \cdot a_1 \cdot (t_1)^2\right) \\ y_B + \frac{1}{2} \cdot a_3 \cdot (t_3)^2 + u_3 \cdot (t_x - t_3), \text{ when } t_3 \le t_x < t_1 \text{ and } d_{AB} < \left(0.5 \cdot a_1 \cdot (t_1)^2\right) \end{cases}$	(6.85)
D	$y_D = y_F - \frac{1}{2} \cdot a_3 \cdot (t_3)^2$	(6.86)
E	$y_E = y_F$	(6.87)
F	$y_F = \frac{B}{2} + \frac{PL}{2} + Buf_{PL} + Buf + \frac{B_B - B}{2}$	(6.88)
G	$y_G = y_F$	(6.89)
H	$y_H = y_F - \frac{1}{2} \cdot a_3 \cdot (t_2)^2$	(6.90)
I	$y_I = y_J + \frac{1}{2} \cdot a_3 \cdot (t_2)^2$	(6.91)
J	$y_J = y_A$	(6.92)
	Z-coordinate	
A	$z_A = VCG_c^{deck} + \frac{con_h}{2}$	(6.93)
B	$z_B = z_A + 1.0$	(6.94)
C	$z_C = \begin{cases} z_B + \frac{1}{2} \cdot a_1 \cdot (t_x)^2, \text{ when } t_x \le t_3 \text{ and } d_{AB} < \left(0.5 \cdot a_1 \cdot (t_1)^2\right) \\ z_B + \frac{1}{2} \cdot a_1 \cdot (t_1)^2, \text{ when } t_3 \le t_1 \text{ and } d_{AB} \ge \left(0.5 \cdot a_1 \cdot (t_1)^2\right) \\ z_B + \frac{1}{2} \cdot a_1 \cdot (t_1)^2, \text{when } t_1 < t_3 \text{ and } d_{AB} \ge \left(0.5 \cdot a_1 \cdot (t_1)^2\right) \\ z_B + \frac{1}{2} \cdot a_1 \cdot (t_x)^2, \text{ when } t_3 \le t_x < t_1 \text{ and } d_{AB} < \left(0.5 \cdot a_1 \cdot (t_1)^2\right) \end{cases}$	(6.95)
D	$z_D = z_C$	(6.96)
E	$z_E = \begin{cases} z_D - \frac{1}{2} \cdot a_1 \cdot (t_1)^2 - u_1 \cdot (t_3 - t_1), \text{ when } t_1 \le t_3 \\ z_D - \frac{1}{2} \cdot a_1 \cdot (t_3)^2, \text{ when } t_3 < t_1 \end{cases}$	(6.97)
F	$z_F = \frac{T_{st} + T_{end}}{2} + con_h + cl$	(6.98)
G	$z_G = z_H - \frac{1}{2} \cdot a_2 \cdot (t_2)^2$	(6.99)
H	$z_H = z_I$	(6.100)
I	$z_I = z_J + \frac{1}{2} \cdot a_2 \cdot (t_2)^2$	(6.101)
J	$z_J = z_A + con_h + 0.5$	(6.102)

Note: The values of 0.5m and 1.0m at the z-coordinates of points J and B, respectively, are taken for safety reasons.

where, the various magnitudes have been defined in the previous sections.

Below deck:

For the below deck TEUs, the coordinates of the most control points for each separate 40ft bay are the same as in Table 6.12. The points with different parametric coordinates were calculated as follows:

Table 6.13: Coordinates of control points for the below deck TEU, in the case of loading using SSPC units.

Point	Y-coordinate	
A	$y_A=TCG_c^{holds}$	(6.103)
	Z-coordinate	
A	$z_A=VCG_c^{holds}+\frac{con_h}{2}$	(6.104)
B	$z_B=D+h_{HC}$	(6.105)
J	$z_J=D+h_{HC}+con_h$	(6.106)

where, the various magnitudes have been defined in the previous section.

From this point and onwards, the procedure is identical to the one described in the unloading cycle (see sub-section 6.2.1.1).

Chapter 7

Techno-Economic Assessment

At this point, since the definitions of the main data of the vessels have been analyzed, the techno-economic assessment can follow. This stage is very critical, in order to evaluate the investment. As mentioned above, the analysis was made from the perspective of a ship owner. The objective of the assessment was to calculate the annual number of transported TEUs, the estimation of the fuel and lubricants consumption of the vessel and the determination of the transportation cost for each TEU for a specific route. For this reason, the Fuel Cost per TEU (FCT) index was introduced, which was based on the idea of the required cost of transporting goods; in this case, containers. For the calculation of the required cost of transporting containers to be more accurate, the total annual costs of the vessel should be estimated. However, the total annual cost can be divided into the following subcategories:

- Capital cost –based mainly on the building cost of the ship
- Fuel cost (consumption) – relative to the fuel consumed during two different states; underway and while located at ports. In each case, the load of the main and auxiliary engines varies. In this group of costs, the consumption of the lubricants is included
- Operation cost – consists of the expenses: crew cost, stores cost, maintenance cost, insurance cost, administration cost, port cost etc.

According to the above, the only category that may differ among cases is the fuel cost. The capital cost has been assumed constant for the various cases. It is based on the Lightship of the vessel and the materials used for the construction. A further design and strength analysis are needed, in order to make a more accurate determination of this cost. A typical difference in Lightship is 1000-1500 tons, for these cases[i]. A typical operation time of a vessel is 25 years. In addition, the operation costs have been considered constant between the various vessels' cases. One parameter that could not be defined was the port costs. At the moment, it is not clear how the port operators will determine the cost of the tariffs for the new design cranes (SSPCs). For these reasons, the capital and operation costs were excluded from the required cost of transporting containers calculation.

More precisely, the FCT calculation was based on the following formula:

$$FCT=\frac{(\text{Total annual fuel cost})}{(\text{Trips/Year})\cdot(\text{TEUs})} \tag{7.1}$$

---

[i] A study for steel prices was made according to (World Steel Prices, 2020) (Updated: 23^{th} of January 2020)

For the estimation of fuel cost, the determination of a specific route was needed. The chosen voyage was between the ports of Rotterdam and Shanghai (and vice versa), distance of 10525 sea miles passing by Suez Canal. The reasons these regions were chosen are, that ships of this type and size, usually, travel on Europe-Asia routes (Southbound), ranking in the top 15 largest ports in the world (Rotterdam: 11th in the World & 1st in Europe, Shanghai: 1st in the World) and also these ports have the ability to "receive" such vessels. At the same time, it was verified (according to the study of Appendix A) that there was no restriction on the passage of these vessels through the Suez Canal. In order to simplify the calculations, no intermediate ports (or stops) were taken into account, as the purpose of this Diploma Thesis was to compare the different designs.

The trip was divided into route time (the time needed to capture the distance from port A to port B) and port time (net operation time – only operation of loading/unloading is undertaken). It could also be considered a delay factor which may include any delays at the port due to conjunction on the terminal, as well as any delays during travel (refueling, damages, etc.). Because this factor is constant for each design, it was considered negligible and excluded from the study.

$$\text{(Trip Time)}=\text{(Route Time)}+\text{(Port Time)} \tag{7.2}$$

The calculations were made based on the following proposed methods; method A and B, respectively. It has been assumed that the vessel is fully loaded. For this reason, the ship is fully unloaded and fully loaded while remaining at port. During this time, any provisions and refueling are carried out by the stern. The ship begins its journey fully loaded.

To simplify the reading process, in the following sections 7.1, 7.2 and 7.3, “CSV” will be an abbreviation for Case Study Vessel and “NEW” for the proposed cases.

7.1 Method A

For CSV, the first step was to calculate the time needed for the vessel to capture the distance between the port A and port B (route time) with the maximum service speed (V_{max}). With the route time and port time (according to the procedure of Chapter 6) known, the trip time can be estimated. The trip time is calculated for each crane type. The port time is the total operation time (loading and unloading cycle). Then, the calculation of the annual number of trips is made (Trips/Year) and the result is rounded to the first decimal place for a more precise comparison. This value is multiplied by the total TEU capacity of the vessel and the annual number of transported containers is calculated (TEUs/Year). The next step is to calculate the annual fuel consumption and the cost of the Main and Auxiliary Engines fuels and lubricants (see Section 7.3). With all the above known, the FCT for the CSV can be determined.

For the NEW, the maximum service speed remains constant (V_{max}), thus the route time remains also constant. Then, the calculation of the trip time is made (the port time is different in this case and is expected less than the CSV). The procedure for the remaining calculations is identical to those that were made for the CSV.

It is crucial to mention that, all the above times are measured in hours (hr), the consumption in tons per hour (t/hr) and the cost in US dollars ($).

For a further understanding of the method, the algorithmic procedure is depicted below:

- $V_{CSV\ (ALL)} = V_{max} = V_{NEW\ (ALL)}$
- Calculate (Route Time) $_{CSV\ (ALL)}$ = f (Dist. AB, V_{max}) = (Route Time) $_{NEW\ (ALL)}$
- Calculate (Port Time) $_{CSV\ (ALL)}$ = (T_{unl} + T_{load}) $_{CSV\ (ALL)}$
- Calculate (Trip Time) $_{CSV\ (ALL)}$ = f (Route Time, Port Time) $_{CSV\ (ALL)}$
- Calculate (Trips/Year) $_{CSV\ (ALL)}$ = f (Trip Time) $_{CSV\ (ALL)}$
- Calculate (TEU/Year) $_{CSV\ (ALL)}$ = f (TEUs, Trips/Year) $_{CSV\ (ALL)}$
- Calculate (Port Time) $_{NEW\ (ALL)}$ = (T_{unl}+T_{load}) $_{NEW\ (ALL)}$ < (Port Time) $_{CSV\ (ALL)}$
- Calculate (Trip Time) $_{NEW\ (ALL)}$ = f (Route Time, Port Time) $_{NEW\ (ALL)}$
- Calculate (Trips/Year) $_{NEW\ (ALL)}$ = f (Trip Time) $_{NEW\ (ALL)}$
- Calculate (TEU/Year) $_{NEW\ (ALL)}$ = f (TEUs, Trips/Year) $_{NEW\ (ALL)}$
- Calculate for both cases (CSV, NEW) consumption and costs (according to Section 7.3)
- Calculate for both cases (CSV, NEW) the FCT ($/TEU)
- Compare FCTs

Where, “f (…)” means one magnitude as a function of another. Indicators “SSG”, “SSPC”, “ALL” refer to the types of operating cranes. Indicator “ALL” shows that the parameter applies to both the SSG and the SSPC concept.

Note: Modifications can be made and instead of a maximum speed (V_{max}), it could be considered a slower service speed (e.g. 16 knots), based on the idea of "slow steaming". Such change will affect the outcome quantitatively rather than qualitatively, as designs are compared.

7.2 Method B

Method B is similar to method A. The only difference is that the annual number of trips (Trips/Year) for NEW vessels for any crane type equals to the respective annual number of the CSV, when SSGs are operated. In method A, the maximum service speed (V_{max}) was assumed constant. For this reason, the service speed of the new design vessels must be determined. All the other steps are identical to those in method A.

For a further understanding of the method, the algorithmic procedure is depicted below:

- $V_{CSV\ (SSG)} = V_{max}$
- Calculate (Route Time) $_{CSV\ (SSG)}$ = f (Dist. AB, V_{max}) $_{CSV\ (SSG)}$
- Calculate (Port Time) $_{CSV\ (SSG)}$ = (T_{unl} + T_{load}) $_{CSV\ (SSG)}$
- Calculate (Trip Time) $_{CSV\ (SSG)}$ = (Route Time + Port Time) $_{CSV\ (SSG)}$
- Calculate (Trips/Year) $_{CSV\ (SSG)}$ = f (Trip Time) $_{CSV\ (SSG)}$ = (Trips/Year) $_{CSV\ (SSPC)}$ =(Trips/Year) $_{NEW\ (ALL)}$
- Calculate (TEU/Year) $_{CSV\ (ALL)}$ = f (TEUs, Trips/Year) $_{CSV\ (ALL)}$
- Calculate (Trip Time) $_{CSV\ (SSPC)}$ = f (Trips/Year) $_{CSV\ (SSPC)}$
- Calculate (Port Time) $_{CSV\ (SSPC)}$ = (T_{unl} + T_{load}) $_{CSV\ (SSPC)}$
- Calculate (Route Time) $_{CSV\ (SSPC)}$ = f (Trips/Year, Port Time) $_{CSV\ (SSPC)}$

- Calculate $V_{CSV\ (SSPC)}$ = f (Dist. AB, Route Time) $_{CSV\ (SSPC)}$
- Calculate (Trip Time) $_{NEW\ (ALL)}$ = f (Trips/Year) $_{NEW\ (ALL)}$
- Calculate (Port Time) $_{NEW\ (ALL)}$ = (T_{unl} + T_{load}) $_{NEW\ (ALL)}$
- Calculate (Route Time) $_{NEW\ (ALL)}$ = f (Trip Time, Port Time) $_{NEW\ (ALL)}$
- Calculate $V_{NEW\ (ALL)}$ = f (Route time, Distance AB) $_{NEW\ (ALL)}$
- Calculate (TEU/Year) $_{NEW\ (ALL)}$ = f (TEUs, Trips/Year) $_{NEW\ (ALL)}$
- Calculate for both cases (CSV, NEW) consumption and costs (according to Section 7.3)
- Calculate for both cases (CSV, NEW) the FCT ($/TEU)
- Compare FCTs

Where, "f (…)" means one magnitude as a function of another. Indicators "SSG", "SSPC", "ALL" refer to the types of operating cranes. Indicator "ALL" shows that the parameter applies to both the SSG and the SSPC concept.

7.3 Calculation of consumption and fuel costs

For both methods A and B, the estimation of consumption and fuel costs were needed. The procedure of calculations is similar for both methods. The calculation of consumption was divided into two levels. In the first one, the consumption was calculated as long as the ship is in underway condition (at sea) and in the second, for the time remaining at port (at harbor). In both levels the fuel and lubricant consumption of the Main Engine (ME) and the Auxiliary Engines (AE) are calculated.

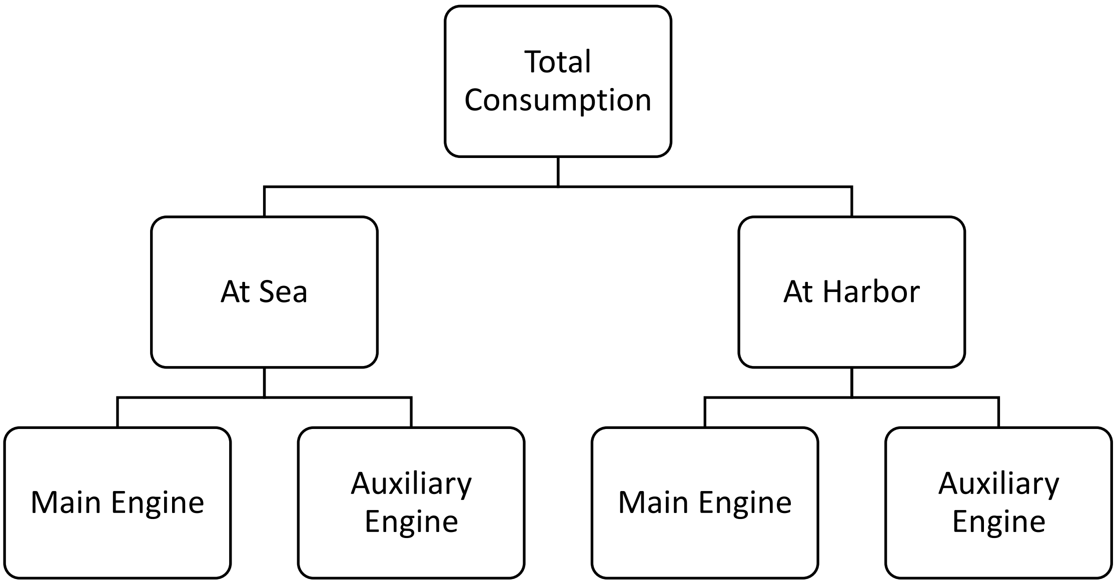

Figure 7.1: Flow chart of consumption calculations

For the underway condition (at sea), the ME operates at 100 % load of the Maximum Continuous Rating (100 % load MCR) and the AE at the 30 % of the installed power (30 % P_{AE}). Throughout this time, 90% of the voyage, the vessel is operated using Very Low Sulfur Fuel Oil (VLSFO) and the remainder with Low Sulfur Marine Gas Oil (LSMGO) due to coastal areas along the route. These types of fuels were selected in order to comply with the Regulations of IMO on the reduction of Sulphur emissions from the exhaust gases. Other types of fuels and the operation of scrubbers could be taken into consideration. However, at the present study, the aim was to compare different vessels' designs and not to find the optimum solution to comply with the regulation "Sulphur Cap 2020".

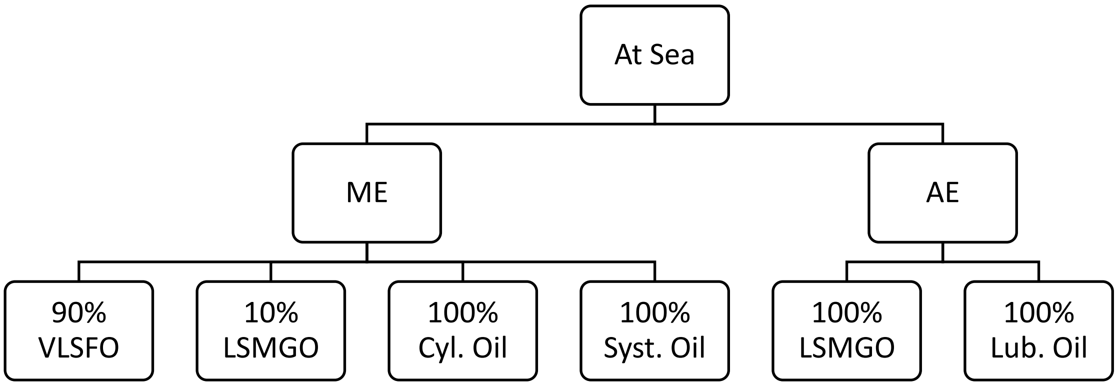

Figure 7.2: Analysis of consumption factors when the ship is in underway condition.

Respectively, when the vessel remains at port, the ME is operated at the 25 % load and the AE at the 95 % load. At this condition, only LSMGO is used.

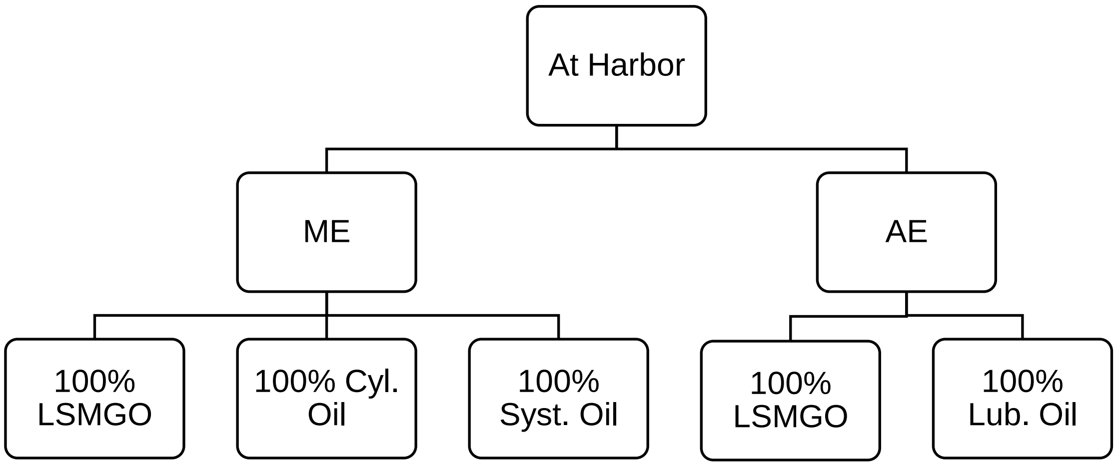

Figure 7.3: Analysis of consumption factors when the ship is at port.

In general, the consumption rate is calculated as:

$$\dot{m}=\frac{b \cdot P}{10^6} \tag{7.3}$$

where, $\dot{m}$: consumption rate (t/hr)
b: specific consumption (gr/kWh)
P: power (kW)

The total consumption was estimated by the following formula:

$$C=\sum_i \dot{m}_i \cdot t_i^{sea} \cdot K_i + \sum_j \dot{m}_j \cdot t_j^{harbor} \cdot K_j \tag{7.4}$$

where, C: total consumption ($)
t^{sea}: time at underway condition (hr)
K: cost of fuel or lubricant per ton ($/ton)
t^{harbor}: time at port (hr)
i: number of factors in underway condition
j: number of factors when the ship is at port

The specific consumption of fuel is depicted in the manufacturer's project guides of the ME and the AE regarding standard fuel (ISO). The specific consumption of the fuels under study was calculated in proportion to their calorific values (Hu- kJ/kg):

$$b_{Fuel}=b_{ISO} \cdot \left(\frac{Hu_{\ ISO}}{Hu_{\ Fuel}}\right) \tag{7.5}$$

The calorific values were obtained as:

Table 7.1: Calorific values of fuels. Source: (MAN B&W, 2019) (DNV-GL)

Hu_{ISO}	42700	kJ/kg
Hu_{VLSFO}	41000	kJ/kg
Hu_{LSMGO}	45000	kJ/kg

The lubricants were divided in: cylinder and system oil for the ME and in lubricant oil for the AE. Usually, the specific consumption of lubricants is found in the manufacturers' project guides for the ME and the AE. For the present study, the specific consumptions that were taken, are depicted below:

Table 7.2: Specific consumption of lubricants.

Cyl. Oil @ ME	0.6	gr/kWh
Syst. Oil @ ME	6.0	kg/day/cylinder
Lub. Oil @ AE	0.7	gr/kWh

The costs of the fuels and of the lubricants are presented in the following table:

Table 7.3: Fuel oil and lubricants costs. (Updated 27th December 2019). Source: (LiveBunkers)

	Rotterdam ($/ton)	Shanghai ($/ton)	Average ($/ton)
VLSFO	573.0	626.0	599.5
LSMGO	592.0	725.0	658.5
Cyl. Oil	4400.0	4400.0	4400.0
Syst. Oil/Lub. Oil	5180.0	5180.0	5180.0

Chapter 8

Numerical Simulations – Case Studies

In this chapter the two case study vessels and their results are presented. Utilizing the calculations and the tools described in Chapters 5, 6 and 7 to accomplish the aim of the Thesis. The main objective of the study was to investigate the possible changes in the principal dimensions of large container vessels, in order to comply better with the COFASTRANS system for loading/unloading from both sides. The analysis was made for a 14000 TEUs vessel (14K) and for a 20000 one (20K). For each case, six new design sub-scenarios have been proposed (see Section 4.4). The results of each scenario are depicted below. In addition, the case study vessels' data used for the calculations are presented in the following sections. A further discussion of the results is made in Chapter 9.

8.1 Case Study A: 14000 TEU Vessel

The necessary data of the 14K case study vessel was obtained from the ship-owning company. The basic magnitudes that were used in the calculations are listed below:

Table 8.1: Basic magnitudes for 14K case study vessel.

	Magnitude	Symbol	Value
Principal Dimensions	Length overall	L_{OA} (m)	368.991
	Length between perpendiculars	L_{BP} (m)	353
	Beam at amidships	B (m)	51
	Depth	D (m)	29.9
	Draught @ full load	T_{st} (m)	15.822
	Draught @ ballast condition	T_{end} (m)	8.906
	Air draught from keel	H (m)	65
Main & Auxiliary Engines	Service speed	V_S (kn)	23
	Main Engine	1 x MAN D&T 11S90ME-C10.2	
	Power	P (kW)	49200
	Generators	4 x Himsen 7H32/40	
	Each Generator Power	P_{AE} (kW)	3360
Coefficients	Block	C_B	0.6765
	Water plane area	C_{WL}	0.8645
	Mid-ship section	C_M	0.9811
	Prismatic	C_P	0.6895
Weights	Lightship	LS (t)	43950
	Deadweight	DWT (t)	153631
	Displacement	Δ (t)	197581
Bay plan information	Capacity	TEU	14424
	Number of 40ft bays	$Bays_n$	22
	Maximum number of above deck container rows	$rows_d$	20
	Maximum number of below deck container rows	$rows_h$	18
	Maximum number of above deck container tiers	$tiers_d$	11
	Maximum number of below deck container tiers	$tiers_h$	11
Other	Double bottom height	h_{DB} (m)	2.3
	Height of hatch covers	h_{HC} (m)	2.88
	Transverse spacing	s (m)	2.52
	Transverse sectional area of the bulb	A_{BT} (m^2)	43
	Immersed part of the transverse area of the transom at zero speed	A_T (m^2)	21.83
	Bow thruster diameter	d_b (m)	2.3
	Deck thickness at side	t (mm)	150

All necessary information about compartments and superstructure was obtained from the Trim and Stability Booklet (T&S) and the General Arrangement (GA), respectively. The detailed bay plan was needed in order to incorporate the case study vessel into the developed algorithm (see Chapter 6).

Firstly, the preliminary design calculations (see Chapter 5) were undertaken in order to define the basic data of the proposed cases. The obtained results are depicted in the following table.

Table 8.2: Results of basic data for each 14K vessel.

Magnitudes	Case Study A	Case 1.1	Case 1.2	Case 2.1	Case 2.2	Case 3.1	Case 3.2
TEUs[i]	14424	14492	14446	14456	14466	14522	14428
L_{BP} (m)	353	353	353	338.3	323.7	338.3	323.7
B (m)	51	53.6	56	53.6	56	56	61
D (m)	29.9	27.3	24.7	29.9	29.9	27.3	24.7
L/B	6.92	6.59	6.30	6.31	5.78	6.04	5.30
B/T	3.22	3.55	3.86	3.42	3.58	3.72	4.22
L/D	11.8	12.93	14.29	11.31	10.83	12.39	13.1
C_B	0.6765	0.6765	0.6765	0.6765	0.6765	0.6765	0.6765
C_{WL}	0.8645	0.8645	0.8645	0.8645	0.8645	0.8645	0.8645
DWT (t)	153631	153631	153631	153631	153631	153631	153631
W_{HULL} (t)	31226	31409	31490	30807	30196	30885	30442
W_{OUT} (t)	6794	7172	7536	6922	7007	7274	7698
W_M (t)	5930	5941	5953	5924	5913	5934	5930
LS (t)	43950	44522	44979	43653	43117	44094	44070
Δ (t)	197581	198153	198610	197285	196748	197725	197701
T_{ST} (m)	15.822	15.1	14.49	15.69	15.65	15.05	14.44
T_{END} (m)	8.906	8.52	8.19	8.82	8.78	8.47	8.13
T_{IILC} (m)	20.12	18.77	16.46	20.74	20.70	18.74	16.72
V_S (kn)	23	23	23	23	23	23	23
γ_{homo} (t/TEU)	7.64	7.74	7.92	7.62	7.61	7.72	7.93
GM @ FLD (m)	0.64	3.84	7.08	2.39	4.02	5.56	11.69
GM @ FLA (m)	0.87	4.09	7.35	2.65	4.30	5.83	12.00
Req.EEDI ($grCO_2$/tnm)	11.06	11.06	11.06	11.06	11.06	11.06	11.06
Att. EEDI ($grCO_2$/tnm)	9.08	9.28	9.50	9.31	9.56	9.51	9.85
EIV ($grCO_2$/tnm)	10.72	10.96	11.22	10.99	11.29	11.23	11.63
Rtotal (kN)	2702.8	2774.8	2854.6	2783.6	2872.0	2858.5	2978.3
EHP (kW)	31980.0	32832.2	33776.1	32936.3	33981.9	33822.0	35240.3
SHP_{real} (kW)	49200.0	50511.0	51963.4	50671.2	52279.9	52033.9	54215.9

Note: With red color the EEDI values that do not comply to the requirements are mentioned. The EHP magnitude is related with the SHP_{real} by the propulsive coefficient (P.C.).

[i] In more accurate design stages, the total number of TEUs will be slightly different.

Comments: Increasing the beam of the vessels, was expected to lead to greater resistance and better stability. However, increasing resistance means greater propulsion power demand (SHP) and therefore higher fuel consumption (qualitatively), which will be quantified by the techno-economic analysis. The stability is expressed by the GM index (see section 5.6), which in some cases is extremely large. This is a major problem for such ships. Large GM values trigger intense roll motions (parametric rolling) and transverse accelerations on the ship's deck, in other words these values make the ship stiffer. It can cause nausea or injuries to passengers and crew and the shift or damage of higher up stacked cargo. However, it does not mean that these ships should not be built. In order to decrease GM, stronger lashing systems or additional above deck tiers are required. The stronger lashing systems will increase the Lightship. Furthermore, adding an extra above deck tier will increase the ship's capacity, but this is not within the scope of the present analysis.

Another issue is that in some cases the Estimated Index Value (EIV) is greater than the required EEDI. This was expected, due to the greater power demand of the proposed cases. However, a service speed reduction or the introduction of Power Take-Off (PTO) and Power Take-In (PTI) systems are needed in order to meet the requirements. However, at this point the calculated EEDI is not so accurate, due to lack of data. In further design stages, a more precise calculation could be made.

In the following figure, the relationship between the main dimensions of the proposed cases and those resulting from literature statistical analysis are illustrated. It is observed that the proposed designs are different from the conventional ones.

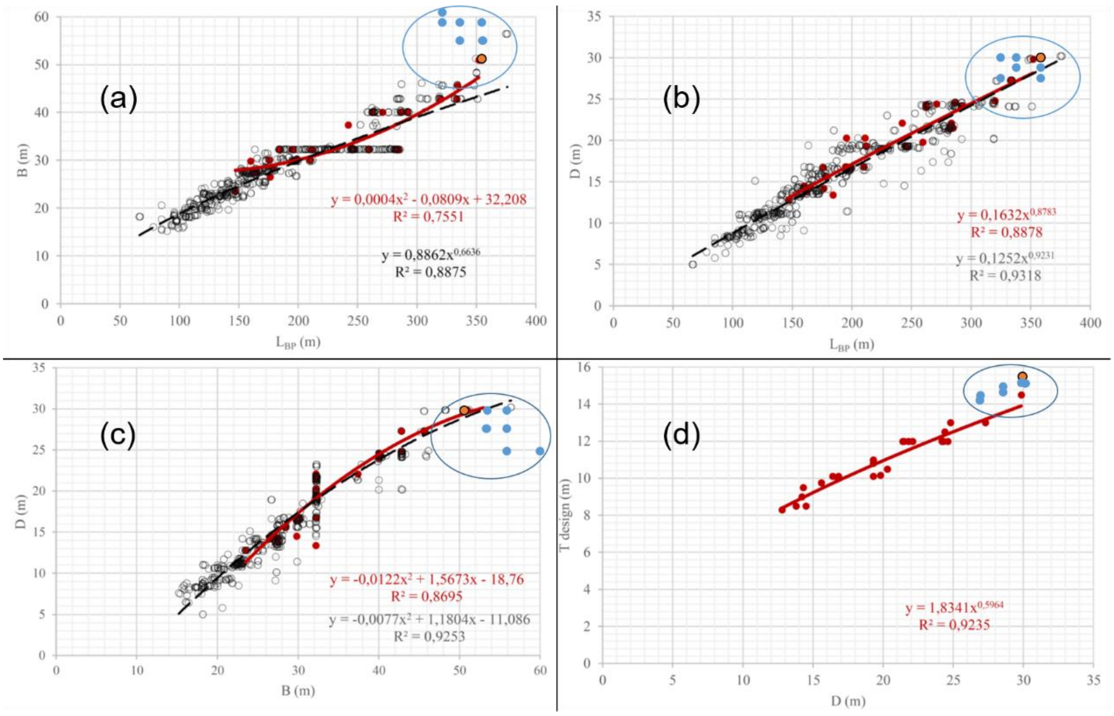

Figure 8.1: Relationship between the main dimensions of the proposed 14K cases and those resulting from statistical analysis. With orange color the case study vessel A is mentioned. Diagrams: (a) B-L_{BP}, (b) D-L_{BP}, (c) D-B, (d) T_{Design}-D. Source: (Chrysikopoulos, 2016)

After the determination of the alternative cases' main data, the calculations of operation times were conducted. The obtained results for each operation (unloading, loading and total) and for each case are presented in Table 8.3, Table 8.4 and Table 8.5, respectively. It is reminded that there are two types of SSPC units, with different indented berths' widths; Type A and Type B. The Case 3.2 vessel cannot enter the indented berth of SSPC Type A unit due to her beam. A clearance between vessel's beam and indented berth's width is needed.

In the following tables, the "Crane Type" column represents the crane type used for the operation and the "No." column, the number of cranes deployed along the vessel. The "Max. Cycle Time (sec)" column shows the maximum cycle time observed for above deck (Deck) and below deck (Holds) TEUs. The maximum cycle time is a very essential parameter for the operation. Further details will be described below. The "Tot. Time (hr)" column represents the total time of the operation. The percentage difference in total times with respect to the SSG concept and to the case study vessel A are presented in the last two columns, respectively.

Table 8.3: Unloading times results for 14K cases.

Ship	Crane Type	No.	Max. Cycle Time (sec)		Tot. Time (hr)	Percentage Difference with respect to the SSG concept	Percentage Difference with respect to the Case Study A
			Deck	Holds			
Case Study A	SSG	6	94.27	96.19	21.55	0.0	0.0
	SSPC (A)	3	105.26	108.18	14.49	32.8	0.0
		4			10.69	50.4	0.0
	SSPC (B)	3	111.02	113.94	15.28	29.1	0.0
		4			11.27	47.7	0.0
Case 1.1	SSG	6	92.86	93.47	21.08	0.0	2.1
	SSPC (A)	3	103.26	104.86	14.92	29.2	-3.0
		4			11.02	47.7	-3.1
	SSPC (B)	3	109.02	110.62	15.76	25.3	-3.1
		4			11.64	44.8	-3.3
Case 1.2	SSG	6	91.32	90.61	20.49	0.0	4.9
	SSPC (A)	3	99.92	100.23	13.68	33.3	5.6
		4			10.10	50.7	5.5
	SSPC (B)	3	105.68	105.99	14.44	29.6	5.5
		4			10.66	48.0	5.4
Case 2.1	SSG	6	95.02	96.92	22.61	0.0	-4.9
	SSPC (A)	3	105.41	108.30	16.08	28.9	-11.0
		4			11.67	48.4	-9.2
	SSPC (B)	3	111.17	114.06	16.96	25.0	-11.0
		4			12.31	45.5	-9.3
Case 2.2	SSG	6	95.65	97.55	21.73	0.0	-0.9
	SSPC (A)	3	104.24	107.13	13.95	35.8	3.8
		4			10.31	52.5	3.5
	SSPC (B)	3	110.00	112.89	14.70	32.4	3.8
		4			10.86	50.0	3.6
Case 3.1	SSG	6	93.50	94.10	22.32	0.0	-3.6
	SSPC (A)	3	102.09	103.69	14.76	33.9	-1.8
		4			10.70	52.0	-0.2
	SSPC (B)	3	107.85	109.45	15.56	30.3	-1.8
		4			11.28	49.4	-0.2
Case 3.2	SSG	6	90.60	87.88	20.02	0.0	7.1
	SSPC (B)	3	102.55	100.84	13.07	34.7	14.4
		4			9.77	51.2	13.3

Note: Light green color denote cells for which operation time is reduced, while pink color and negative sign (-) denote increase of operation time.

Table 8.4: Loading times results for 14K cases.

Ship	Crane Type	No.	Max. Cycle Time (sec)		Tot. Time (hr)	Percentage Difference with respect to the SSG concept	Percentage Difference with respect to the Case Study A
			Deck	Holds			
Case Study A	SSG	6	96.27	98.19	21.99	0.0	0.0
	SSPC (A)	3	107.26	110.18	14.76	32.9	0.0
		4			10.89	50.5	0.0
	SSPC (B)	3	113.02	115.94	15.52	29.4	0.0
		4			11.45	48.0	0.0
Case 1.1	SSG	6	94.86	95.47	21.54	0.0	2.0
	SSPC (A)	3	105.26	106.86	15.24	29.3	-3.2
		4			11.25	47.8	-3.3
	SSPC (B)	3	111.02	112.62	16.04	25.6	-3.4
		4			11.84	45.1	-3.4
Case 1.2	SSG	6	93.32	92.61	20.97	0.0	4.6
	SSPC (A)	3	101.92	102.23	13.92	33.6	5.7
		4			10.28	51.0	5.6
	SSPC (B)	3	107.68	107.99	14.72	29.8	5.2
		4			10.87	48.2	5.1
Case 2.1	SSG	6	97.02	98.92	23.09	0.0	-5.0
	SSPC (A)	3	107.41	110.30	16.40	29.0	-11.1
		4			11.90	48.4	-9.3
	SSPC (B)	3	113.17	116.06	17.24	25.3	-11.1
		4			12.51	45.8	-9.3
Case 2.2	SSG	6	97.65	99.55	22.21	0.0	-1.0
	SSPC (A)	3	106.24	109.13	14.19	36.1	3.9
		4			10.49	52.8	3.6
	SSPC (B)	3	112.00	114.89	14.95	32.7	3.7
		4			11.04	50.3	3.5
Case 3.1	SSG	6	95.50	96.10	22.81	0.0	-3.7
	SSPC (A)	3	104.09	105.69	15.04	34.1	-1.3
		4			10.90	52.2	-0.2
	SSPC (B)	3	109.85	111.45	15.88	30.4	-2.3
		4			11.51	49.5	-0.6
Case 3.2	SSG	6	92.60	89.88	20.47	0.0	6.9
	SSPC (B)	3	104.55	102.84	13.34	34.8	14.0
		4			9.96	51.3	13.0

Note: Light green color denote cells for which operation time is reduced, while pink color and negative sign (-) denote increase of operation time.

Table 8.5: Total operation times results for 14K cases.

Ship	Crane Type	No.	Tot. Time (hr)	Percentage Difference with respect to the SSG concept	Percentage Difference with respect to the Case Study A
Case Study A	SSG	6	43.54	0.0	0.0
	SSPC (A)	3	29.25	32.8	0.0
		4	21.58	50.5	0.0
	SSPC (B)	3	30.80	29.3	0.0
		4	22.72	47.8	0.0
Case 1.1	SSG	6	42.63	0.0	2.1
	SSPC (A)	3	30.16	29.3	-3.1
		4	22.27	47.8	-3.2
	SSPC (B)	3	31.80	25.4	-3.3
		4	23.48	44.9	-3.4
Case 1.2	SSG	6	41.47	0.0	4.8
	SSPC (A)	3	27.60	33.5	5.7
		4	20.38	50.9	5.6
	SSPC (B)	3	29.16	29.7	5.3
		4	21.53	48.1	5.2
Case 2.1	SSG	6	45.70	0.0	-4.9
	SSPC (A)	3	32.48	28.9	-11.0
		4	23.58	48.4	-9.3
	SSPC (B)	3	34.20	25.2	-11.0
		4	24.83	45.7	-9.3
Case 2.2	SSG	6	43.95	0.0	-0.9
	SSPC (A)	3	28.13	36.0	3.8
		4	20.81	52.7	3.6
	SSPC (B)	3	29.64	32.6	3.8
		4	21.91	50.2	3.6
Case 3.1	SSG	6	45.13	0.0	-3.6
	SSPC (A)	3	29.80	34.0	-1.9
		4	21.61	52.1	-0.2
	SSPC (B)	3	31.44	30.3	-2.1
		4	22.80	49.5	-0.4
Case 3.2	SSG	6	40.50	0.0	7.0
	SSPC (B)	3	26.42	34.8	14.2
		4	19.74	51.3	13.1

Note: Light green color denote cells for which operation time is reduced, while pink color and negative sign (-) denote increase of operation time.

In the following figures (8.2-8.6) the unloading (blue), loading (orange) and total times (grey) for the various 14K vessels' cases and for the various concepts are illustrated in charts. The diagrams assist to draw conclusions about operation times. Figure 8.2 shows the unloading, loading and total times for 14K ships cases when six SSG cranes are deployed. Figure 8.3 illustrates the unloading, loading and total times for 14K ships cases, when three Type A SSPC units are deployed and Figure 8.4 the case of four Type A SSPC units deployed along the vessels. In the same way, Figure

8.5 shows the unloading, loading and total times for 14K ships cases when three Type B SSPC units are deployed and Figure 8.6 the case of four Type B SSPC units deployed along the vessels.

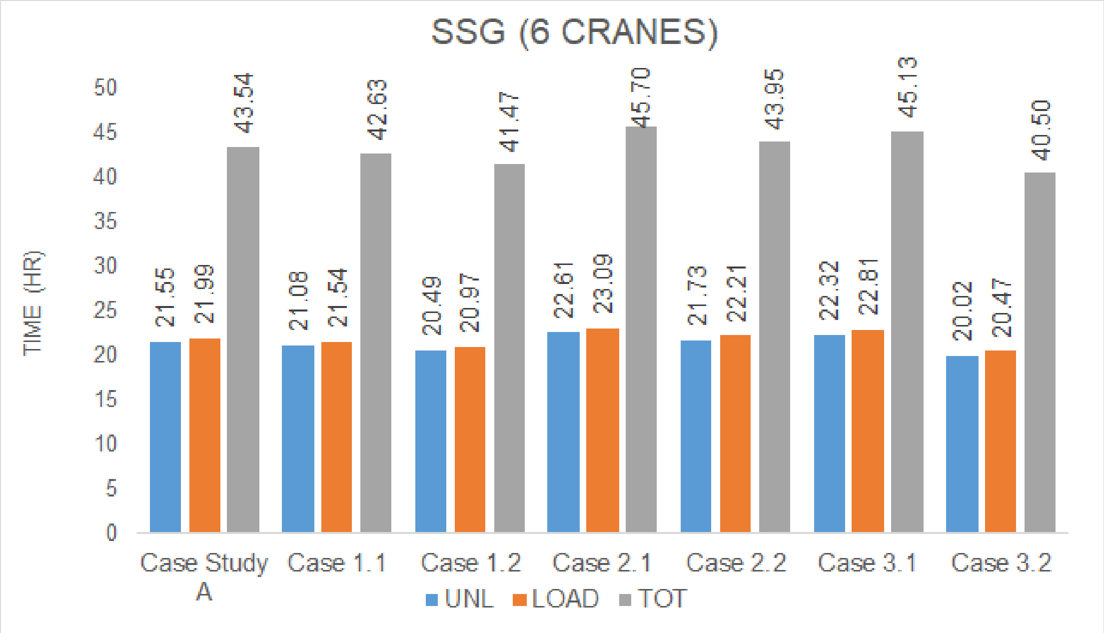

Figure 8.2: Unloading, Loading and Total times for 14K ship cases using 6 SSG cranes.

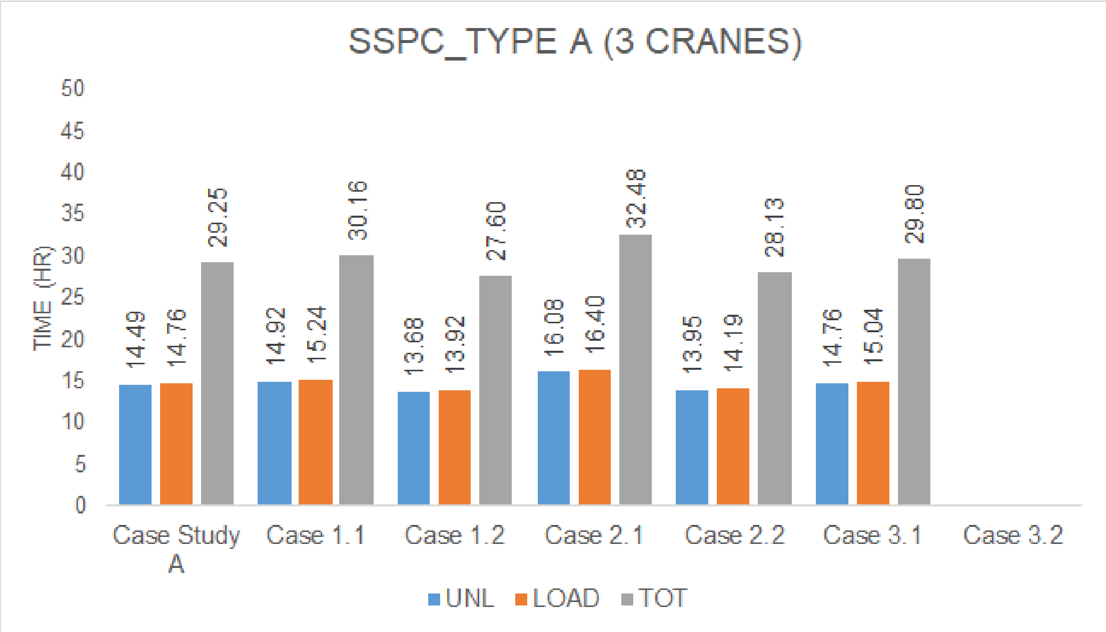

Figure 8.3: Unloading, Loading and Total times for 14K ship cases using 3 Type A SSPC units.

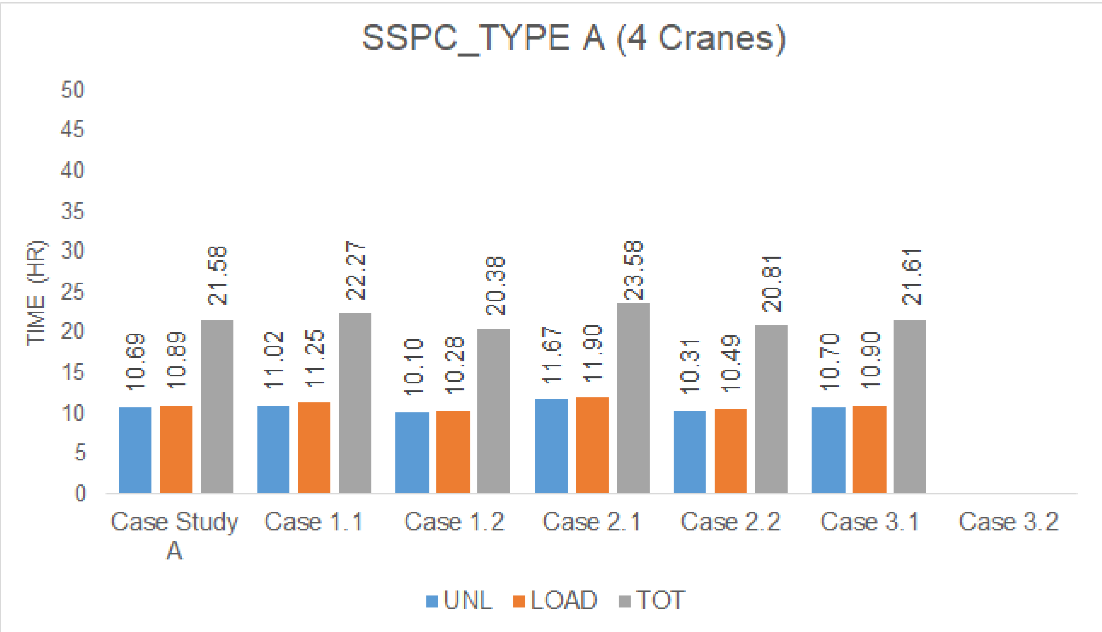

Figure 8.4: Unloading, Loading and Total times for 14K ship cases using 4 Type A SSPC units.

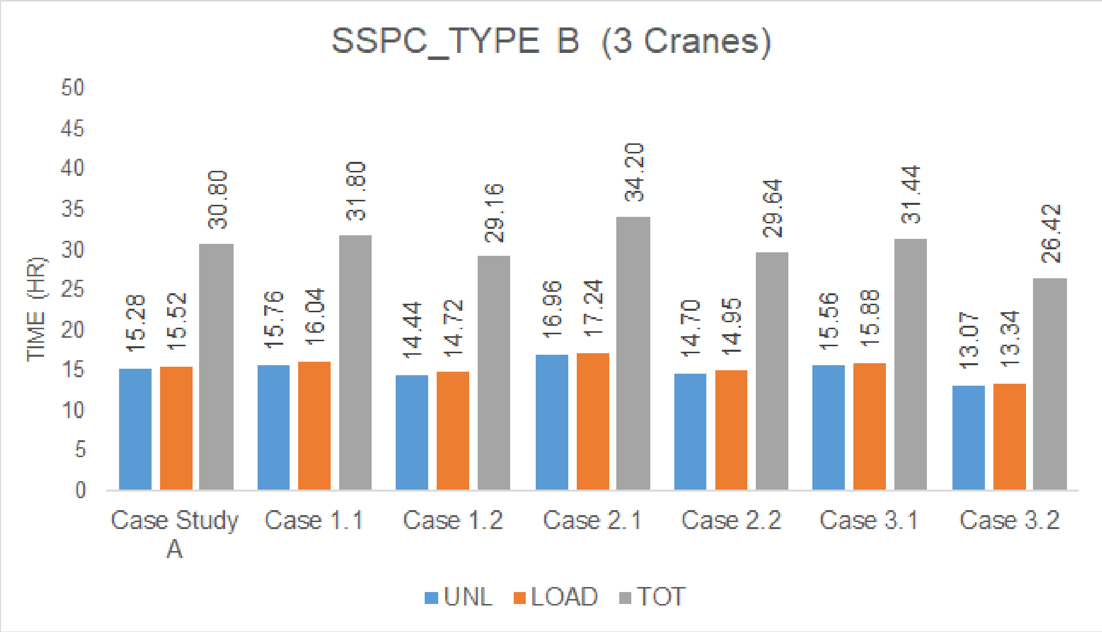

Figure 8.5: Unloading, Loading and Total times for 14K ship cases using 3 Type B SSPC units.

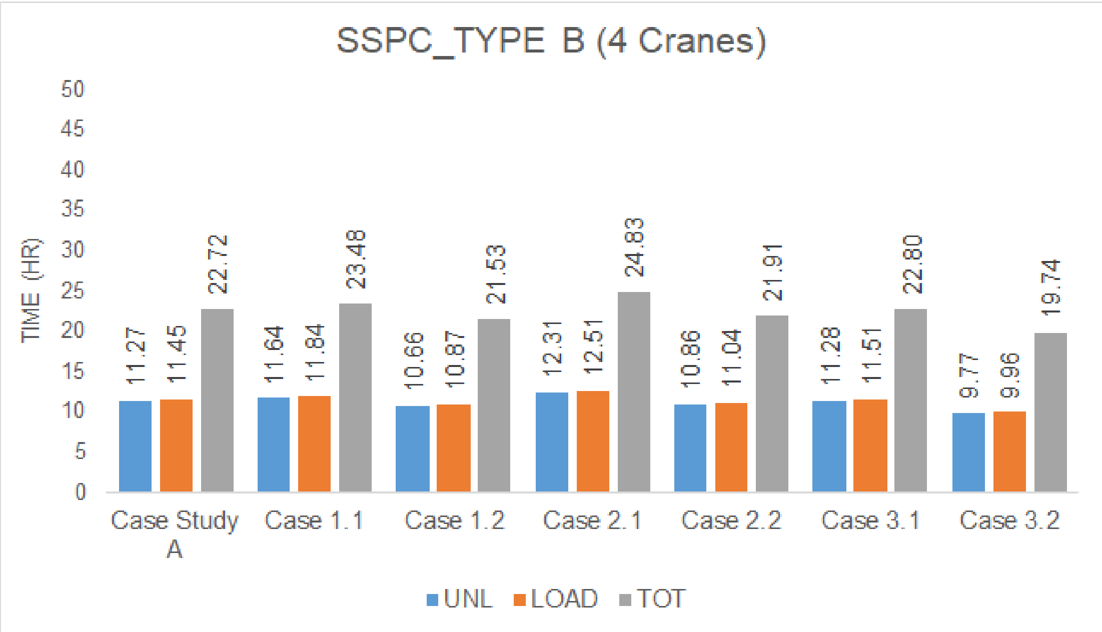

Figure 8.6: Unloading, Loading and Total times for 14K ship cases using 4 Type B SSPC units.

In the following figures (8.7 and 8.8), the comparison between the SSG cranes and Type A SSPC units (Figure 8.7) and Type B SSPC units (Figure 8.8) is illustrated.

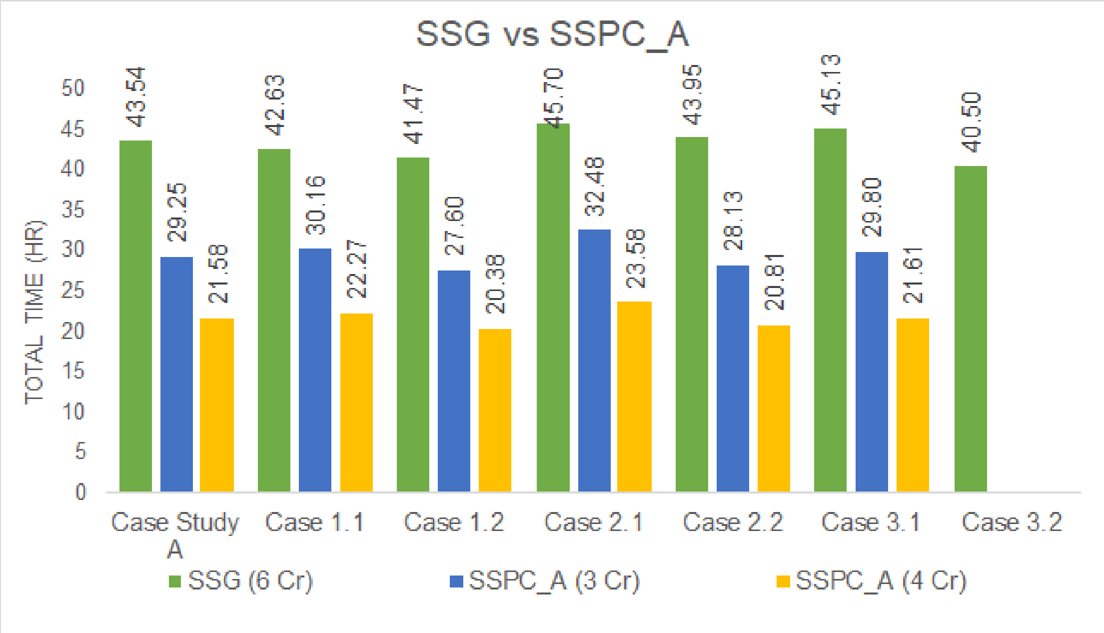

Figure 8.7: Comparison between the total operation times of SSGs and Type A SSPCs units in 14K cases.

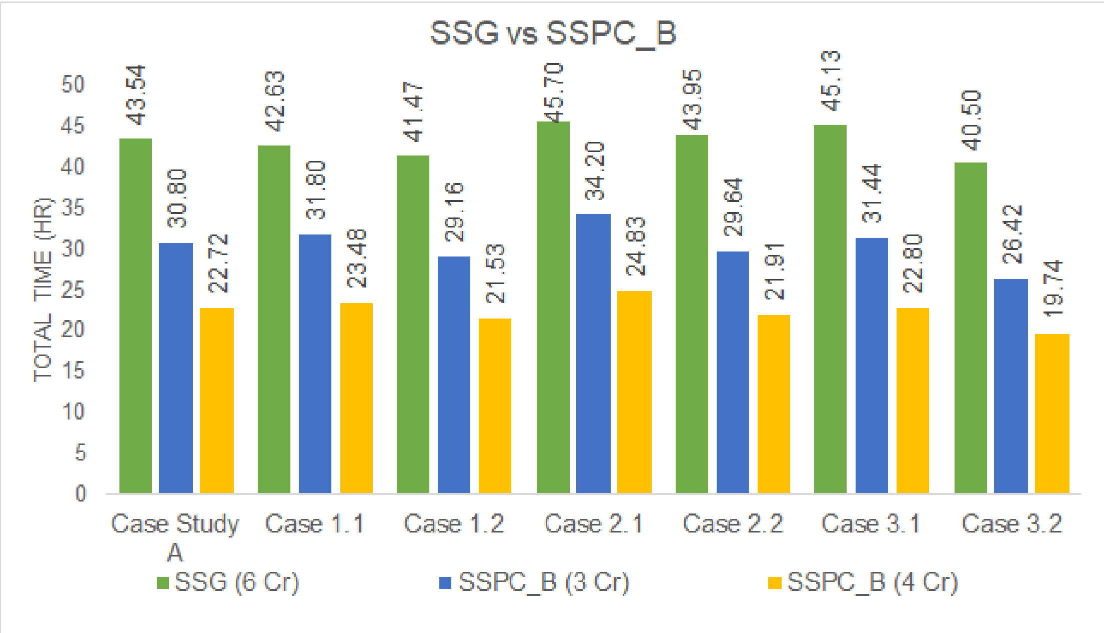

Figure 8.8: Comparison between the total operation times of SSGs and Type B SSPCs units in 14K cases.

Comments: From the above analysis it was confirmed that the use of new-concept cranes reduces the loading/unloading time. Therefore, the gain in time when using SSPCs compared to the usage of 6 conventional SSG cranes for loading/unloading the ship is almost 25-35 % in the case of 3 SSPCs, and almost 45-53% in the case of 4 SSPCs. The percentage reduction varies between cases and depends largely on the width of the berth. For this kind of vessels, the Type A SSPCs are preferred. In this case, the berth is narrower, so the containers are closer to the quayside (supposing unloading cycling) and the trolley has to cover a shorter distance than in the case of Type B SSPCs.

In figures 8.7 and 8.8, the blue color stands for the total operation times, when three cranes of Type A and Type B SSPC units used. From Figure 8.7, the maximum gain of time when three Type A SSPC cranes are deployed, in comparison to the usage of six SSG cranes, is observed in Case 2.2 vessel (36%). The minimum operation time is observed in Case 1.2 vessel (27.6 hr). From Figure 8.8, the maximum gain of time (34.8%) and the minimum operation time (26.42 hr) when three Type B SSPC cranes are deployed, in comparison to when six SSG cranes are deployed, are observed in Case 3.2 vessel. However, these differences are negligible in comparison with the case study vessel A, when three Type A and Type B SSPC units are deployed.

In the same way, the yellow color stands for the total operation times, when four cranes of Type A and Type B SSPC units are used. From Figure 8.7, the maximum gain of time when four Type A SSPC cranes are deployed, in comparison to when six SSG cranes are deployed, is observed in Case 2.2 vessel (52.7%). The minimum operation time is observed in Case 1.2 vessel (20.38 hr). From Figure 8.8, the maximum gain of time (51.3%) and the minimum operation time (19.74 hr) when three Type B SSPC cranes are deployed, in comparison to when six SSG cranes are deployed, are observed in Case 3.2 vessel. However, these differences are negligible compared to the case study vessel A, when four Type A and Type B SSPC units are deployed.

Final assessments of whether changes to the main dimensions of case study vessel A are appropriate were made after the techno-economic analysis, which is described in Chapter 7.

An increase of total operation times in some cases (1.1, 2.1 and 3.1) has been observed with respect to the case study vessel A when SSPC units are used. An expected result for all alternative cases was the reduction of total operation time, when SSPC units are used, due to the increase of the beam. For a wider vessel the distance between the quay and the vessel decreases, so the trolley has to cover shorter distances. However, the total operation time is increased. This phenomenon was first called “time paradox”. The times’ results are affected by several factors and it is impossible to build an equation that will include all these parameters and give a qualitative assessment of the times. For this reason, all the factors affecting the total operation times were identified and analyzed below.

Despite the crane concept, the total operation time depends on the number of 40ft bays (depending on the length of the ship) but also on the operation time of each 40ft bay. In case of SSPCs, apart from the total number of bays, the distribution of bays along the length of the ship also plays an important role; the number of bays in the forefront of the superstructure, the number of aft most of the funnel and the number of those in between.

The total loading/unloading times for each bay are the sum of the times required to load/unload the containers above and below the deck, expressed in terms of the number of containers (TEUs) and the time required for the spreader to make one move (cycle time). The general formula for calculating loading/unloading times is:

$$T=\frac{TEU \cdot CT}{3600 \cdot ex} \tag{8.1}$$

where, T: total loading/unloading time for each bay (hr)
TEU: the capacity of the bay (TEUs)
CT: cycle time, the time required for the spreader to make one move (sec)
ex: the number of TEU exchanged in one move and depends on the type of the spreader (TEU/move)

The proposed cases have the same capacity with the case study vessel, “i.e.” the total number of TEU capacity remains constant (Total TEU = constant). Consequently, from case to case the number of TEUs above and below deck is modified so that the total remains constant.

The cycle time depends on the coordinates of the geometric center of the bays (VCG, TCG). When conventional cranes are used, the increase of the vessel’s beam, typically, increases the bay's cycle time, while in new design cranes it reduces it. However, in some cases, this trend is not followed by the total operational time of each bay, due to the product of the bay’s TEU capacity by the cycle time. For instance, the Case 1.1 vessel takes longer to be loaded/unloaded when SSPC units are operated than the case study vessel, but the maximum cycle time is shorter. For Case 1.1 vessel, the beam was increased by one row, the depth was reduced by one tier and the length was considered constant (the same configuration plan of cranes is used). Inside the berth, each side of the vessel is closer to the quayside by almost half width of container than the case study vessel. The maximum number of rows is an odd number, so the port side trolley undertakes to load/unload the remaining row. The TCG fends off the quayside by almost half a distance of the transverse spacing than the case study vessel's one. The transverse spacing distance is almost equal to the width of a container. According to this, the cycle time was expected to be marginally longer. However, the VCG is lower by half a height of a container to the quayside, and this reduces the cycle time. In this case, the impact of VCG in cycle time is bigger than the TCG. Therefore, the maximum cycle time of Case 1.1 vessel is shorter than the case study one. When simultaneously changing of beam and depth is occurred, no qualitative conclusion about operation time can be drawn, though. This is why the maximum cycle time was mentioned above as “an essential parameter of the operation”.

The parameters that affect the “time paradox” phenomenon, are illustrated below:

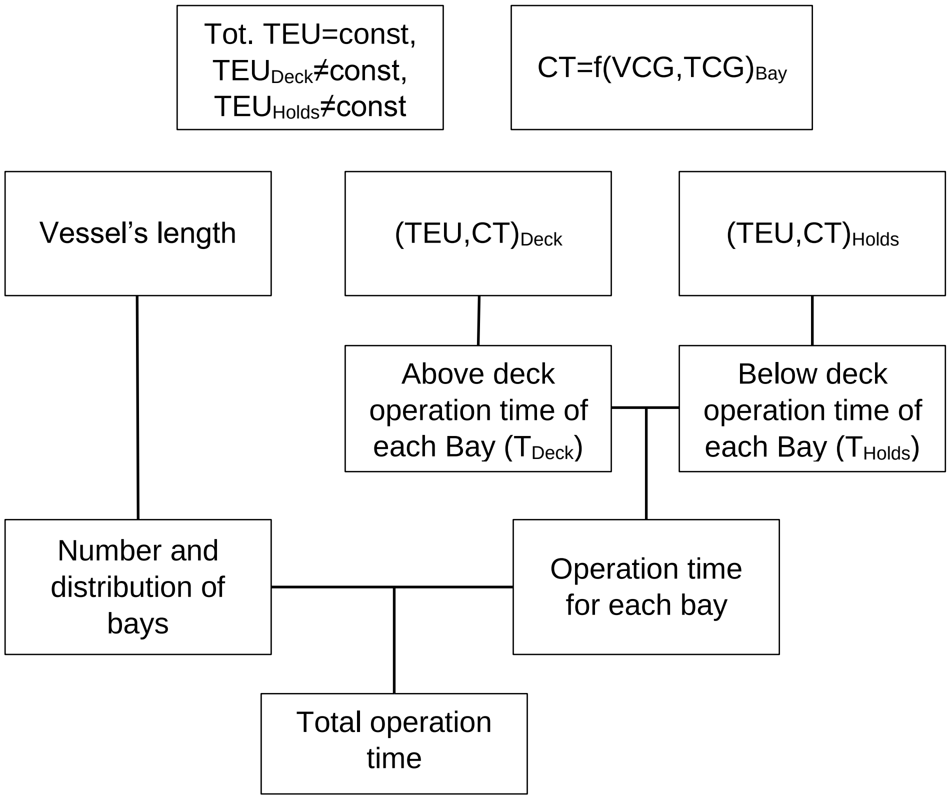

Figure 8.9: Schematic Analysis of the parameters that affect the total operation time.

In conventional cranes, the reduction of the depth has been observed as a very essential magnitude in reducing the cycle time, even when the beam was increased. In new-concept cranes, the simultaneous increase of the beam and decrease of the depth may reduce the cycle time, but no qualitative conclusions can be drawn in any case. A higher efficiency of the portal cranes can be achieved when the maximum number of rows is an even number. These remarks were made to offer a better understanding of the way that these magnitudes impact the total operation times.

After calculating the loading/unloading times, the techno-economic assessment was performed to quantify whether the investment is beneficial for the ship owners. The analysis was described in Chapter 7. The results of the assessment are depicted in the following tables.

The “Crane Type” column represents the crane type used for the operation and the “No.” column the number of cranes deployed along the vessel. The “V (kn)” column denotes the service speed of the vessels. The “Trips/Year” and “TEUs/Year” columns show the annual number of Trips and transported TEUs for each vessel, respectively. The annual consumption (based on the fuel costs) and the Fuel Costs per TEU are presented in the last two columns.

Table 8.6: Techno-Economic Assessment's results for 14K cases according to method A.

Ship	Crane Type	No.	V (kn)	Trips/ Year	TEUs/Year	Annual Consumption ($)	FCT ($/TEU)
Case Study A	SSG	6	23	17.4	251569	$45,912,842	182.51
	SSPC (A)	3		17.9	258798	$46,527,326	179.78
		4		18.2	263136	$46,922,200	178.32
	SSPC (B)	3		17.9	258798	$46,603,447	180.08
		4		18.2	263136	$46,979,356	178.54
Case 1.1	SSG	6	23	17.5	253610	$47,237,193	186.26
	SSPC (A)	3		17.9	259407	$47,694,424	183.86
		4		18.2	263754	$48,093,360	182.34
	SSPC (B)	3		17.8	257958	$47,509,378	184.18
		4		18.2	263754	$48,154,769	182.57
Case 1.2	SSG	6	23	17.5	252805	$48,403,574	191.47
	SSPC (A)	3		18.0	260028	$49,081,093	188.75
		4		18.3	264362	$49,525,812	187.34
	SSPC (B)	3		17.9	258583	$48,887,317	189.06
		4		18.2	262917	$49,314,315	187.57
Case 2.1	SSG	6	23	17.4	251534	$47,250,611	187.85
	SSPC (A)	3		17.8	257317	$47,679,704	185.30
		4		18.2	263099	$48,298,997	183.58
	SSPC (B)	3		17.8	257317	$47,765,202	185.63
		4		18.1	261654	$48,096,801	183.82
Case 2.2	SSG	6	23	17.4	251708	$48,514,417	192.74
	SSPC (A)	3		18	260388	$49,380,706	189.64
		4		18.3	264728	$49,823,997	188.21
	SSPC (B)	3		17.9	258941	$49,182,955	189.94
		4		18.2	263281	$49,608,461	188.42
Case 3.1	SSG	6	23	17.4	252683	$48,366,138	191.41
	SSPC (A)	3		17.9	259944	$48,980,172	188.43
		4		18.2	264300	$49,379,833	186.83
	SSPC (B)	3		17.9	259944	$49,063,168	188.75
		4		18.2	264300	$49,441,065	187.06
Case 3.2	SSG	6	23	17.5	252490	$50,251,733	199.02
	SSPC (B)	3		18	259704	$50,956,978	196.21
		4		18.3	264032	$51,453,883	194.88

Table 8.7: Techno-Economic Assessment's results for 14K cases according to method B.

Ship	Crane Type	No.	V (kn)	Trips/ Year	TEUs/Year	Annual Consumption ($)	FCT ($/TEU)
Case Study A	SSG	6	23.0	17.4	251569	$45,912,842	182.51
	SSPC (A)	3	22.2			$45,333,406	180.20
		4	21.8			$45,023,268	178.97
	SSPC (B)	3	22.3			$45,396,427	180.45
		4	21.9			$45,068,980	179.15
Case 1.1	SSG	6	22.8	17.4	252161	$46,911,978	186.04
	SSPC (A)	3	22.2			$45,800,394	181.63
		4	21.8			$45,059,338	178.69
	SSPC (B)	3	22.3			$45,985,658	182.37
		4	21.9			$45,244,602	179.43
Case 1.2	SSG	6	22.7	17.4	251360	$47,994,572	190.94
	SSPC (A)	3	22.1			$46,848,910	186.38
		4	21.7			$46,085,136	183.34
	SSPC (B)	3	22.1			$46,848,910	186.38
		4	21.8			$46,276,079	184.10
Case 2.1	SSG	6	22.9	17.4	251534	$47,079,843	187.17
	SSPC (A)	3	22.3			$45,970,199	182.76
		4	21.9			$45,230,437	179.82
	SSPC (B)	3	22.4			$46,155,140	183.49
		4	21.9			$45,230,437	179.82
Case 2.2	SSG	6	22.9	17.4	251708	$48,514,676	192.74
	SSPC (A)	3	22.1			$46,983,899	186.66
		4	21.8			$46,409,857	184.38
	SSPC (B)	3	22.2			$47,175,246	187.42
		4	21.8			$46,409,857	184.38
Case 3.1	SSG	6	22.9	17.4	252683	$48,248,054	190.94
	SSPC (A)	3	22.2			$46,917,438	185.68
		4	21.8			$46,157,087	182.67
	SSPC (B)	3	22.2			$46,917,438	185.68
		4	21.8			$46,157,087	182.67
Case 3.2	SSG	6	22.7	17.4	251047	$49,925,532	198.87
	SSPC (B)	3	22.0			$48,528,830	193.31
		4	21.7			$47,930,244	190.92

For better understanding of the relation of the values, the following diagrams were made. In Figure 8.10 all the FCT values calculated by Method A (Section 7.1) for each 14K ship cases and for each crane type are presented. In same way, all the FCT values calculated by Method B (Section 7.2) for each 14K ship cases and for each crane type are depicted in Figure 8.11.

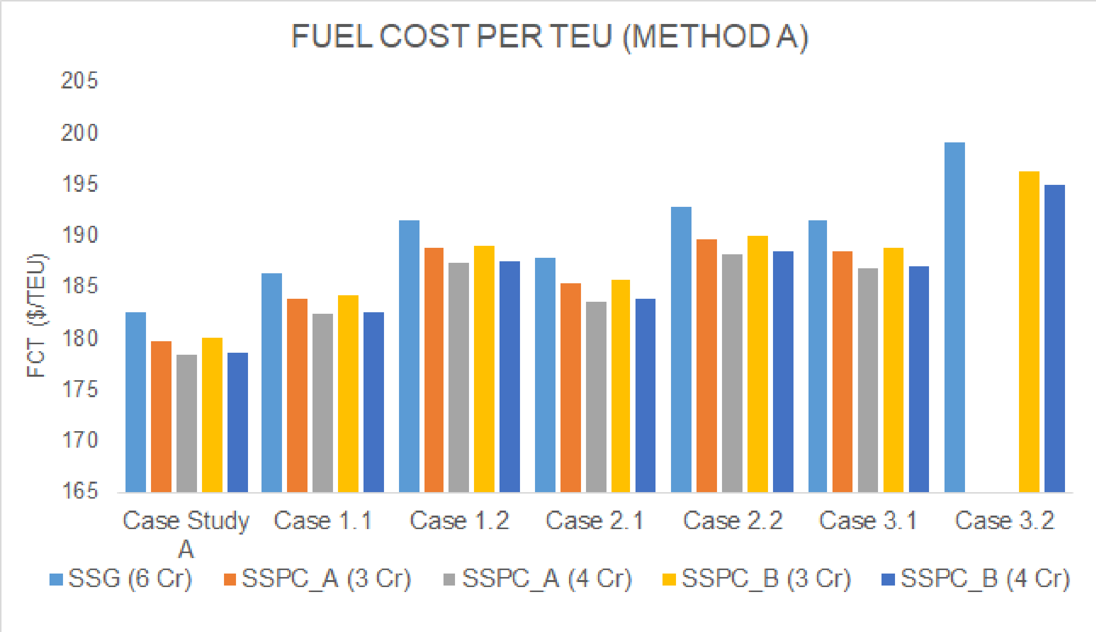

Figure 8.10: Fuel Cost per TEU (FCT) for 14K vessels according to method A.

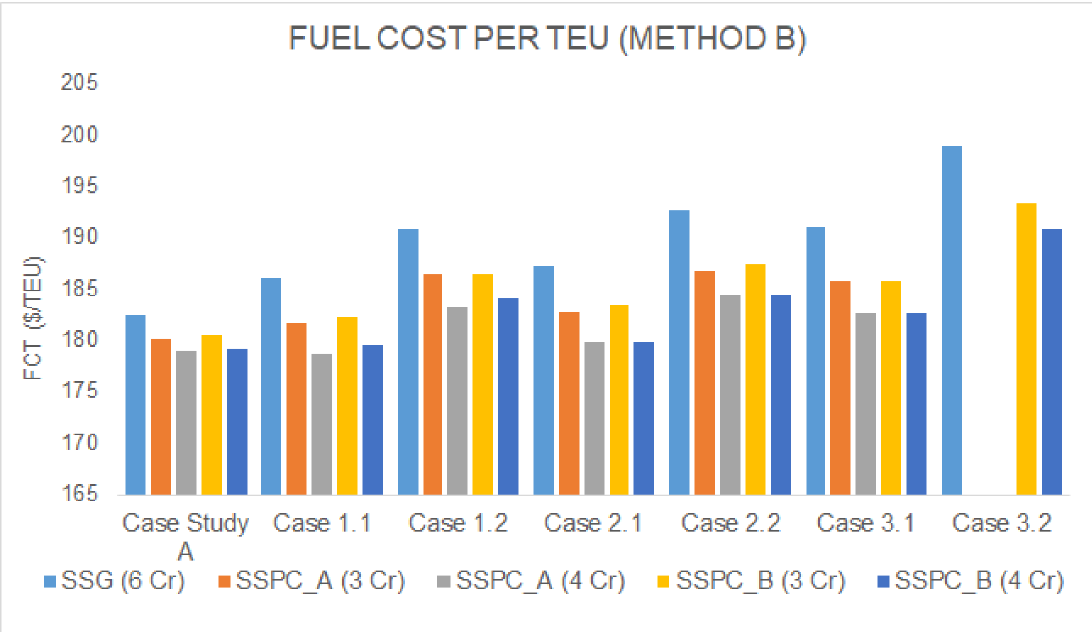

Figure 8.11: Fuel Cost per TEU (FCT) for 14K vessels according to method B.

Comments: According to method A results, the FCT is slightly decreased (1-2%) when SSPC units are operated in comparison to the SSG usage. In SSPC concept, the vessels could make more trips annually and could transfer more TEUs too. Thus results the increase of the annual consumption. The simultaneous increase of consumption and of the annual number of transported TEUs leads to a slightly decreased FCT. This reduction is negligible, but it has to be mentioned. Furthermore, in case of SSPCs operation, the vessels gain 0.5-0.8 Trips/Year, “i.e.” 1.0-1.6 Trips/ 2 Years, “i.e.” 5.0-8.0 Trips/ 10 Years, which is almost half a year trips. For the 25-year life of these vessels the gain is negligible. However, the minimum FCT is observed in the case study vessel. All proposed designs indicate an FCT's increase of 2-9%. The alternative designs are more expensive than the case study vessel.

According to method B results, the FCT is, also, decreased (1-4%) when SSPC units are operated in comparison to the SSG usage. The minimum FCT is observed in Case 1.1 vessel when 4 Type A SSPC units are operated, though. In this case, the gain of FCT value is almost 0.2% and the annual consumption is greater than $20000 with respect to the case study vessel. The Case 2.1 vessel has almost equal FCT values with the case study vessel too. However, the total annual consumption meets its minimum in case study vessel. All of these differences are negligible in relation to case study vessel A. All the other proposed designs indicate an FCT's increase of 0.2-9%.

In conclusion, no changes in the main dimensions of the case study vessel A are proposed. Further analysis is required to obtain more accurate results, however, the results of this analysis are not expected to change significantly.

8.2 Case Study B: 20000 TEU Vessel

The necessary data of the 20K case study vessel was obtained from the classification society's portal (ABS, 2020), where she is registered. However, some magnitudes could not be determined. For this reason, some assumptions were made. The basic magnitudes that were used in the calculations are listed below:

Table 8.8: Basic magnitudes for 20K case study vessel.

	Magnitude	Symbol	Value
Principal Dimensions	Length overall	L_{OA} (m)	399.87
	Length between perpendiculars	L_{BP} (m)	383
	Beam at amidships	B (m)	58.8
	Depth	D (m)	32.5
	Draught @ full load	T_{st} (m)	16.03
	Draught @ ballast condition	T_{end} (m)	9.285[i]
	Air draught from keel	H (m)	73.5
Main & Auxiliary Engines	Service speed	V_S (kn)	23
	Main Engine	1 x MAN B&W 11G95ME-C9.5	
	Power	P (kW)	61530
	Generators	4 x Daihatsu 8DE-33	
	Each Generator Power	P_{AE} (kW)	4300
Coefficients	Block	C_B	0.6840[ii]
	Waterplane area	C_{WL}	0.8645[iii]
	Mid-ship section	C_M	0.9826
	Prismatic	C_P	0.6961
Weights	Maximum Ballast	$W_{BALLAST}$ (t)	65243.0
	Lightship	LS (t)	61682.8
	Deadweight	DWT (t)	191421.9
	Displacement	Δ (t)	253104.7
Bay plan information[xii]	Capacity	TEU	20000[iv]
	Number of 40ft bays	$Bays_n$	24
	Maximum number of above deck container rows	$rows_d$	23
	Maximum number of below deck container rows	$rows_h$	21
	Maximum number of above deck container tiers	$tiers_d$	11
	Maximum number of below deck container tiers	$tiers_h$	12[xii]
Other	Double bottom height	h_{DB} (m)	2.4
	Height of hatch covers	h_{HC} (m)	2.88[xi]
	Transverse spacing	s (m)	2.52[xi]
	Transverse sectional area of the bulb	A_{BT} (m^2)	43
	Immersed part of the transverse area of the transom at zero speed	A_T (m^2)	30[v]
	Bow thruster diameter	d_b (m)	2.3[xi]
	Deck thickness at side	t (mm)	150[xi]

[i] Calculated according to equations (5.7) and (5.13) with Δ=LS+$W_{BALLAST}$
[ii] Calculated according to equation (5.1).
[iii] Assumed equal with the 14K case study vessel.
[iv] The bay plan was developed by images on the internet. According to the acquired data from the classification society, the maximum capacity of the vessel is 21413 TEUs. However, this capacity could not be reached. Furthermore, the maximum number of below deck container tiers was assumed in order to achieve the depth height.
[v] Approximate calculation according to the geometry.

The Trim and Stability Booklet (T&S), as well as the General Arrangement (GA), were not found. The data for compartments, superstructure and bay plan could not be obtained. For this reason, the Deadweight analysis and the initial stability calculations were not conducted. The dimensions of the superstructure were roughly estimated by images on the internet, in relation to the containers' dimensions. In a similar way, the bay plan was developed. The detailed bay plan was needed in order to incorporate the case study vessel into the algorithm (see Chapter 6).

Firstly, the preliminary design calculations (see Chapter 5) were undertaken in order to define the basic data of the proposed cases. The obtained results are depicted in the following table:

Table 8.9: Results of basic data for each 20K vessel.

Magnitudes	Case Study B	Case 1.1	Case 1.2	Case 2.1	Case 2.2	Case 3.1	Case 3.2
TEUs[i]	20000	20016	19916	19998	20030	20026	20074
L_{BP} (m)	383	383	383	368.4	353.8	368.4	353.8
B (m)	58.8	61.3	63.8	61.3	63.8	63.8	68.8
D (m)	32.5	29.91	27.32	32.5	32.5	29.91	27.32
L/B	6.51	6.25	6.00	6.01	5.55	5.77	5.14
B/T	3.67	3.98	4.29	3.84	4.01	4.15	4.64
L/D	11.79	12.81	14.02	11.34	10.89	12.32	12.95
C_B	0.684	0.684	0.684	0.684	0.684	0.684	0.684
C_{WL}	0.8645	0.8645	0.8645	0.8645	0.8645	0.8645	0.8645
DWT (t)	191422	191422	191422	191422	191422	191422	191422
W_{HULL} (t)	44222	44403	44585	43572	42799	43747	43138
W_{OUT} (t)	9565	10019	10474	9695	9789	10136.2	10642
W_M (t)	7895	7910	7922	7886	7874	7898	7898
LS (t)	61682.8	62332.9	62981.2	61153.5	60463.0	61781.5	61677.9
Δ (t)	253105	253755	254403	252575	251885	253203	253100
T_{ST} (m)	16.03	15.42	14.85	15.96	15.92	15.37	14.84
T_{END} (m)	9.28	8.95	8.64	9.23	9.18	8.90	8.59
T_{IILC} (m)	22.62	21.21	18.94	23.18	23.13	21.16	19.09
V_S (kn)	23	23	23	23	23	23	23
Req. EEDI ($grCO_2$/tnm)	10.58	10.58	10.58	10.58	10.58	10.58	10.58
Att. EEDI ($grCO_2$/tnm)	9.09	9.22	9.37	9.22	9.35	9.34	9.58
EIV ($grCO_2$/tnm)	10.73	10.89	11.07	10.89	11.04	11.04	11.32
Rtotal (kN)	3380.1	3441.1	3509.8	3439.2	3496.2	3496.3	3603.2
EHP (kW)	39994.5	40715.4	41528.5	40692.8	41367.9	41368.7	42633.3
SHP_{real} (kW)	61530.0	62639.1	63890.0	62604.3	63642.9	63644.1	65589.7

Note: With red color the EEDI values that do not comply with the requirements are mentioned. The EHP magnitude is related with the SHP_{real} by the propulsive coefficient (P.C.).

Comments: Similarly, in case study vessel A, increasing the beam of the vessels was expected to lead to greater resistance and better stability. However, increasing resistance means greater propulsion power demand (SHP) and therefore higher consumption (qualitatively), which will be quantified by the techno-economic analysis.

[i] In more accurate design stages, the total number of TEUs will be slightly different.

The stability was not examined due to lack of data. The determination of the GM index will be made in later design stages. Furthermore, in all cases the EIVs are greater than the required EEDIs. A service speed reduction or the introduction of Power Take-Off (PTO) and Power Take-In (PTI) systems are needed in order to meet the requirements. However, at this point the calculated EEDI is not so accurate due to lack of data. In further design stages, a more precise calculation could be made.

In the following figure, the relationship between the main dimensions of the proposed cases and those resulting from literature statistical analysis are illustrated. It is observed that the proposed designs are different from the conventional ones.

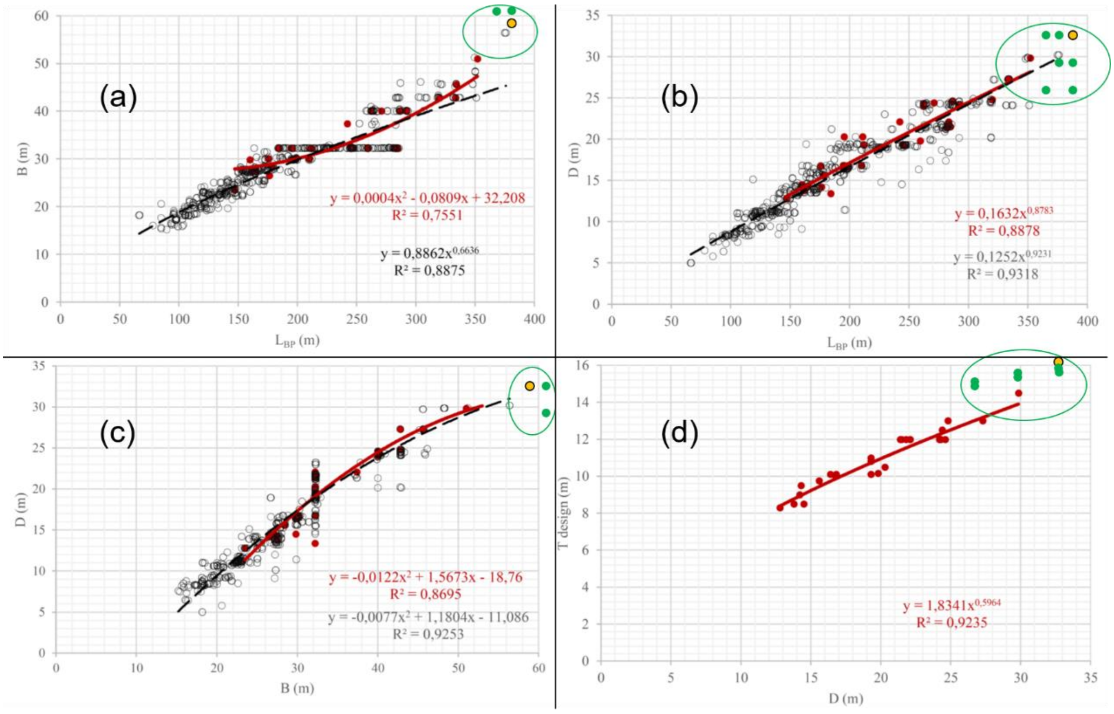

Figure 8.12: Relationship between the main dimensions of the proposed 20K cases and those resulting from statistical analysis. With yellow color the case study vessel B is mentioned. Diagrams: (a) B-L_{BP}, (b) D-L_{BP}, (c) D-B, (d) T_{Design}-D. Source: (Chrysikopoulos, 2016)

After the determination of the alternative cases' main data, the calculations of operation times were conducted. The obtained results for each operation (unloading, loading and total) and for each case are depicted in Table 8.10, Table 8.11 and Table 8.12, respectively. It is recalled that there are two types of SSPC units, with different indented berths' widths; Type A and Type B. The case study vessel B is the only one that can enter in the indented berth of SSPC Type A unit. The alternative designs cannot due to their beam. A clearance between vessel's beam and indented berth's width is needed. To the best of our knowledge, there are not existing SSG cranes that can load/unload vessels with greater beam than 62m wide. The Cases 1.2, 2.2, 3.1 and 3.2 are wider than 62m. For study's purposes, existence of such cranes has been assumed.

In the following tables, the "Crane Type" column represents the crane type used for the operation and the "No." column the number of cranes deployed along the vessel.

The “Max. Cycle Time (sec)” column shows the maximum cycle time observed for above deck (Deck) and below deck (Holds) TEUs. The maximum cycle time is very essential parameter for the operation. The “Tot. Time (hr)” column represents the total time of the operation. The percentage difference in total times with respect to the SSG concept and to the case study vessel B are presented in the last two columns.

Table 8.10: Unloading times results for 20K cases.

Ship	Crane Type	No.	Max. Cycle Time (sec)		Tot. Time (hr)	Percentage Difference with respect to the SSG concept	Percentage Difference with respect to the Case Study B
			Deck	Holds			
Case Study B	SSG	6	100.21	101.82	32.44	0.0	0.0
	SSPC (A)	3	107.92	110.74	20.25	37.6	0.0
		4			15.31	52.8	0.0
	SSPC (B)	3	113.68	116.50	21.37	34.1	0.0
		4			16.16	50.1	0.0
Case 1.1	SSG	6	98.68	99.01	31.72	0.0	2.2
	SSPC (B)	3	110.35	111.87	19.81	37.5	7.3
		4			15.00	52.7	7.2
Case 1.2	SSG	6	97.13	96.15	30.90	0.0	4.8
	SSPC (B)	3	108.19	108.45	20.17	34.7	5.6
		4			15.29	50.5	5.4
Case 2.1	SSG	6	100.64	102.26	33.36	0.0	-2.8
	SSPC (B)	3	112.30	115.13	20.59	38.3	3.7
		4			15.58	53.3	3.6
Case 2.2	SSG	6	101.52	103.14	33.33	0.0	-2.8
	SSPC (B)	3	112.59	115.40	22.42	32.7	-4.9
		4			16.77	49.7	-3.7
Case 3.1	SSG	6	99.34	99.66	32.60	0.0	-0.5
	SSPC (B)	3	110.40	111.94	21.18	35.0	0.9
		4			15.88	51.3	1.8
Case 3.2	SSG	6	98.36	97.39	31.50	0.0	2.9
	SSPC (B)	3	107.02	107.27	21.00	33.3	1.8
		4			15.59	50.5	3.6

Note: Light green color denote cells for which operation time is reduced, while pink color and negative sign (-) denote increase of operation time.

Table 8.11: Loading times results for 20K cases.

Ship	Crane Type	No.	Max. Cycle Time (sec)		Tot. Time (hr)	Percentage Difference with respect to the SSG concept	Percentage Difference with respect to the Case Study B
			Deck	Holds			
Case Study B	SSG	6	102.21	103.82	33.09	0.0	0.0
	SSPC (A)	3	109.92	112.74	20.50	38.0	0.0
		4			15.61	52.8	0.0
	SSPC (B)	3	115.68	118.50	21.57	34.8	0.0
		4			16.42	50.4	0.0
Case 1.1	SSG	6	100.68	101.01	32.38	0.0	2.2
	SSPC (B)	3	112.35	113.87	20.04	38.1	7.1
		4			15.28	52.8	6.9
Case 1.2	SSG	6	99.13	98.15	31.53	0.0	4.7
	SSPC (B)	3	110.19	110.45	20.42	35.2	5.3
		4			15.58	50.6	5.1
Case 2.1	SSG	6	102.64	104.26	34.01	0.0	-2.8
	SSPC (B)	3	114.30	117.13	20.94	38.4	2.9
		4			15.85	53.4	3.5
Case 2.2	SSG	6	103.52	105.14	34.03	0.0	-2.7
	SSPC (B)	3	114.59	117.40	22.82	32.9	-5.8
		4			17.04	49.9	-3.7
Case 3.1	SSG	6	101.34	101.66	33.24	0.0	-0.5
	SSPC (B)	3	112.40	113.94	21.55	35.2	0.1
		4			16.16	51.4	1.6
Case 3.2	SSG	6	100.36	99.39	32.15	0.0	2.8
	SSPC (B)	3	109.02	109.27	21.44	33.3	0.6
		4			15.91	50.5	3.1

Note: Light green color denote cells for which operation time is reduced, while pink color and negative sign (-) denote increase of operation time.

Table 8.12: Total operation times results for 20K cases.

Ship	Crane Type	No.	Tot. Time (hr)	Percentage Difference with respect to the SSG concept	Percentage Difference with respect to the Case Study B
Case Study B	SSG	6	65.52	0.0	0.0
	SSPC (A)	3	40.76	37.8	0.0
		4	30.93	52.8	0.0
	SSPC (B)	3	42.95	34.5	0.0
		4	32.59	50.3	0.0
Case 1.1	SSG	6	64.09	0.0	2.2
	SSPC (B)	3	39.86	37.8	7.2
		4	30.29	52.7	7.1
Case 1.2	SSG	6	62.42	0.0	4.7
	SSPC (B)	3	40.60	35.0	5.5
		4	30.88	50.5	5.3
Case 2.1	SSG	6	67.37	0.0	-2.8
	SSPC (B)	3	41.54	38.3	3.3
		4	31.42	53.4	3.6
Case 2.2	SSG	6	67.37	0.0	-2.8
	SSPC (B)	3	45.25	32.8	-5.4
		4	33.81	49.8	-3.7
Case 3.1	SSG	6	65.84	0.0	-0.5
	SSPC (B)	3	42.74	35.1	0.5
		4	32.04	51.3	1.7
Case 3.2	SSG	6	63.65	0.0	2.9
	SSPC (B)	3	42.44	33.3	1.2
		4	31.50	50.5	3.4

Note: Light green color denote cells for which operation time is reduced, while pink color and negative sign (-) denote increase of operation time.

In the following figures (8.13-8.15) the unloading (blue), loading (orange) and total times (grey) for the various 20K vessels' cases and for the various concepts are illustrated in charts. The diagrams assist to draw conclusions about operation times. Figure 8.13 shows the unloading, loading and total times for 20K ships cases when six SSG cranes are deployed. Figure 8.14 shows the unloading, loading and total times for 20K ships cases when three Type B SSPC units are deployed and Figure 8.15 the case of four Type B SSPC units deployed along the vessels.

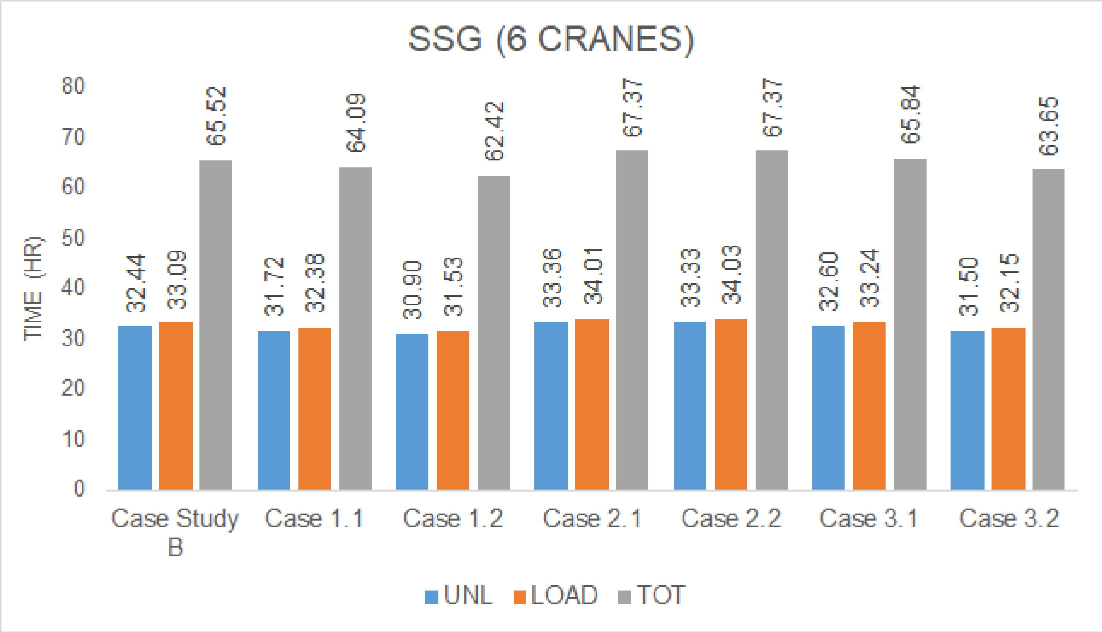

Figure 8.13: Unloading, Loading and Total times for 20K ship cases using 6 SSG cranes.

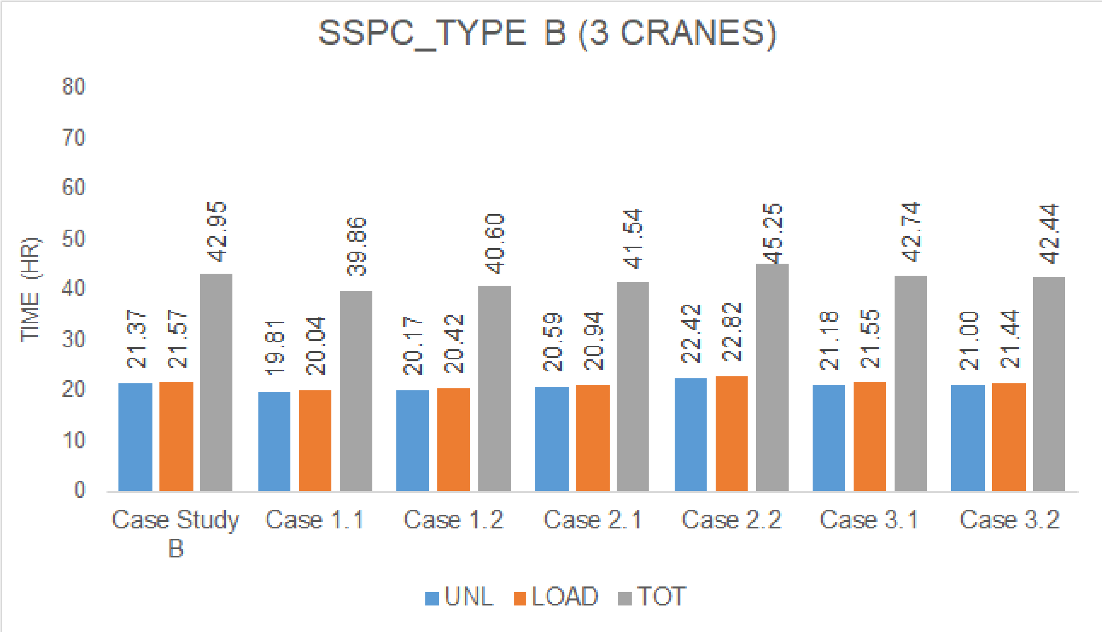

Figure 8.14: Unloading, Loading and Total times for 20K ship cases using 3 Type B SSPC units.

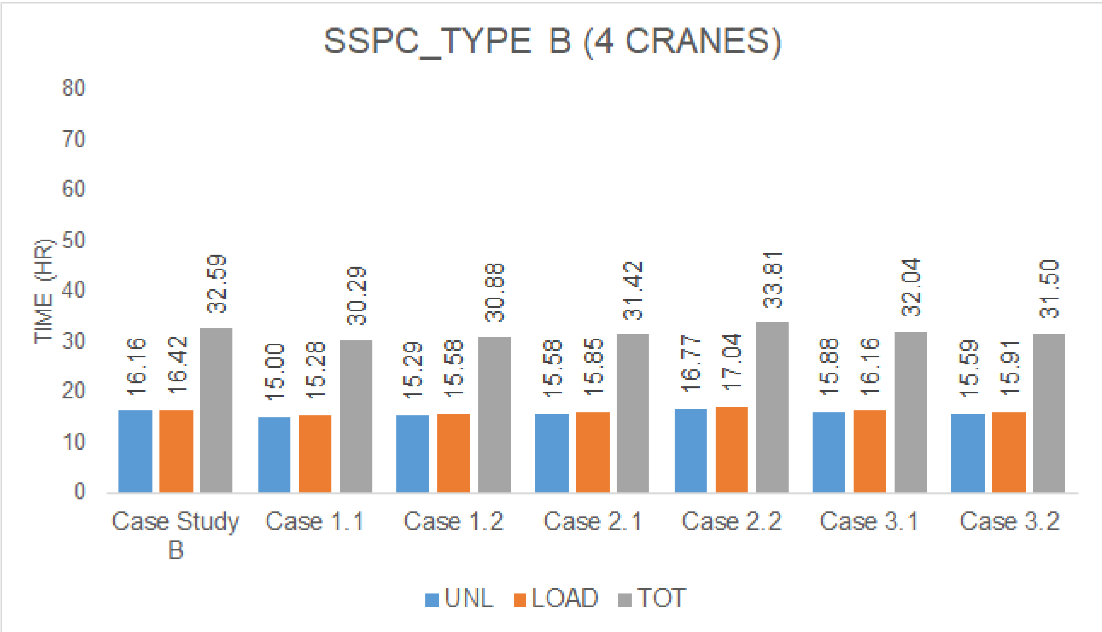

Figure 8.15: Unloading, Loading and Total times for 20K ship cases using 4 Type B SSPC units.

Figure 8.16 illustrates the comparison between the SSG cranes and Type B SSPC units.

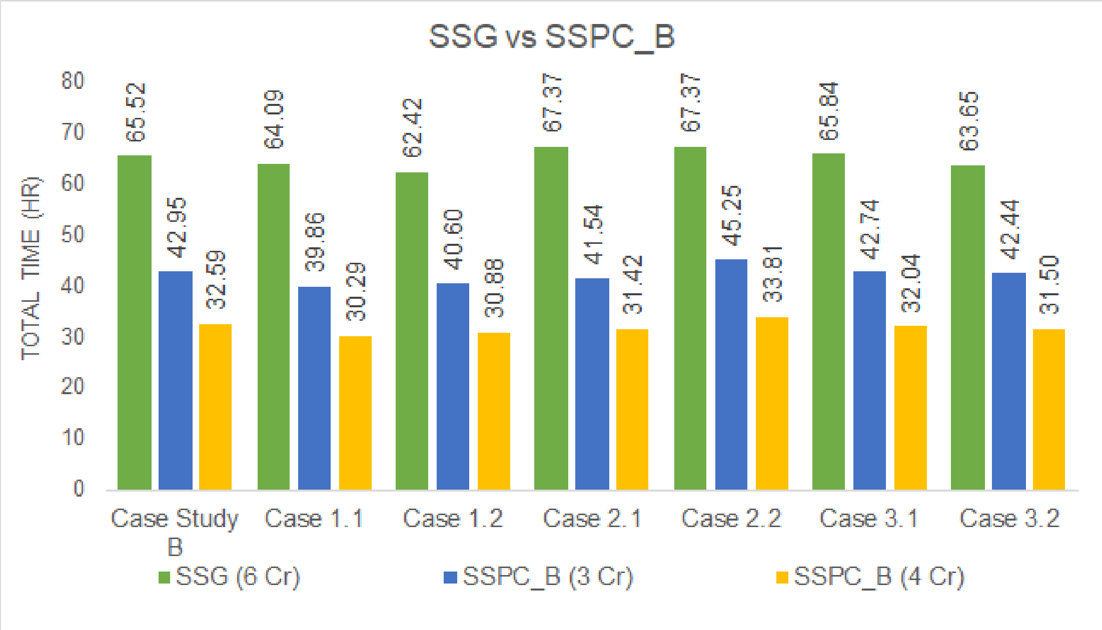

Figure 8.16: Comparison between the operation of SSG and Type B SSPC units in 20K cases.

Comments: The above analysis confirmed that the use of the new-concept cranes reduces the loading/unloading time. Therefore, the gain in time when using SSPCs compared to the usage of 6 conventional SSG cranes for loading/unloading the ship is almost 32-38 % in the case of 3 SSPCs, and almost 49-53% in the case of 4 SSPCs. The percentage reduction varies between cases. For this kind of vessels, the Type B SSPCs could only be used.

In Figure 8.16, the blue color stands for the total operation times, when three cranes of Type B SSPC units used. From Figure 8.16, the maximum gain of time when three Type B SSPC cranes are deployed, in comparison to when six SSG cranes are deployed, is observed in Case 2.1 vessel (38.3%). The minimum operation time is observed in Case 1.1 vessel (39.86 hr). However, these differences are negligible in comparison with the case study vessel B, when three Type B SSPC units are deployed.

In the same way, the yellow color stands for the total operation times, when four cranes of Type B SSPC units used. From Figure 8.16, the maximum gain of time when four Type B SSPC cranes are deployed, in comparison to when six SSG cranes are deployed, is observed in Case 2.1 vessel (53.4%). The minimum operation time is observed in Case 1.1 vessel (30.29 hr). However, these differences are negligible compared to the case study vessel A, when four Type B SSPC units are deployed.

Final assessments of whether changes to the main dimensions of case study vessel B are appropriate were made after the techno-economic analysis, described in Chapter 7.

The “time paradox” is observed in Case 2.2 vessel. The parameters that affect it, are identical to those described in case study vessel A (see section 8.1). In conventional cranes, the reduction of the depth plays a significant role in reducing the cycle time, even when the beam has increased. In new concept cranes, the simultaneous increase of the beam and decrease of the depth may reduce the cycle time, but no qualitative conclusions can be drawn in any case. A higher efficiency of the portal cranes can be achieved when the maximum number of rows is an even number.

After calculating the loading/unloading times, the techno-economic assessment was performed to quantify whether the investment is beneficial for the ship owners. The analysis was described in Chapter 7. The results of the assessment are depicted in the following tables.

The “Crane Type” column represents the crane type used for the operation and the “No.” column the number of cranes deployed along the vessel. The “V (kn)” column denotes the service speed of the vessels. The “Trips/Year” and “TEUs/Year” columns show the annual number of Trips and transported TEUs for each vessel, respectively. The annual consumption (based on the fuel costs) and the Fuel Costs per TEU are presented in the last two columns.

Table 8.13: Techno-Economic Assessment's results for 20K cases according to method A.

Ship	Crane Type	No.	V (kn)	Trips/ Year	TEUs/Year	Annual Consumption ($)	FCT ($/TEU)
Case Study B	SSG	6	23	16.7	334000	$57,083,135	170.91
	SSPC (A)	3		17.5	350000	$58,267,568	166.48
		4		17.9	358000	$58,970,046	164.72
	SSPC (B)	3		17.5	350000	$58,404,651	166.87
		4		17.8	356000	$58,746,293	165.02
Case 1.1	SSG	6	23	16.7	334267	$57,905,182	173.23
	SSPC (B)	3		17.6	352282	$59,488,141	168.87
		4		17.9	358286	$59,884,578	167.14
Case 1.2	SSG	6	23	16.8	334589	$59,179,478	176.87
	SSPC (B)	3		17.5	348530	$60,256,177	172.89
		4		17.9	356496	$61,000,650	171.11
Case 2.1	SSG	6	23	16.6	331967	$57,725,921	173.89
	SSPC (B)	3		17.5	349965	$59,226,626	169.24
		4		17.9	357964	$59,927,696	167.41
Case 2.2	SSG	6	23	16.6	332498	$58,572,156	176.16
	SSPC (B)	3		17.4	348522	$59,997,358	172.15
		4		17.8	356534	$60,637,280	170.07
Case 3.1	SSG	6	23	16.7	334434	$58,833,105	175.92
	SSPC (B)	3		17.5	350455	$60,183,662	171.73
		4		17.8	356463	$60,523,857	169.79
Case 3.2	SSG	6	23	16.8	337243	$60,652,841	179.85
	SSPC (B)	3		17.5	351295	$61,813,887	175.96
		4		17.9	359325	$62,506,024	173.95

Table 8.14: Techno-Economic Assessment's results for 20K cases according to method B.

Ship	Crane Type	No.	V (kn)	Trips/ Year	TEUs/Year	Annual Consumption ($)	FCT ($/TEU)
Case Study B	SSG	6	23.0	16.7	334000	$57,083,135	170.91
	SSPC (A)	3	21.8			$55,804,019	167.08
		4	21.3			$55,312,417	165.61
	SSPC (B)	3	21.9			$55,914,988	167.41
		4	21.4			$55,394,708	165.85
Case 1.1	SSG	6	22.8	16.7	334267	$57,793,377	172.90
	SSPC (B)	3	21.7			$55,327,512	165.52
		4	21.2			$54,206,664	162.17
Case 1.2	SSG	6	22.7	16.7	332597	$58,683,011	176.44
	SSPC (B)	3	21.7			$56,390,513	169.55
		4	21.3			$55,473,514	166.79
Case 2.1	SSG	6	23.0	16.7	333967	$58,023,692	173.74
	SSPC (B)	3	21.7			$55,126,176	165.06
		4	21.3			$54,234,633	162.40
Case 2.2	SSG	6	23.0	16.7	334501	$58,874,132	176.01
	SSPC (B)	3	21.9			$56,381,715	168.55
		4	21.4			$55,248,799	165.17
Case 3.1	SSG	6	22.9	16.7	334434	$58,738,590	175.64
	SSPC (B)	3	21.8			$56,240,065	168.16
		4	21.3			$55,104,372	164.77
Case 3.2	SSG	6	22.8	16.7	335236	$60,228,186	179.66
	SSPC (B)	3	21.8			$57,879,237	172.65
		4	21.3			$56,704,763	169.15

For a better understanding of the relation of the values, the following diagrams were made. Only the results of SSGs and Type B SSPCs are illustrated, due to the fact that the Type A SSPCs cannot operate in the 20K vessels. In Figure 8.17 all the FCT values calculated by Method A (Section 7.1) for each 20K ship cases and for each crane type are presented. Similarly, all the FCT values calculated by Method B (Section 7.2) for each 20K ship cases and for each crane type are depicted in Figure 8.18.

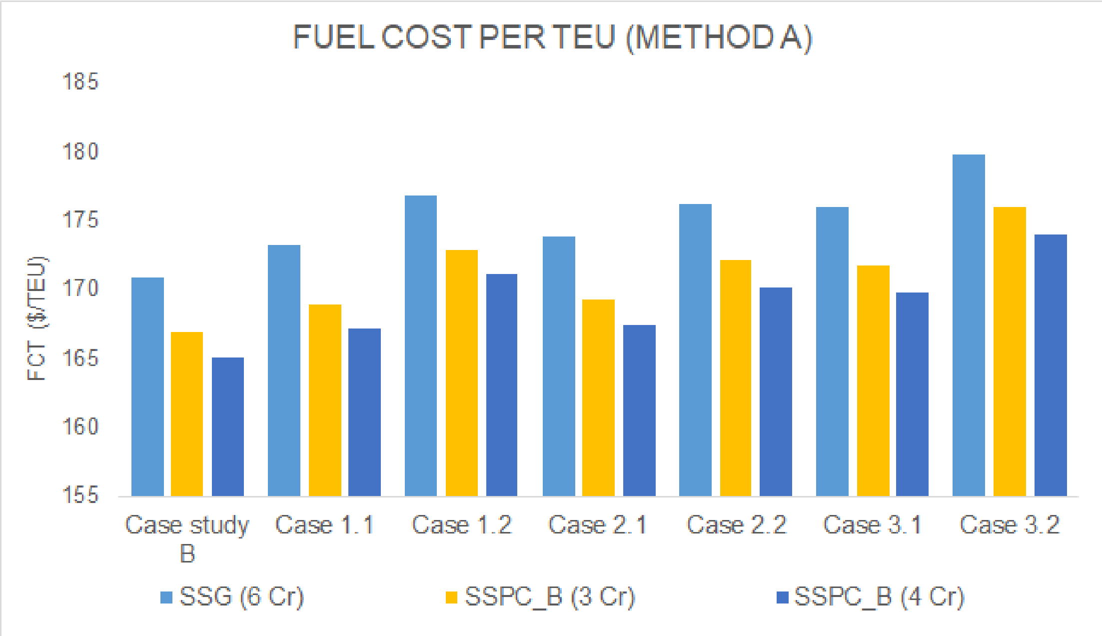

Figure 8.17: Fuel Cost per TEU (FCT) for 20K vessels according to method A.

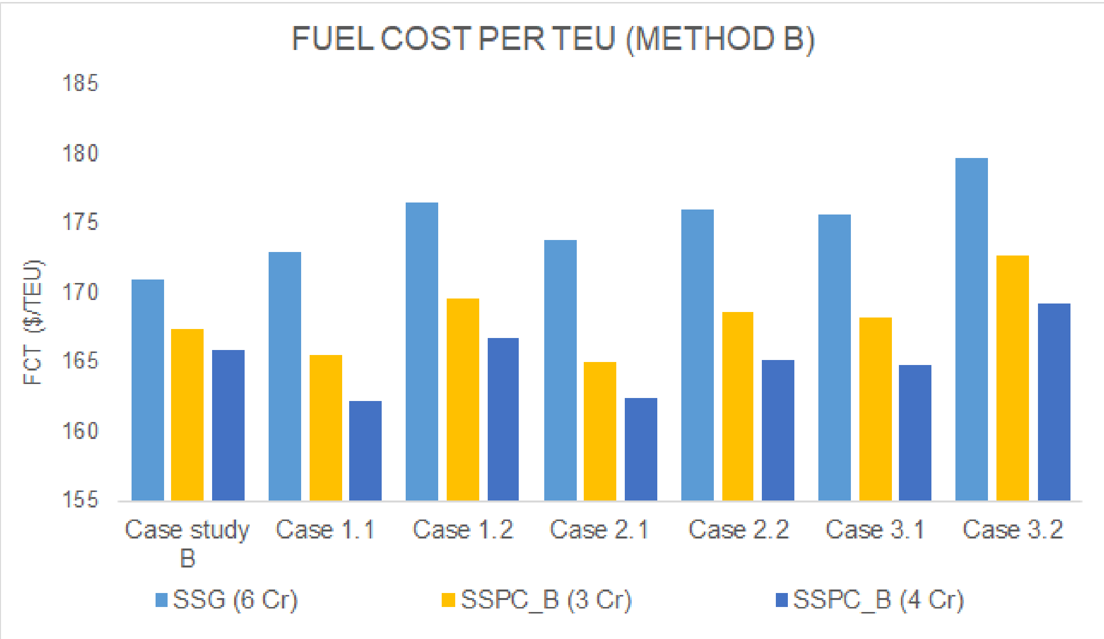

Figure 8.18: Fuel Cost per TEU (FCT) for 20K vessels according to method B.

Comments: According to method A results, the FCT is slightly decreased (2-3%) when SSPC units are operated in comparison to when the SSG cranes are used. In SSPC concept, the vessels could make more trips annually and could transfer more TEUs too. Thus results the increase of the annual consumption. The simultaneous increase of consumption and of the annual number of transported TEUs leads to a slightly decreased FCT. This reduction is negligible, but it has to be mentioned. Furthermore, in case of SSPCs operation, the vessels gain 0.8-1.1 Trips/Year, "i.e." 1.6-2.2 Trips/ 2 Years, "i.e." 8.0-11.0 Trips/ 10 Years, which is more than a half year of trips. For the 25-year life of these vessels the gain is negligible. However, the minimum FCT is observed in the case study vessel. All proposed designs indicate an FCT's increase of 1-5%. The alternative designs are more expensive than the case study vessel.

According to method B results, the FCT is, also, decreased (2-6%) when SSPC units are operated in comparison to when the SSG cranes are used. However, the FCT is observed in many cases to be less than the case study vessel. The Cases 1.1 and 2.1 have better FCT and annual consumption with almost the same TEU capacity. For this reason, these designs seem to be more efficient. The Cases 2.2 and 3.1 have also better FCT and annual consumption when 3 Type B SSPC are operated. However, the difference in this cases is almost 0.4-0.7% with respect to the case study vessel. It is important to note that all of the previous results may change in the latter design stages. All of these differences are negligible with respect to the case study vessel B. All the other proposed designs indicate an FCT's increase of 0.6-5%.

In conclusion, no changes in the main dimensions of the case study vessel B are proposed. Further analysis is required to obtain more accurate results, however, the results of this analysis are not expected to change significantly.

8.3 Comparison of Case Studies

At this point, the question which case study is affected more from the SSPCs is raised. The impact of the cranes on the case study vessels is distinguished in two levels; time and cost.

According to the time calculations, the gain of time when SSPC units are operated, compared to the usage of SSGs, is slightly higher for the 20K vessels than for the 14K ones. As the number of TEU capacity increases, more hoist movements are needed. The SSPCs were designed to have faster process of loading/unloading than the SSG cranes. Therefore, the impact of the SSPCs on loading/unloading time increases with the increase of the vessel's TEU capacity. For instance, for the 14K vessels, the gain in time when using SSPCs compared to the usage of 6 conventional SSG cranes for loading/unloading the ship is almost 25-35% in the case of 3 SSPCs, and almost 45-52% in the case of 4 SSPCs, instead of 32-38% in the case of 3 SSPCs and 49-53% in the case of 4 SSPCs for the 20K vessels.

According to the techno-economic assessment, improved FCT and annual consumption values have emerged for the 20K vessels compared to the 14K ones. These magnitudes are affected by the propulsive power (resistance) and the trip time, or better yet, the port time. 20K vessels have greater power demand than the 14K ones, but the port times are less. This has led to improved FCT and annual consumption values. According to the calculations, the ship owners' theory that "the bigger vessels are more efficient" (see Chapter 2) is verified, due to the higher number of TEU transported with less cost per TEU. Moreover, the differences in FCT values are negligible and the modifications on the main dimensions are not advised. However, the comparison of the present calculated FCTs is not valid due to different capital and operation costs of the two case study vessels. Nevertheless, this analysis shows a tendency.

Last but not least, the COFASTRANS system opens the horizons of building larger vessels. As the vessels get bigger the efficiency of the conventional cranes concept decreases. On the other hand, the efficiency of the new-concept cranes seems to increase. However, a further analysis of the optimum vessel design is needed.

Chapter 9

Discussion

Summarizing, in the present work, the research of changes in the principal dimensions of the ULCVs in order to comply better with COFASTRANS system for loading/unloading from both sides has been conducted. The investigation made focused on the ship owners' view. For this reason, it was conducted for two case study vessels; 14K and 20K. For each case, six different design cases were proposed. During the course of this Thesis, several preliminary methodologies were applied and several tools were developed in order to compare the proposed cases. Proper modifications of the main dimensions of both case study vessels were made in order to reduce the total operation time, during which the vessels remain at port. Some basic preliminary design methodologies were applied in order to examine the sea worthiness of the proposed cases. The loading/unloading time calculation was made by using the developed tool. This algorithm was developed in Hypertext Preprocessor (or simply PHP) programming language, which is originally designed for web development. The tool is extractable and can be used by anyone. At first, the algorithm was developed in MATLAB, but it was very complex to use. Then a Techno-Economic Assessment was made in order to evaluate whether the investment is profitable or not. For this reason, two methodologies were developed and applied. Although, the chosen economic method can be modified in order to comply better with an actual scenario that the ship owners prefer. However, further analysis is needed in order to verify the worthiness of the results.

According to the preliminary design calculations:

- The alternative designs are quite different than the conventional ones, that were found in literature based on regression analysis.
- The alternative designs have better stability with higher GM values than the case study vessels due to the increase of the beam. Large GM values trigger intense roll motions (parametric rolling) and transverse accelerations on the ship's deck. Nausea or injuries to the crew and loss or damage of the cargo could be caused.
- For large GM values, stronger (heavier) lashing systems are needed or an extra tier can be added on the above deck containers. In this case, the alternative designs can carry on more containers without increasing significantly the building cost of the vessel. The reduction of the GM values was not within the objective of the present study.

According to the loading/unloading times calculations:

- The operation of SSPCs can decrease the time for which the vessel remains at port.

- For 14K vessels, the gain in time when using SSPCs compared to the usage of 6 conventional SSG cranes for loading/unloading the ship is almost 25-35 % in the case of 3 SSPCs, and almost 45-52% in the case of 4 SSPCs.
- For 20K vessels, the gain in time when using SSPCs compared to the usage of 6 conventional SSG cranes for loading/unloading the ship is almost 32-38 % in the case of 3 SSPCs, and almost 49-53% in the case of 4 SSPCs.
- The selection of which type of crane can reach better operation rates depends on the dimensions of the vessel. For a 14K vessel the Type A SSPCs units are preferred, due to the narrow berth and the fact that shorter hoist movements are required.
- A “time paradox” phenomenon was observed.
- Some basic parameters that affect the “time paradox” phenomenon are: the length of the vessel, the distribution of the bays, the number of TEUs in each bay, the number of rows and the tiers of each bay.
- In SSG concept, the reduction of depth (or height in general) decreases the operation time.
- In SSPC concept, the simultaneous reduction of depth and increase of beam, decreases the operation time.
- The odd number of rows decreases the efficiency of the SSPCs, due to the fact that one trolley of the beam remains idle for some time. In this case the port side trolley undertakes to load/unload the remaining row of containers.

According to the Techno-Economic Assessment:

- SSPC concept offers slightly lower FCT values than the SSG one. In some cases, this is achieved by the simultaneous increase of the annual consumption and the annual number of transported TEUs (depends largely on the applied method).
- The impact in FCTs is slightly greater for the 20K vessels than the 14K ones due to larger TEU capacity.
- The proposed 20K Cases 1.1 and 2.1, when SSPC units are operated, have shown slightly positive results – but negligible.
- No modifications on the case study vessels are advised.
- The increase of the beam over 60-62m, which is the structural limit nowadays, due to the SSG outreach, seems to be realistic and very interesting.
- Further analysis is needed.

Consequently, the ship owners’ theory that larger vessels make the operations more efficient, is strengthened. The tendency shows that the vessels will get bigger as time goes on. However, the question whether the whole container supply chain (ship owners, ship operators, port operators, shore transportation companies etc.) is ready to handle this, has raised. From the ship owner’s view, the COFASTRANS system seems to be a profitable solution for the future. A further analysis is needed in order to cover the fields that could not be investigated in the present study. This report is the first step, in a series of required studies, for the installation of the COFASTRANS system in ports globally.

Chapter 10

Future Work

This Diploma Thesis leaves as a repository the research of suitable statistical preliminary design methods for ULCVs and the loading/unloading time calculation tool. Future work, in continuation of the present, could include the following topics:

- A more detailed analysis based on the results and on the assumptions of the present study.
- A feasibility study for the proposed types of SSPC units.
- An optimization analysis for identifying optimal slope parameters that minimize the operation time and the fuel costs.
- An optimization analysis for identifying optimal slope parameters that maximize TEU capacity in a reasonable cost scaling. Increasing the beam and the maximum number of above deck container tiers along with the simultaneous reduction of depth, enables the construction of bigger vessels. Increasing the length is not advisable due to strength issues that may arise (bending and twisting moments).
- A similar investigation from the port operators' scope based on the above data and results. The main question is whether ports can manage the faster rates of inbound and outbound containers. Possible introduction of automations should be examined.
- A study of the design of a triple-beam crane (extension of SSPC). Strength study and techno-economic assessment should be made. It is possible to lead in decreased deployed number of cranes along the vessel.
- Modification of the algorithm for the time calculation in case of odd number of container rows. Examine the possibility for the trolleys to work alternately on the remaining container row so that one does not remain idle for a long time.
- The longitudinal spacing between container bays would be specific and could remain constant for all new vessels. This will lead to a better designation of the SSPC units (optimum distance of the spanning beams).
- Extension of the algorithm to a simulation tool based on genetic algorithms and Artificial Intelligence (AI), which could optimize the stowage planning.

Literature

ABS. (2020). *Eagle*. Retrieved from ABS Record: https://www.eagle.org/portal/?fbclid=IwAR2NMKV9DaHJo4dUzNlo71yT-F3GKSB1QGPBSJm-5pGJx_1yso0b6zztWE0#/absrecord/search

Alba, D., & Risemberg, R. (2011, September 5). How Would the Ports Stack Up? *Los Angeles Business Journal*. Retrieved from https://labusinessjournal.com/news/2011/sep/05/how-would-ports-stack/

Bazari, Z. (2016). *Module 2 – Ship Energy Efficiency Regulations and Related Guidelines.* London: International Maritime Organization.

Birk, L. (2019). *Fundamentals of Ship Hydrodynamics* (1st ed.). New Orleans, USA: Wiley.

Blendermann, W. (1986). *Die Windkräfte am Schiff.* Hamburg.

Blendermann, W. (1994). Parameter identification of wind loads on ships. *Journal of Wind Engineering and industrial aerodynamics*(51), 339-351.

Borkowski et.al, T. (2012). Energy Efficiency Design Index of Container Vessel. *Journal of Kones Powertrain and Transport*(Vol. 19, No. 4).

Chambers, S. (2020, February 10). Coronavirus costing liners up to $350m in lost revenues every week. *Splash247*. Retrieved from https://splash247.com/coronavirus-costing-liners-up-to-350m-in-lost-revenues-every-week/

Chrysikopoulos, A. (2016). *Concentration and Statistical Analysis of Containerships technical data.* Diploma Thesis, National Technical University of Athens, School of Naval Architecture and Marine Engineering, Athens.

COFASTRANS. (2017, May 4). Retrieved from http://www.cofastrans.com/

(2015). *COFASTRANS-Indented Berths Feasibility Study.* H2020 FTI Project Report, version 3.0.

DNV-GL. (n.d.). (Future) Fuels and Fuel Converters. Retrieved from https://www.ntnu.edu/documents/20587845/1266707380/01_Fuels.pdf/1073c862-2354-4ccf-9732-0906380f601e

GRID Logistics Inc. (n.d.). *Putting the "Good" into Goods-Movements*. Retrieved from http://www.gridinc.biz/

Hamalainen, J., A., M., Baharova, L., & Virkkunen, J. (1995, Janouary). Optimal path planning for a trolley crane: Fast and smooth transfer of load. *IEE Proceedings - Control Theory and Applications, Volume 142*(Issue 1), 51-57. doi:10.1049/ip-cta:19951593

Han, M., & Son, S. (2000). *Gantry Crane having Circulating Trolley.* International Patent No. WO 2000/048937, World International Property Organization, Publication Date 24 August 2000. Retrieved from https://patentscope.wipo.int/search/en/detail.jsf?docId=WO2000048937&tab=PCTBIBLIO

Holtrop, J. a. (1978). A statistical power prediction method. In *International Shipbuilding Progress.*

Holtrop, J. a. (1982). An approximate power prediction method. In *International Shipbuilding Progress.*

International Chamber of Shipping. (2019). *Shipping and World Trade*. Retrieved from http://www.ics-shipping.org/shipping-facts/shipping-and-world-trade

Kim, K., Phan, M., & Woo, Y. (2012). *New Conceptual Handling Systems in Container Terminals.* Paper, Pusan National University, Department of Industrial Engineering, Busan.

KONECRANES. (2020). *Rail Mounted Gantry Cranes*. Retrieved from https://www.konecranes.com/en-us/equipment/container-handling-equipment/rail-mounted-gantry-cranes

KONECRANES. (2020). *Rubber Tired Gantry Cranes*. Retrieved from https://www.konecranes.com/en-us/equipment/container-handling-equipment/rubber-tired-gantry-cranes

Ligteringen, H., Winkel Buiter, T., & Vermeer, A. (2002). Ceres-Paragon Container Terminal in the Port of Amsterdam-Design and realisation of a high-productivity terminal. *PIANC 2002.* Sydney. Retrieved from http://www.graduadosportuaria.com.ar/seminario/Ligteringen.pdf

LiveBunkers. (n.d.). Fuel Prices. Retrieved December 29, 2019, from http://livebunkers.com/

MAN B&W, E. S. (2019). *Marine Engine Programme* (2nd ed.).

Marine Traffic. (2017). *Density Maps*. Retrieved from https://www.marinetraffic.com/

MEPC.1-Circ.866. (2017). Guidelines on the method of calculation of the attained energy efficiency design index (EEDI) for new ships. London.

Miller, D. (1968). *The economics of the container ship subsystem.*

MSC. (2019, August 19). *World's largest container ship completes first voyage from Asia to Europe*. Retrieved from MSC Press Realease: https://www.msc.com/irl/press/press-releases/2019-august/world-s-largest-container-ship-completes-first-voy

MSC.143(77). (2003). Resolution MSC.143(77). *Maritime Safety Committe.* IMO.

Nevsimal, W. (2017). STS Multi-Trolley Portal Gantry Container Crane (International Patent WO 2017/071736A1). *World International Property Organization.*

Nevsimal-Weidenhoffer, V., & Oja, H. (2018). Next-Gen STS Cranes-A model for the future. *Port Technology International Journal* (Edition 77).

New Crane Concept from Konecranes. (2018, March). *World Cargo News*.

Nikolakakis, D. (2006). *VISIONS – NoE: Visionary Concepts for Vessels and floating structures-Initiation of Academic Contest Loop II.* Presentation, University of Rockstock.

Papanikolaou, A. (2014). *Ship Design-Methodologies of Preliminary Design.* Athens: Springer.

Perumpalath, B. (2004). Product Management Systems: Group Project. Portsmouth. Retrieved from http://pms2004.tripod.com/formulae_and_definitions.html

PNGWAVE. (2020). Spreader Container crane Intermodal container Machine. Retrieved from https://www.pngwave.com/png-clip-art-ltsnw

Politis, G. (2019). *Ship Resistance and Propulsion* (5th ed.). Athens: NTUA.

Port Technology. (2011, April 6). APM Terminals honored for FastNet Crane concept. *Port Technology*. Retrieved from https://www.porttechnology.org/news/apm_terminals_honored_for_fastnet_crane_concept_at_awards/

Rankine, G. (1999). Developing a Container Vessel "Docking System". *Seminar on Port Design and Operation Technology .* Singapore.

Rankine, G., Netherstreet, I., Perez Romero, D., & Palmer, J. (2018). COFASTRANS (Container Vessel Fast Transhipment System). *PIANC-World Congress.* Panama.

Rodrigue, J.-P. (2017). *The Geography of Transport Systems* (4th ed.). New York: Routledge. Retrieved from https://transportgeography.org

Schneekluth, H., & Bertram, V. (1998). *Ship Design for Efficiency and Economy* (2nd ed.). Butterworth-Heinemann.

Steenken, D., Voβ, S., & Stahlbock, R. (2004). Container terminal operation and operations research - a classification and literature review. In *OR Spectrum* (pp. 3-49). doi:10.1007/s00291-003-0157-z

Turbosquid. (2017 & 2019). *Straddle Carrier and Automated Guided Vehicle*. (3.-m. International, & ConstantinOs, Producers) Retrieved from https://www.turbosquid.com/de/3d-models/3d-straddle-carrier-20ft-iso-container-model-1365110 and https://www.turbosquid.com/3d-models/3d-automated-guided-vehicle-model/1134987

UNCTAD. (2015). *Review of Maritime Transport.* Retrieved from https://unctad.org/en/PublicationChapters/rmt2015ch3_en.pdf

UNCTAD. (2019). *Review of Maritime Transport.* New York.

Ventura, M. (n.d.). *Hull Form.* Master Thesis Presentation, Instituto Superior Tecnico, Marine Engineering, Lisboa. Retrieved from http://oa.upm.es/14340/2/Documentacion/3_Formas/SD-1.5.1-Hull%2520Form.pdf

Vis, I. F. (2008, December 9). *Processes at a container terminal*. Retrieved from IrisVis: http://www.irisvis.nl/container/processes.html

Watson, D. (1998). *Practical Ship Design.* Elsevier Science Ltd.

Wikipedia. (2019). *Gantry Cranes*. Retrieved from Wikipedia: https://en.wikipedia.org/wiki/Gantry_crane

World Shipping Council. (2018). Retrieved from Top 50 world container ports: http://www.worldshipping.org/about-the-industry/global-trade/top-50-world-container-ports

World Shipping Council. (2020). Ανάκτηση από http://www.worldshipping.org/

World Steel Prices. (2020, January 23). *World Steel Prices*. Retrieved from https://worldsteelprices.com/

Young, B. (2012, September 3). *The Load Star*. Retrieved from Amsterdam’s 'White Elephant' is put out of its misery: https://theloadstar.com/amsterdams-white-elephant-is-put-out-of-its-misery/

Appendix A

Table of Ports and Sea Routes Limitations

In the present Appendix A, all the results of the conducted research for Ports and Sea Routes limitations are presented.

In Table A.1, the port limitations are depicted. The research was conducted for almost 80 ports worldwide. The 50 busiest container ports were ranked in descending order according to the 2018th results (World Shipping Council, 2018). The rest of them were placed below in random order. The column "No." denotes the port's position on the worldwide list. The columns "Length (m)", "Beam (m)", "Draught (m)" and "Air Draught (m)" declare the restrictions for each one of these magnitudes. Some remarks are depicted in the last column. Furthermore, the term "und.", used in several cells, is an abbreviation for "undefined". In the same way, the sea routes limitations are depicted in Table A.2.

Table A.1: Port Limitations.

Ports	No.	Length (m)	Beam (m)	Draught (m)	Air Draught (m)	Remarks
Shanghai Port, China	1	-	-	14.2	-	Berth depth: 17.5m @ Guandong International Container Terminal Company
PSA, Singapore	2	-	-	16	-	-
Shenzhen Port, China	3	Terminal Length: 7047m	-	16	-	-
Port of Ningbo-Zhoushang, China	4	Terminal Length: 4465m	-	13.5-17	-	-
Port of Guangzhou, China	5	-	60	15.5	-	Nansha Terminal
Port of Bussan, South Korea	6	-	-	15-17	-	-
Port of Hong Kong	7	Depends on Terminal	-	15.5	73.5	Stonecutters Bridge
Port of Qingdao, China	8	-	65	15	-	-
Port of Tianjin, China	9	-	-	13.8-16	-	Depends on Terminal

Ports	No.	Length (m)	Beam (m)	Draught (m)	Air Draught (m)	Remarks
Jebel Ali Port. Dubai, UAE	10	-	-	17	-	-
Port of Rotterdam, the Netherlands	11	-	-	24	-	-
Port Klang, Malaysia	12	300	-	15	-	Westport
Port of Antwerp, Belgium	13	-	-	13.5	-	-
Kao Ming. Kaohsiung, Taiwan	14	375	-	16.5	-	-
Port of Xiamen, China	15	-	-	17	-	-
Port of Dalian, China	16	-	-	9.8-16	-	DCT. DPCM. and DICT have a total of 13 berths with alongside depths from 9.8m to 16m
Port of Los Angeles, USA	17	-	-	15.84	-	-
Port of Tanjung Pelepas, Malaysia	18	720 (turning basin)	25 rows outreach	15-19	-	-
Port of Hamburg, Germany	19	-	-	16.7	-	-
Port of Long Beach, USA	20	-	-	15.2	-	-
Laem Chabang, Thailand	21	600 (turning basin)	-	16	-	-
Port of Tanjung Priok, Indonesia	22	450	-	16	-	New Priok Terminal 1
New York/New Jersey, USA	23	-	-	15.2	69.4	Verrazano Bridge
Port of Colombo, Sri Lanka	24	-	-	18	-	Colombo South Container Terminal
Port of Yingkou, China	25	430	-	15.5	-	-
Saigon Port, Vietnam	26	-	-	12.1	-	-
Port of Bremerhaven, German	27	-	-	12-15	-	-

Ports	No.	Length (m)	Beam (m)	Draught (m)	Air Draught (m)	Remarks
Port of Manila, Philippines	28	-	-	14	-	South Harbor International Container Terminal (SHICT)-26 vessels at the same time
Jawaharlal Nehru Port. Mumbai, India	29	330	-	16.2 (max). 14 (Tidal)	-	-
Port of Piraeus, Greece	30	700	-	16.5	-	For Pier II. West Side
Port of Algeciras, Spain	31	Over 152.4	-	17-18.5	-	APM Terminals Algeciras: 17 meters/Total Terminal International Algeciras: 17.5m-18.5m
Lianyungang, China	32	322	-	13.4	-	Berths 29 and 30
Port of Tokyo, Japan	33	Terminal Length: 2354m	-	15	-	Oi Container Terminal
Mundra Port, India	34	275	-	15.5	-	Berth 1
Garden City Terminal. Savannah. Georgia, USA	35	366	22 Containers Across without slowdown-24 into slowdown zone	14.8	56.3	Berth 3. Talmadge Memorial Bridge
Jeddah Islamic Port, Saudi Arabia	36	-	-	16	-	-
Port of Santos, Brazil	37	-	-	9	-	Dredging to 17m in future
Rizhao Port, China	38	-	-	11-12.2	-	-
Port of Colon, Panama	39	-	-	12.5-13.7	-	-
Port of Felixstowe, UK	40	-	-	14.5	-	-
Port of Seattle-Tacoma, USA	41	-	-	15.2-15.5	-	-
Port of Dongguan, China	42					

Ports	No.	Length (m)	Beam (m)	Draught (m)	Air Draught (m)	Remarks
APM Terminals Tangier, Morocco	43	-	-	18	-	Fast handling rates
Port of Barcelona, Spain	44	-	-	16	-	South entrance
Vancouver Fraser Port Authority, Canada	45	-	-	15	55.9	Pg. 179 Appendix A
Port of Salalah, Oman	46	-	-	16	-	-
Port of Fuzhou, China	47	-	-	-	-	-
Marsaxlokk Port, Malta	48	-	-	17	-	-
Port of Nanjing, China	49	-	-	12.5	-	-
Port of Cai Mep, Vietnam	50	600	-	14	-	Channel Access
Khor Fakkan, UAE	und.	400	-	16	-	-
Port of Taicang, China	und.	-	-	12.5	-	-
Port of Valencia, Spain	und.	-	-	17	-	Modern Valencia Port
Port of Tanjung Perak, Indonesia	und.	-	-	16	-	Can serve 15000 TEUs
Port Said, Egypt	und.	297	-	13	70	Suez Canal Bridge
Port Newark–Elizabeth Marine Terminal. New York, USA	und.	-	-	15.2	65.5	Bayonne Bridge
Halifax, Canada	und.	333	-	16.2	-	Pier C
Seagirt. Baltimore, USA	und.	373	-	15.2	56	Francis Scott Key Bridge
Dundulk. Baltimore, USA	und.	-		13.7	56.3	Berth 5-6. Francis Scott Key Bridge
Norfolk International Terminals. Virginia, USA	und.	-	22 container wide	15.2	-	-
Fairview Terminal-Prince Rupert, Canada	und.	380	-	16.8	-	-

Ports	No.	Length (m)	Beam (m)	Draught (m)	Air Draught (m)	Remarks
Port of Portland, USA	und.	-	-	12.19	59	Astoria–Megler Bridge
Port of Oakland, USA	und.	502.9 (turning basin)	57.3	15.2	67 (West)	Golden Gate Bridge (San Francisco-Oackland Bay Bridge)
Port of Houston, USA	und.	-	-	13.7	-	-
Port of New Orleans, USA	und.	-	-	13.7	51.8	Crescent City Connection bridge
Port of Mobile. Alabama, USA	und.	-	-	13.7	-	-
Port of Gulfport. Missisipi, USA	und.	-	-	11.8	-	-
Port of Miami, USA	und.	-	-	15.2	-	-
Port Everglades, USA	und.	-	-	13.1	-	-
Port of Palm Beach, USA	und.	-	-	10.9	-	-
Port of Jacksonville, USA	und.	-	-	12.19	53.3	Dames Point Bridge
Port of Charleston, USA	und.	-	-	13.7	0/56.6/47.24	(Union Pier)/ Arthur Ravenel Jr. Bridge (Wando Welch. Leatherman Sr. Veterans)/ Don N. Holt Bridge (North Charlestone
Port of Wilmington (North Carolina), USA	und.	-	-	12.8	-	-
Port of Wilmington (Delaware) , USA	und.	-	-	11.5	53	-
Port of Philadelphia, USA	und.	-	-	12.19	57.3	Delaware Memorial Bridge
Port Jersey, USA	und.	-	-	15.2	69.4	Verrazano Bridge

Ports	No.	Length (m)	Beam (m)	Draught (m)	Air Draught (m)	Remarks
Port of Boston, USA	und.	-	-	12.19	-	-
Port of Corpus Christi.Texas, USA	und.	-	-	13.7	-	-
Port of Freeport. Texas, USA	und.	-	-	13.7	-	-
Gwadar Port, Pakistan	und.	-	-	12.5	-	*Under construction dredging until 20.5m (Phase II)
Port of Durrës, Albania	und.	-	-	11.5	-	-
DP World London Gateway, UK	und.	-	-	14.5-21 tidal	-	Depth alongside: 17m chart datum/Quay cranes among the largest in the world. 138m tall with the booms up
Khalifa Port, UAE	und.	-	-	16	-	Develop to deepen its main channel and basin to 18 metres
CERES Paragon Container Terminal Amsterdam, the Netherlands	und.	400	57	17.5	-	High Productivity
GCT Delta Port, Canada	und.	Each Terminal Length: 1000m	-	15.9	-	Fast handling rates

Table A.2: Sea Routes Limitations.

Route	Length (m)	Beam (m)	Draught (m)	Air Draught (m)	Remarks
Neo-Panamax Canal	366	51.25	14.94	61.3	Bridge of the Americas
Suez Canal	-	77.5	20.1	70	Suez Canal Bridge
Malacca Straits	470	und.	20	-	Limitation on speed
Bosphorus	-	-	min. 13	64	Bosphorus Bridge
Northeast Passage (NEP)	-	-	min. 13	-	Varieties of depths because of different routes
Northwest Passage (NWP)	-	-	15	-	Varieties of depths because of different routes
Isthmus of Tehuantepec	-	-	10	-	
Cape Horn	-	-	-	-	
Isthmus of Corinth	-	17.6	7.3	-	

Appendix B

User Manual of Time Calculations Tool

In the present Appendix B, the “User Manual” of time calculation software tool is depicted and the whole process of data entry and the obtained results are described.

In order to run the software, the user should have the main folder of “cofastrans”. The installation of a free and open-source cross-platform web server solution stack package (like XAMPP) is needed. This package runs both for Windows and for Linux. The “cofastrans” folder should be pasted on the “htdocs” directory of the XAMPP file on the disk (C:\xampp\htdocs).

The user opens the XAMPP program and then enables the Apache service. After that the user opens the browser. The software’s link is the following: http://localhost/cofastrans/index.php. Then the software’s portal page opens (Figure B.1).

In the following figure, the portal page of the tool is illustrated. This page is the main menu and contains four options (buttons). From top to bottom, the first button is called “New Ship” and the user enters the data for the visual creation of the ship. The second button is called “Modify Ship” and offers to the user the ability to the user to change the loading condition of the vessel. The third and the fourth can be used for calculations of loading/unloading times for the SSG and SSPC concept, respectively.

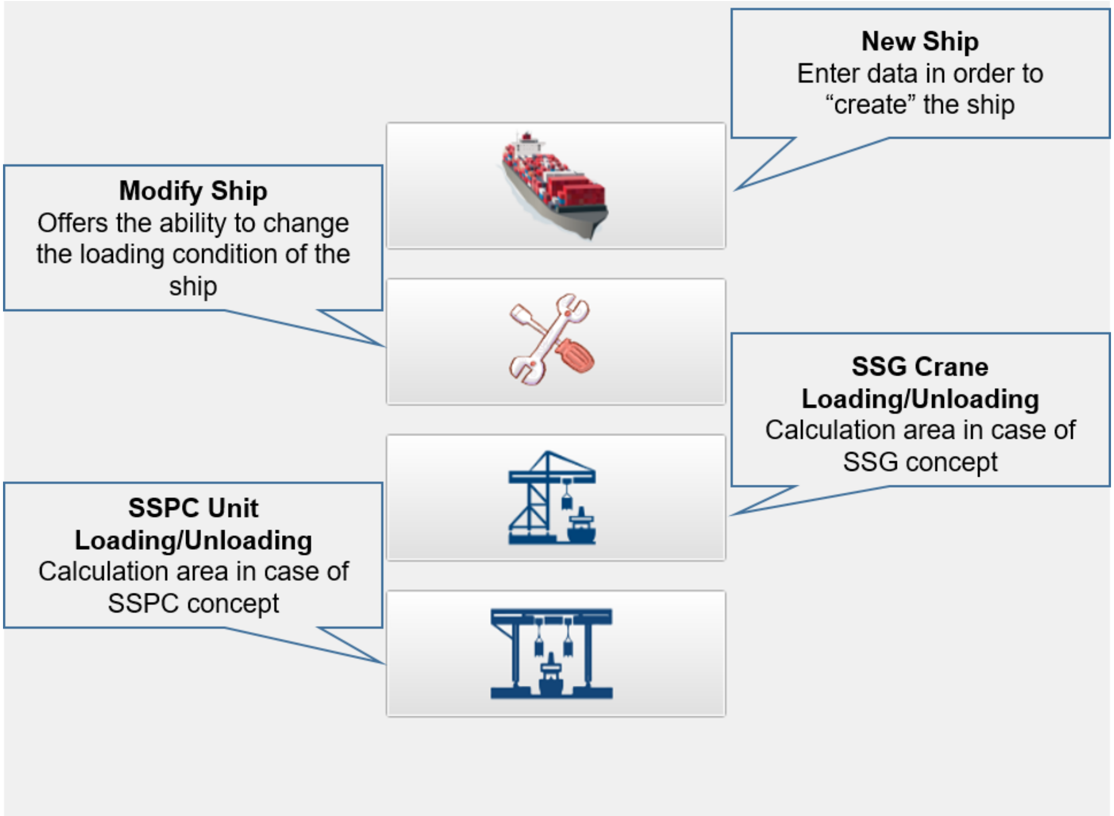

Figure B.1: Main Menu.

For the data entry process, the user has to click the "New Ship" button. An input area window opens (see Figure B.2). The fields are completed according to the vessel's data. Note that the fields "Aft Bays", "Mid Bays", "Forward Bays" indicate the distribution of the 20ft bays along the ship. The tool was developed for vessels with different position of funnel and superstructure. However, this has no impact on the total calculation of loading/unloading time. The final calculation has to be made by the user, due to the fact that the optimum configuration plan is needed. The procedure of total operation time calculations is described in Chapter 6. The separation of the funnel and the superstructure was made for visual reasons, in order the allocation of bays to be distinct. In case the funnel and the superstructure are not separated, choosing the number zero for 'Mid Bays", is advised.

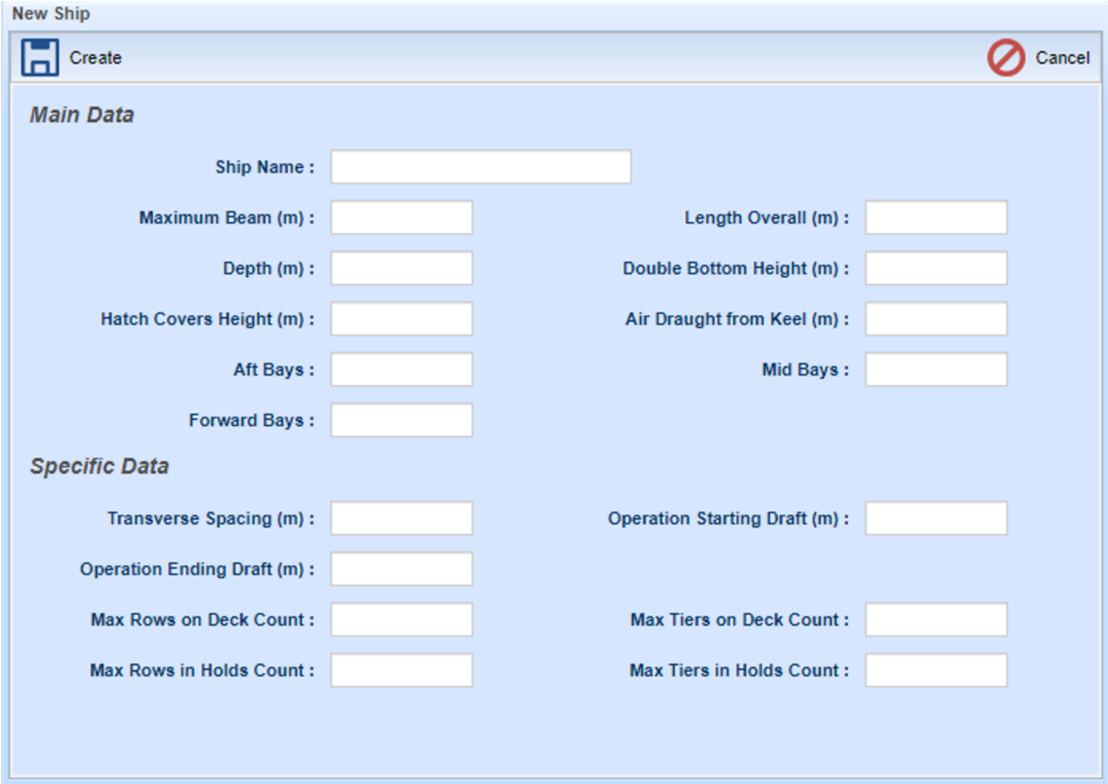

Figure B.2: Input Area window.

The specific data are described below (see also Chapter 6):

- Transverse Spacing (m): the transverse distance between the centers of two adjacent containers.
- Operation Starting Draft (m): the draught when operation starts. During the operation the vessel's draught changes. The calculations are made for the average draught.
- Operation Ending Draft (m): the draught at the end of operation.
- Max Rows on Deck Count: the maximum number of rows on above deck TEUs.
- Max Tiers on Deck Count: the maximum number of tiers on above deck TEUs.
- Max Rows on Holds Count: the maximum number of rows on below deck TEUs.
- Max Tiers on Holds Count: the maximum number of tiers on below deck TEUs.

After entering the necessary data, a new window with the bay list is shown (Figure B.3). In the upper part of the window, some basic vessel data are presented. The list below indicates the distribution of 20ft bays along the ship. For a faster data entry, a helpful option appears on the right; the "Copy Bay" and the "Paste Bay".

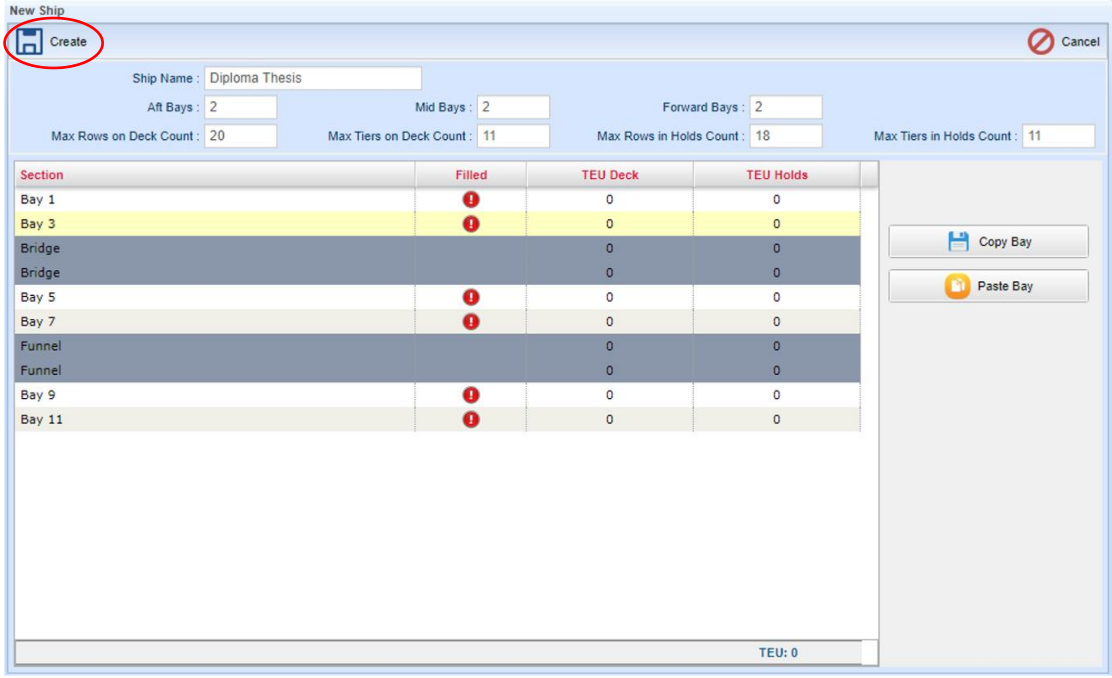

Figure B.3: Bay List window.

By double clicking on one bay, the "Bay Plan" for above deck (DECK) and below deck containers (HOLD) window opens (Figure B.4). The software creates a table of boxes depending on the maximum number of rows and tiers that the user gave. In order to create the bay Plan, the user must input the actual position of any TEU, by clicking the respective box, that denotes the aforementioned position, on this table. Some additional features appear on the right. These features help the user fill/erase all the area or fill/erase one row or tier. A very useful feature is the "Mirror" which copies the allocation of TEUs from one side and mirrors it to the other. At this point, the visualization of the bay is achieved.

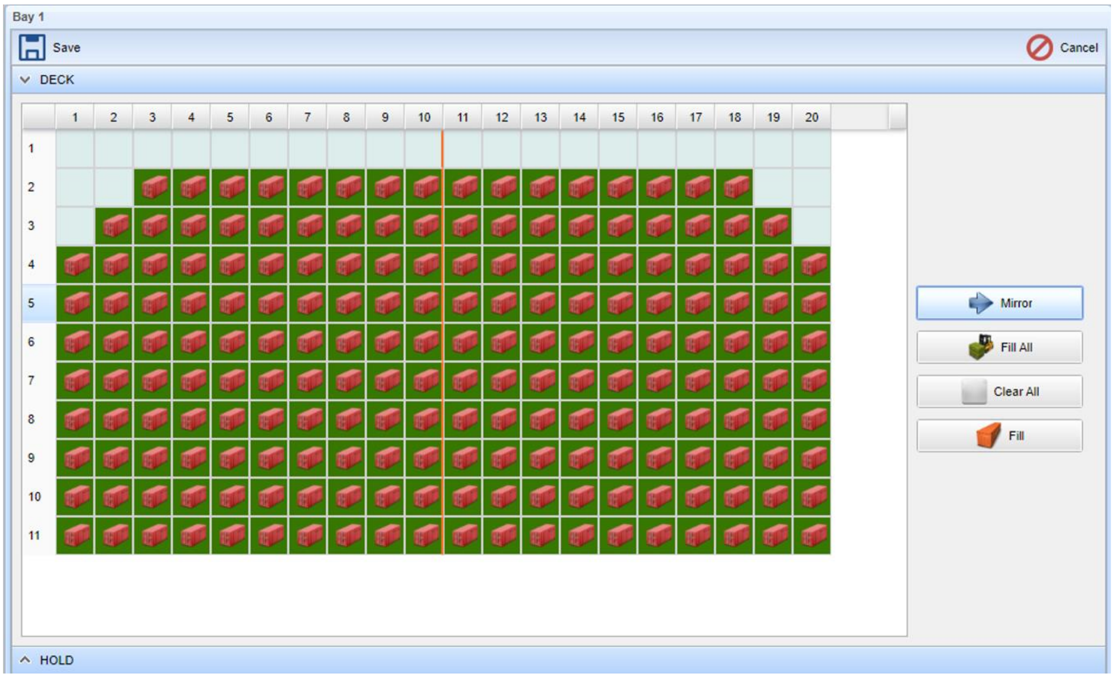

Figure B.4: Bay Plan window.

This procedure has to be made for each bay. After the fulfillment of visual bays, the software creates the visual vessel by clicking the "Create" button (red circle in Figure B.3).

The second button of the Main Menu is called "Modify Ship". The user can change the loading condition of the vessel and make the time calculations. By clicking the "Modify Button" a list of the saved vessels appears. The user selects the vessel that needs to be modified. Then, the same interface with the bay List opens, in which the changes can be made.

The third button of the Main Menu is called "SSG Crane Loading/Unloading". By clicking it, the calculation area window appears (Figure B.5). First, the main data of the crane has to be incorporated, on the left side of the window. The user can choose between loading and unloading, on the top left corner. The selection of the vessel can be made in the list of ships. By double clicking on the ship of the user's choice, the operation time results for above and below deck TEUs for each bay, as well as the total time for each bay.

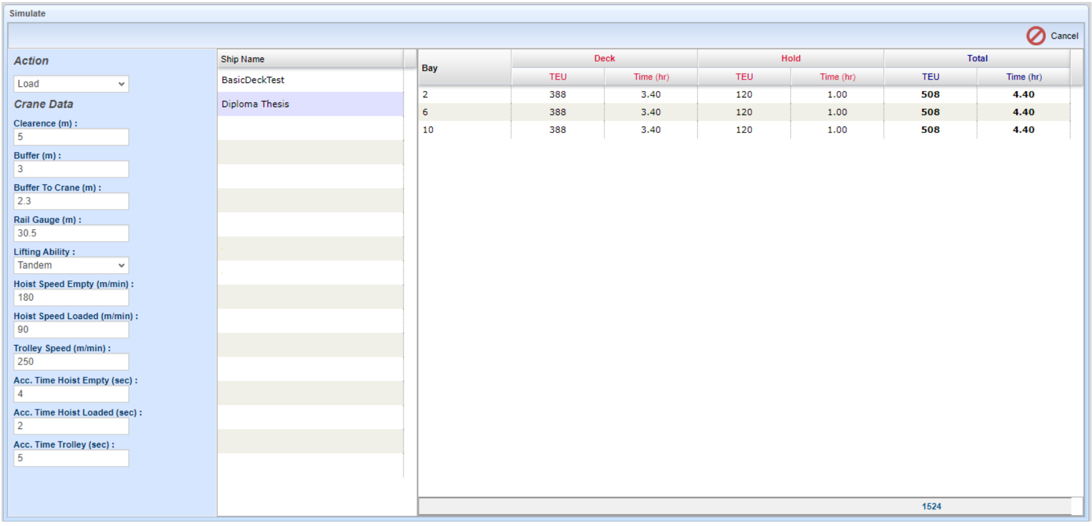

Figure B.5: Calculation area of SSG concept.

The calculations for the SSPC concept can be made, in the same way, on the fourth Main Menu's button, called "SSPC Unit Loading/Unloading". For the sake of simplicity, the interface of this option is similar to the SSG concept. An illustration is presented below.

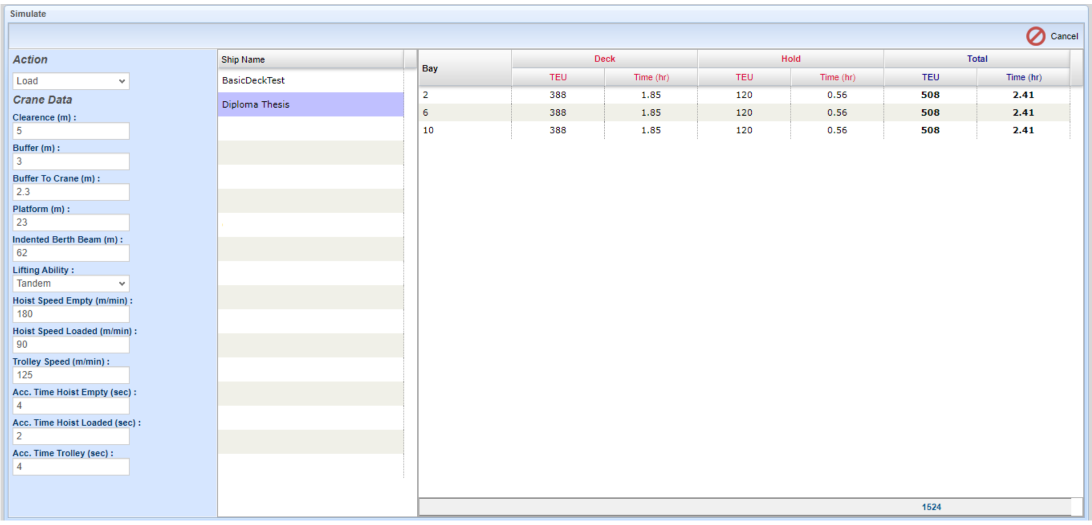

Figure B.6: Calculation area of SSPC concept.

The "lifting ability" selection is divided in two cases; tandem and twin lift spreader. In case of tandem lift spreader, the numbers of TEU transported in one full move of operation equal to 3.2 TEU/move, and the dwell time for docking and undocking the TEUs from the spreader equals to 15 seconds. In case of twin lift spreader, the numbers of TEU transported in one full move of operation equal to 1.6 TEU/move, and the dwell time for docking and undocking the TEUs from the spreader equals to 10 seconds.

The tool can export the results of mass centers of each bay, the cycle times of each bay and the total times of each bay into a ".txt" and ".csv" format. The files are saved automatically as “results” in the software’s directory (C:\xampp\htdocs\cofastrans\results).

The “results” folder path is the following:

Results → Ship’s name folder → SSG/SSPC folder → Loading/Unloading folder (with run Date and Time, based on XAMPP’s timezone)

The results files are located inside the Loading/Unloading folders, which are:

- “**crane_config.txt**”: the user’s crane input data
- “**center_gravity.txt**” (only in SSG concept): the center of gravity of each group (above deck-DECK, below deck-HOLDS) of each bay
- “**result.csv**”: the results that are depicted in the output window in editable format
- “**Cycle Time.txt**”: the cycle times of each group of each bay
  (*) In SSPC concept the groups are divided into port side and starboard side sub-groups. In this case, the results for both sub-groups are depicted on this file. Only the maximum cycle times should be taken into account.
  (*) In case of empty group, the center of gravity is located in (0,0). The calculation of cycle time is undertaken for this point. However, the total operation time of each bay equals to zero. The cycle time should be considered as zero, too.

For further information, please contact me: leotsagan@gmail.com